NAVAL POSTGRADUATE SCHOOL

MONTEREY, CALIFORNIA

THESIS

THE INTERACTION OF ATMOSPHERIC RIVERS AND HIGH-PRESSURE SYSTEMS

by

Justin P. Van Es

December 2020

Thesis Advisor:	Wendell A. Nuss
Second Reader:	Joel Feldmeier, Meteorology: MR

THIS PAGE INTENTIONALLY LEFT BLANK

REPORT DOCUMENTATION PAGE	*Form Approved OMB No. 0704-0188*

1. AGENCY USE ONLY *(Leave blank)*	**2. REPORT DATE** December 2020	**3. REPORT TYPE AND DATES COVERED** Master's thesis

4. TITLE AND SUBTITLE THE INTERACTION OF ATMOSPHERIC RIVERS AND HIGH-PRESSURE SYSTEMS	**5. FUNDING NUMBERS**
6. AUTHOR(S) Justin P. Van Es	
7. PERFORMING ORGANIZATION NAME(S) AND ADDRESS(ES) Naval Postgraduate School Monterey, CA 93943-5000	**8. PERFORMING ORGANIZATION REPORT NUMBER**
9. SPONSORING / MONITORING AGENCY NAME(S) AND ADDRESS(ES) N/A	**10. SPONSORING / MONITORING AGENCY REPORT NUMBER**

11. SUPPLEMENTARY NOTES The views expressed in this thesis are those of the author and do not reflect the official policy or position of the Department of Defense or the U.S. Government.

12a. DISTRIBUTION / AVAILABILITY STATEMENT Approved for public release. Distribution is unlimited.	**12b. DISTRIBUTION CODE** A

13. ABSTRACT (maximum 200 words)

As Midlatitude Pacific storms migrate east, some develop moisture plumes that can stretch from the western United States to Hawaii. These events are commonly known as atmospheric rivers (ARs) and have been associated with some of worst flooding in the western United States. There is evidence that both extratropical ARs and low-level high-pressure systems form near the Hawaiian Islands, and the low-level high-pressure system aids moisture transport into the AR. Four AR events were analyzed, and this study found that ARs from these extratropical cyclones 1) result from the interaction of the surface high- and low-pressure system centers to form major (Pineapple Express) AR events; 2) are fed moisture from the high-pressure system to the east; and 3) have different relative sources of moisture that impact on observed downstream precipitation.

14. SUBJECT TERMS atmospheric rivers, ARs, floods, California	**15. NUMBER OF PAGES** 111
	16. PRICE CODE

17. SECURITY CLASSIFICATION OF REPORT	**18. SECURITY CLASSIFICATION OF THIS PAGE**	**19. SECURITY CLASSIFICATION OF ABSTRACT**	**20. LIMITATION OF ABSTRACT**
Unclassified	Unclassified	Unclassified	UU

NSN 7540-01-280-5500

Standard Form 298 (Rev. 2-89)
Prescribed by ANSI Std. 239-18

THIS PAGE INTENTIONALLY LEFT BLANK

Approved for public release. Distribution is unlimited.

THE INTERACTION OF ATMOSPHERIC RIVERS AND HIGH-PRESSURE SYSTEMS

Justin P. Van Es
Lieutenant Commander, United States Navy
BS, San Francisco State University, 2005

Submitted in partial fulfillment of the
requirements for the degree of

MASTER OF SCIENCE IN METEOROLOGY AND PHYSICAL OCEANOGRAPHY

from the

NAVAL POSTGRADUATE SCHOOL
December 2020

Approved by: Wendell A. Nuss
Advisor

Joel Feldmeier
Second Reader

Wendell A. Nuss
Chair, Department of Meteorology

THIS PAGE INTENTIONALLY LEFT BLANK

ABSTRACT

As Midlatitude Pacific storms migrate east, some develop moisture plumes that can stretch from the western United States to Hawaii. These events are commonly known as atmospheric rivers (ARs) and have been associated with some of worst flooding in the western United States. There is evidence that both extratropical ARs and low-level high-pressure systems form near the Hawaiian Islands, and the low-level high-pressure system aids moisture transport into the AR. Four AR events were analyzed, and this study found that ARs from these extratropical cyclones 1) result from the interaction of the surface high- and low-pressure system centers to form major (Pineapple Express) AR events; 2) are fed moisture from the high-pressure system to the east; and 3) have different relative sources of moisture that impact on observed downstream precipitation.

THIS PAGE INTENTIONALLY LEFT BLANK

TABLE OF CONTENTS

THIS PAGE INTENTIONALLY LEFT BLANK

LIST OF FIGURES

THIS PAGE INTENTIONALLY LEFT BLANK

LIST OF ACRONYMS AND ABBREVIATIONS

AMS	American Meteorological Society
AR	atmospheric river
CBAR	convergent boundary atmospheric rivers
CNRFCP	California Nevada River Forecast Center precipitation
GHT	geopotential heights
GOES	Geostationary Operational Environmental Satellite
IR	satellite infrared
ITCZ	Intertropical Convergence Zone
IVT	vertically integrated water vapor transport
mb	millibars
NOAA	National Oceanographic and Atmospheric Administration
SLP	sea-level-pressure
TQV	total column water vapor

THIS PAGE INTENTIONALLY LEFT BLANK

ACKNOWLEDGMENTS

I would like to thank the following groups and individuals: Professor Wendell Nuss, for his guidance and mentorship in researching this project; CDR Joel Feldmeier, for his reviewing and recommendations; CDR Paula Travis and CDR Ana Tempone, for their leadership and encouragement; my cohort, for all of the tutoring and support; the Naval Postgraduate School Graduate Writing Center, for coaching me throughout my time at NPS; San Francisco State University Meteorology Program Professors Oswaldo Garcia, John Monteverdi, and Dave Dempsey, for teaching me throughout my undergrad program; Tom Chance, who gave me my first weather job as a weather observer at the San Jose Airport; my Mom and Dad, Filomena and Jacobus, for their hard work in raising me; and the 1997 New Year's Day Atmospheric River event, for being the storm that sparked my interest in meteorology. Finally, thanks to my loving family: my wife, Yukiko, and my daughter, Amelia, who have brought so much love, and joy, into my life.

THIS PAGE INTENTIONALLY LEFT BLANK

I. INTRODUCTION

A. MOTIVATION AND HYPOTHESES

Atmospheric rivers (ARs) transport water vapor from tropical regions poleward. They are associated with extratropical cyclones and typically form moisture plumes that are longer than their widths. The moisture plume of one common AR, known as the Pineapple Express, can stretch from Hawaii to the west coast of the continental United States. These ARs commonly occur during November through March and produce a substantial amount of winter precipitation for the western United States. Major AR events have been associated with some of the worst catastrophic flooding in the western United States, and Pineapple Express ARs pose a threat to Department of Defense (DOD) installations throughout that region.

Observation and satellite data suggest that ARs form near Hawaii as the trough associated with a low-pressure system increases in meridional extent (i.e., digs) north of Hawaii and a high-pressure system forms just east of Hawaii. While the moisture plume suggests that moisture flows from near Hawaii, the source of moisture can vary between events. The surface high-pressure system to the east appears to feed moisture into the low-pressure system. It may also transport moisture into the associated cold front, forming what has been termed a convergent boundary atmospheric river (CBAR). The role of the full synoptic-scale pattern in contributing moisture and developing ARs has not been fully explored and may be important to explain variations in the resultant downstream precipitation.

This study has three primary objectives to understand: 1) the interaction of the surface high and low-pressure system centers in forming major (Pineapple Express) AR events; 2) the role of the high-pressure system to feed moisture into the low-pressure system and CBAR; 3) the relative source of moisture in different ARs and its potential impact on observed downstream precipitation. Understanding these aspects of the formation and evolution of ARs will help better predict their occurrence and impacts over the U.S. west coast.

B. BACKGROUND

Though ARs have been studied since the 1990s (Ralph et al. 2017), ARs have gained public interest during the past few years due to their link to extreme precipitation events. ARs can produce 20%-50% of winter precipitation in the western United States, falling on the day of or day after AR landfall (Dettinger et al. 2011). In some extreme cases according to Ingram and Malamud-Roam (2013) they "may contain as much water as ten to fifteen Mississippi Rivers." While these impacts are well documented, the variations from case to case are not as well understood.

The definition of an AR according to the *Glossary of Meteorology* from the American Meteorological Society (AMS) is as follows.

> An atmospheric river is a long, narrow, and transient corridor of strong horizontal water vapor transport that is typically associated with a low-level jet stream ahead of the cold front of an extratropical cyclone. The water vapor in atmospheric rivers is supplied by tropical and/or extratropical moisture sources. Atmospheric rivers frequently lead to heavy precipitation where they are forced upward, for example, by mountains or by ascent in the warm conveyor belt. Horizontal water vapor transport in the midlatitudes occurs primarily in atmospheric rivers and is focused in the lower troposphere. Atmospheric rivers are the largest "rivers" of fresh water on Earth, transporting on average more than double the flow of the Amazon River. (AMS 2019)

At its core, an AR plume can typically be longer than 2000 km long and less than 1000 km wide (Ralph et al. 2004). The AR plume is the result of water vapor transport from tropical and/or extratropical moisture sources. How this transport of water vapor occurs in ARs has been extensively studied for years and hotly debated. Some studies suggest that ARs really represent long range moisture transport (such as a river), while others suggest that they are simply an artifact of a propagating storm that leaves a residual moisture trail. Two studies covered both possibilities. The first study covers the possibility that the plumes are the result of a footprint left behind by poleward traveling storms and not a river transporting water vapor from the tropics (Dacre et al. 2015). The other study examined water vapor traveling northeastward from the (northern hemisphere) Intertropical Convergence Zone (ITCZ) (Newell et al. 1992). This variant is found during a dominant jet stream pattern at the 250 mb level. Strong zonal winds at the 250 mb level

appear to correlate to the size of a long moisture plume, and the 250 mb winds appear to be key contributor to moisture transport during AR events.

While both these interpretations will be investigated in this thesis, an additional possibility will be examined that's rarely mentioned or previously researched. This relates to the interaction of a low-level high-pressure system with a low-pressure system (extratropical cyclone). A study by Hedstrom (2014) stated, "the low-level jet in the warm sector in this case extended well to the east, which suggests that low-level structure associated with the high to the east may be important in setting up the moisture transport." This interaction was not explored any further in the Hedstrom study and is an area that should be explored more closely. In the cases that were studied in this thesis, all cases had a low-level high-pressure system and an AR producing extratropical cyclone interacting with each other near the Hawaiian Islands. Both the low-level high-pressure system and AR extratropical cyclone were observed to migrate eastward together. The low-level high-pressure system would appear to transport moisture from tropics and into the cold front or the CBAR, as well as push moisture ahead of the AR extratropical cyclone for further enhancement as the AR extratropical cyclone approaches the western United States.

C. OBJECTIVES

The overall goal of this research is to help identify the source of water vapor and its transport in the formation of an AR extratropical cyclones near Hawaii. Specifically, the interaction between the high-pressure system and low-pressure systems as they migrate to the west coast of the United States will be examined to establish the role of the high-pressure system in an AR extratropical cyclone formation. In addition, the relative contribution of moisture flowing around the high-pressure system will be examined. Finally, the relationship between the moisture source and the downstream impact on precipitation will be examined. These will give us a better understanding on how AR extratropical cyclones form and identify atmospheric patterns ahead of time that could give us a longer-range forecast of potentially extreme precipitation events.

THIS PAGE INTENTIONALLY LEFT BLANK

II. DATA AND METHODS

For this study, four AR events were analyzed and will be used as case studies. The four were identified from archived geostationary satellite imagery from the National Oceanographic and Atmospheric Administration (NOAA) Geostationary Operational Environmental Satellite (GOES) series. The cases are as follows: Case 1: 26–02 December/January 1996–1997; Case 2: 06–10 February 2007; Case 3: 08–13 February 2019; and Case 4 27–02 November/December 2019. In all cases, it was noted on satellite imagery on the last day of each event that an extensive cloud plume that stretched from the western United States to the Hawaiian Islands.

To verify that the satellite images correspond to AR events, surface precipitation observations were examined. Observed precipitation records from the California Nevada River Forecast Center precipitation analyses (CNRFC), and data from multiple National Weather Services offices throughout California were examined to identify significant precipitation. Heavy rainfall lasting for several days was observed throughout California at the times when the events' extensive cloud plumes arrived into California. This further confirmed that a possible AR event was occurring.

To examine the four AR events, Climate Forecast System Reanalysis (CFSR) data from the National Centers for Environmental Prediction (NCEP) was used. University Corporation for Atmospheric Research (UCAR 2020) defines CFSR as "It is a global, high resolution, coupled atmosphere-ocean-land surface-sea ice system designed to provide the best estimate of the state of these coupled domains over this period." The CFSR can gather multiple atmospheric data from 1979 and this data can be ingested local computer programs for further analysis.

One such computer program that utilizes CFSR is called VISUAL. VISUAL was used to produce graphical atmospheric maps for sea-level-pressure (SLP), 1000 mb winds, 700 mb heights, 500 mb heights, total column water vapor (TQV), and vertically integrated water vapor transport (IVT). VISUAL was developed by Dr. Wendell Nuss and Steve Drake (1990) at the Naval Postgraduate School and uses "graphic kernel system primitives

and National Center for Atmospheric Research Graphics routines to examine meteorological grids and observations." This allows users to create a 2D meteorological synoptic view. By utilizing this software, synoptic patterns can be identified and analyzed to and help determine the formation of an AR event.

Since ARs are characterized by their water vapor transport, the integrated water vapor transport (IVT) was calculated as a vector in the x(zonal) and y(meridional) directions (Sexson 2019). The IVT is then displayed through VISUAL and can give good representation of the origins of the water vapor transport. This will also be useful in identifying clockwise air circulation (high-pressure) associated with the AR extratropical cyclone. To calculate IVT we use:

$$IVT_x = -1/g \int uqdp$$

$$IVT_y = -1/g \int vqdp\,,$$

"where g is the gravitation acceleration, u(v) is the zonal (meridional) wind, q is the specific humidity, and p is the pressure" (Guan and Waliser 2017). These vectors can then be plotted on a horizontal chart to see the regions of strong water vapor transport.

The synoptic scale features and their evolution associated with AR development were assessed with geopotential heights (GHT) at 500 mb and 700 mb as well as sea-level pressure and 1000 mb winds. The development of extratropical cyclone systems was examined to determine the development of ARs. These plots were also used to verify the association of the low-level high-pressure region interacting with the AR extratropical system. Specifically, the sea-level pressure and 1000 mb winds were used to confirm that an IVT clockwise circulation associated with an AR event is a low-level high-pressure system. Finally, 250 mb winds were examined to verify the location, size, strength and support of the development of the cloud plume of an AR.

Another feature of VISUAL is the ability to track air parcel trajectories going back 48 hours. Air parcel trajectories were plotted for all four cases at the 700 mb level. Four geographic locations in the California Sierra foothills were chosen for heightened analysis due to observed heavy rainfall. The time and location for the 1996-1997 event was 02

January 1997 in Pacific River CA. For the 2007 event, time and location was 10 Feb 2007 Blue Canyon CA. For the February 2019 event, time and location was 13 February 2019 Blue Springs. Finally, Blue Springs CA was also chosen for the 03 December 2019 event. By using VISUAL, the origin of air parcels associated with each event can be traced and used to confirm if a low-level high-pressure system is contributing to the formation of an AR extratropical cyclone

The data and methods mentioned above should provide a better understanding of the development of an AR extratropical cyclone system and explore the role that the high-pressure region plays in the moisture transport into the AR extratropical cyclone. In the coming chapters, Chapter III evaluates the synoptic characteristics at the beginning of each AR case study. Results of each case will be shown in Chapter IV, and Chapter V is the summary and its findings.

THIS PAGE INTENTIONALLY LEFT BLANK

III. CASE STUDIES

The author chose the listed case studies because he personally lived through all of them. All of the cases left a lasting impression. While gathering satellite imagery for each case, it became apparent that all of the cases exhibited cloud plumes that stretched from Hawaii to the west coast of the United States. Further investigation using the CNRFC data revealed heavy rainfall throughout California during three of the four events. The 1996-1997 event was not archived in the CNRFC, but rainfall data was found at multiple National Weather Services offices throughout California. Finally, while analyzing the synoptic situation of each event, it became apparent in all four cases that a low-level high-pressure system formed east of Hawaii and began to interact with an AR extratropical cyclone north of Hawaii.

A. CASE 1

Case 1 took place from 26 December 1996 – 03 January 1997. This would become known as the Northern California New Year's Day Flood (KCRA TV Sacramento). Heavy, warmer than normal, precipitation fell throughout Northern California. The greatest daily rainfall occurred on January 2, 1997 at both Auburn and Tahoe City, which corresponds to the arrival of the AR to the central Sierra Mountains. In the Sierra Mountains, snow levels were observed at 9,000 feet Roos (1997). In Auburn CA, temperature departure from climatology was 12.3 F warmer (Figure 1) while in Tahoe City CA (elevation 6,250 feet), temperature departure from climatology was over 15 F warmer (Figure 2). No new snow fell at Tahoe city between 29 December 1996 – 02 January 1997 (NWS Reno) and the warmer than normal conditions contributed to snow melt to further increase the precipitation runoff.

Tracking satellite imagery back from January 2, 1997, when the AR was over the central Sierra Mountains, the initial development time and area was identified. Figure 3 is satellite infrared imagery (IR) for 26 December 1996 and shows a low-pressure system developing north west of Hawaii. To the southeast of the low-pressure system, a plume of

clouds extends southwest to northeast. This cloud plume is the first signature of the AR in this case.

The integrated vapor transport (IVT) and 700 mb geopotential heights (Figure 4) indicate a trough and strong moisture transport south and east of the trough where the cloud band is seen in the satellite image. This pattern of vapor transport is typical of the flow around an extratropical cyclone system. Of particular notice, the IVT displays a clockwise circulation east of Hawaii. Analyzing the IVT (Figure 4) further, it appears this high-pressure system aids water vapor transport into the AR extratropical cyclone, even at this early stage, by producing westward transport to the south of Hawaii. The dominant vapor transport is from the west, which converges with this transport from the east.

The 500 mb geopotential height analysis (Figure 5) shows a broad trough in the region of the developing AR cyclone and a ridge east of the AR extratropical cyclone. The ridge is near 155 E east of the main AR trough at roughly 175 E. This structure is consistent with the development of an extratropical cyclone that is associated with the AR. The ridge to the east of the developing system supports the development of surface high-pressure downstream from the ridge. The role of this surface high in helping form the AR is examined in later sections.

Figure 6 shows winds at the 1000 mb level and sea-level pressure (SLP) and confirms that there was a low-level high-pressure system to the northeast of Hawaii. This surface high occurs downstream of the 500 mb ridge. Although the high is relatively weak, the anticyclonic circulation still produces easterly winds just south of Hawaii that feed into the developing AR. The surface clockwise circulation does not exactly align with the IVT plot circulation (Figure 2) as the IVT tends to be dominated by the mid-level circulation, which is displaced somewhat south of the surface high., However, both show westward transport just south of Hawaii and into the AR.

Figure 7 follows the 250 mb polar jet stream, which correlates to the extensive cloud plume found in the IR images. The strong jet windspeeds found in the 250 mb field support massive cloud development in the AR.

Climatological Data for AUBURN, CA - December 1996

Click column heading to sort ascending, click again to sort descending.

Date	Temperature				HDD	CDD	Precipitation	New Snow	Snow Depth
	Maximum	Minimum	Average	Departure					
1996-12-01	56	35	45.5	-2.5	19	0	0.69	0.0	0
1996-12-02	55	35	45.0	-2.8	20	0	0.00	0.0	0
1996-12-03	51	35	43.0	-4.6	22	0	0.00	0.0	0
1996-12-04	54	37	45.5	-1.9	19	0	0.00	0.0	0
1996-12-05	52	41	46.5	-0.7	18	0	2.59	0.0	0
1996-12-06	49	47	48.0	1.0	17	0	0.11	0.0	0
1996-12-07	52	44	48.0	1.2	17	0	0.00	0.0	0
1996-12-08	59	48	53.5	6.8	11	0	0.00	0.0	0
1996-12-09	60	48	54.0	7.5	11	0	0.07	0.0	0
1996-12-10	53	50	51.5	5.1	13	0	1.34	0.0	0
1996-12-11	53	50	51.5	5.3	13	0	0.29	0.0	0
1996-12-12	60	53	56.5	10.4	8	0	1.99	0.0	0
1996-12-13	60	51	55.5	9.5	9	0	0.68	0.0	0
1996-12-14	59	37	48.0	2.1	17	0	0.00	0.0	0
1996-12-15	63	34	48.5	2.7	16	0	0.00	0.0	0
1996-12-16	57	36	46.5	0.8	18	0	0.00	0.0	0
1996-12-17	60	38	49.0	3.4	16	0	0.00	0.0	0
1996-12-18	65	36	50.5	4.9	14	0	0.00	0.0	0
1996-12-19	58	38	48.0	2.5	17	0	0.00	0.0	0
1996-12-20	52	36	44.0	-1.4	21	0	0.00	0.0	0
1996-12-21	45	33	39.0	-6.4	26	0	1.58	0.0	0
1996-12-22	45	33	39.0	-6.3	26	0	1.77	0.0	0
1996-12-23	46	42	44.0	-1.3	21	0	0.76	0.0	0
1996-12-24	54	37	45.5	0.2	19	0	0.00	0.0	0
1996-12-25	52	36	44.0	-1.3	21	0	0.00	0.0	0
1996-12-26	53	M	M	M	M	M	0.05	0.0	0
1996-12-27	51	42	46.5	1.2	18	0	2.24	0.0	0
1996-12-28	52	48	50.0	4.7	15	0	0.35	0.0	0
1996-12-29	55	48	51.5	6.2	13	0	0.03	0.0	0
1996-12-30	57	51	54.0	8.7	11	0	1.40	0.0	0
1996-12-31	58	55	56.5	11.2	8	0	0.84	0.0	0
Sum	1696	1254	-	-	494	0	16.78	0.0	-
Average	54.7	41.8	48.3	2.2	-	-	-	-	0.0
Normal	54.4	37.7	46.1	-	587	0	6.73	0.1	-

Climatological Data for AUBURN, CA - January 1997

Click column heading to sort ascending, click again to sort descending.

Date	Temperature				HDD	CDD	Precipitation	New Snow	Snow Depth
	Maximum	Minimum	Average	Departure					
1997-01-01	62	M	M	M	M	M	1.62	0.0	0
1997-01-02	62	53	57.5	12.2	7	0	4.12	0.0	0
1997-01-03	55	46	50.5	5.1	14	0	0.67	0.0	0
1997-01-04	57	40	48.5	3.1	16	0	0.00	0.0	0
1997-01-05	50	38	44.0	-1.4	21	0	0.02	0.0	0
1997-01-06	49	36	42.5	-3.0	22	0	0.00	0.0	0
1997-01-07	55	36	45.5	0.0	19	0	0.00	0.0	0
1997-01-08	53	34	43.5	-2.1	21	0	0.00	0.0	0
1997-01-09	53	36	44.5	-1.1	20	0	0.00	0.0	0
1997-01-10	56	37	46.5	0.8	18	0	0.00	0.0	0
1997-01-11	55	36	45.5	-0.2	19	0	0.00	0.0	0
1997-01-12	50	36	43.0	-2.8	22	0	0.01	0.0	0
1997-01-13	42	24	33.0	-12.8	32	0	0.25	0.0	0
1997-01-14	40	23	31.5	-14.4	33	0	0.00	0.0	0
1997-01-15	49	27	38.0	-8.0	27	0	0.09	0.0	0
1997-01-16	45	36	40.5	-5.5	24	0	0.03	0.0	0
1997-01-17	54	39	46.5	0.4	18	0	0.00	0.0	0
1997-01-18	46	40	43.0	-3.2	22	0	0.00	0.0	0
1997-01-19	55	37	46.0	-0.3	19	0	0.00	0.0	0
1997-01-20	53	36	44.5	-1.8	20	0	0.43	0.0	0
1997-01-21	47	41	44.0	-2.4	21	0	0.94	0.0	0
1997-01-22	48	42	45.0	-1.5	20	0	1.51	0.0	0
1997-01-23	50	41	45.5	-1.1	19	0	3.62	0.0	0
1997-01-24	53	41	47.0	0.3	18	0	0.02	0.0	0
1997-01-25	52	M	M	M	M	M	0.78	0.0	0
1997-01-26	56	50	53.0	6.1	12	0	2.02	0.0	0
1997-01-27	57	48	52.5	5.5	12	0	0.08	0.0	0
1997-01-28	58	48	53.0	5.9	12	0	0.06	0.0	0
1997-01-29	63	44	53.5	6.3	11	0	0.00	0.0	0
1997-01-30	59	43	51.0	3.7	14	0	0.00	0.0	0
1997-01-31	58	41	49.5	2.1	15	0	0.00	0.0	0
Sum	1642	1129	-	-	548	0	16.27	0.0	-
Average	53.0	38.9	45.8	-0.4	-	-	-	-	0.0
Normal	54.5	37.8	46.2	-	584	0	6.36	0.0	-

Figure 1. NWS Forecast Office Report for Auburn CA, December-January 1996-1997. Source: NWS Sacramento CA (1996-1997).

Climatological Data for TAHOE CITY, CA - December 1996

Click column heading to sort ascending, click again to sort descending.

Date	Temperature				HDD	CDD	Precipitation	New Snow	Snow Depth
	Maximum	Minimum	Average	Departure					
1996-12-01	44	M	M	M	M	M	0.60	M	1
1996-12-02	35	17	26.0	-5.5	39	0	0.14	0.0	1
1996-12-03	38	17	27.5	-3.8	37	0	0.00	0.0	T
1996-12-04	40	20	30.0	-1.1	35	0	0.00	0.0	T
1996-12-05	40	23	31.5	0.6	33	0	2.48	0.0	0
1996-12-06	40	30	35.0	4.2	30	0	0.79	6.0	6
1996-12-07	39	24	31.5	0.9	33	0	0.02	T	4
1996-12-08	44	M	M	M	M	M	0.00	0.0	1
1996-12-09	50	39	44.5	14.2	20	0	T	0.0	M
1996-12-10	40	33	36.5	6.3	28	0	1.43	4.0	4
1996-12-11	37	32	34.5	4.5	30	0	0.93	1.0	1
1996-12-12	41	35	38.0	8.1	27	0	1.65	0.0	1
1996-12-13	40	35	37.5	7.7	27	0	0.31	0.0	1
1996-12-14	44	22	33.0	3.3	32	0	T	0.0	1
1996-12-15	37	21	29.0	-0.6	36	0	0.00	0.0	0
1996-12-16	40	22	31.0	1.4	34	0	0.00	0.0	0
1996-12-17	43	25	34.0	4.5	31	0	0.00	0.0	0
1996-12-18	37	19	28.0	-1.4	37	0	0.00	0.0	0
1996-12-19	40	22	31.0	1.6	34	0	0.00	0.0	0
1996-12-20	45	25	35.0	5.7	30	0	0.00	0.0	0
1996-12-21	45	22	33.5	4.2	31	0	2.17	37.0	37
1996-12-22	29	24	26.5	-2.8	38	0	1.77	24.0	55
1996-12-23	30	M	M	M	M	M	1.24	12.0	56
1996-12-24	37	15	26.0	-3.2	39	0	0.00	0.0	49
1996-12-25	39	13	26.0	-3.2	39	0	0.00	0.0	47
1996-12-26	44	M	M	M	M	M	0.08	0.0	41
1996-12-27	38	31	34.5	5.3	30	0	1.76	5.0	39
1996-12-28	34	31	32.5	3.3	32	0	0.14	2.0	37
1996-12-29	44	31	37.5	8.3	27	0	0.05	0.0	34
1996-12-30	42	34	38.0	8.8	27	0	1.72	0.0	29
1996-12-31	44	38	41.0	11.8	24	0	1.22	0.0	23
Sum	1240	700	-	-	860	0	18.50	91.0	-
Average	40.0	25.9	32.9	3.0	-	-	-	-	15.6
Normal	39.6	20.2	29.9	-	1088	0	5.97	38.2	-

Climatological Data for TAHOE CITY, CA - January 1997

Click column heading to sort ascending, click again to sort descending.

Date	Temperature				HDD	CDD	Precipitation	New Snow	Snow Depth
	Maximum	Minimum	Average	Departure					
1997-01-01	48	42	45.0	15.7	20	0	2.43	0.0	14
1997-01-02	49	40	44.5	15.2	20	0	4.65	0.0	4
1997-01-03	40	30	35.0	5.7	30	0	1.58	5.0	5
1997-01-04	40	19	29.5	0.2	35	0	0.00	0.0	4
1997-01-05	37	21	29.0	-0.3	36	0	0.01	T	3
1997-01-06	33	10	21.5	-7.8	43	0	T	T	3
1997-01-07	33	15	24.0	-5.3	41	0	0.00	0.0	3
1997-01-08	43	18	30.5	1.1	34	0	0.00	0.0	2
1997-01-09	43	20	31.5	2.1	33	0	0.00	0.0	2
1997-01-10	43	23	33.0	3.6	32	0	0.00	0.0	2
1997-01-11	43	20	31.5	2.1	33	0	0.00	0.0	2
1997-01-12	46	23	34.5	5.1	30	0	0.00	0.0	2
1997-01-13	32	5	18.5	-10.9	46	0	0.15	2.0	4
1997-01-14	15	2	8.5	-20.9	56	0	T	T	4
1997-01-15	32	15	23.5	-5.9	41	0	0.16	3.0	7
1997-01-16	41	22	31.5	2.1	33	0	0.00	0.0	6
1997-01-17	41	24	32.5	3.1	32	0	0.00	0.0	5
1997-01-18	44	27	35.5	6.1	29	0	0.00	0.0	3
1997-01-19	48	25	36.5	7.1	28	0	0.00	0.0	2
1997-01-20	50	26	38.0	8.6	27	0	0.19	4.0	6
1997-01-21	32	23	27.5	-1.9	37	0	0.65	10.0	16
1997-01-22	35	28	31.5	2.1	33	0	0.62	9.0	24
1997-01-23	34	31	32.5	3.1	32	0	3.17	21.0	41
1997-01-24	41	19	30.0	0.6	35	0	0.00	0.0	37
1997-01-25	42	27	34.5	5.1	30	0	1.80	3.0	40
1997-01-26	38	32	35.0	5.6	30	0	2.60	10.0	44
1997-01-27	42	28	35.0	5.5	30	0	0.02	T	38
1997-01-28	41	31	36.0	6.5	29	0	0.20	T	36
1997-01-29	42	27	34.5	5.0	30	0	0.00	0.0	35
1997-01-30	48	25	36.5	7.0	28	0	0.00	0.0	34
1997-01-31	44	27	35.5	6.0	29	0	0.00	0.0	33
Sum	1240	725	-	-	1022	0	18.23	67.0	-
Average	40.0	23.4	31.7	2.3	-	-	-	-	14.9
Normal	39.4	19.4	29.4	-	1104	0	5.89	40.4	-

Figure 2. NWS Forecast Office Report for Tahoe City, CA, December–January 1996–1997. Source: NWS Reno NV (1996–1997).

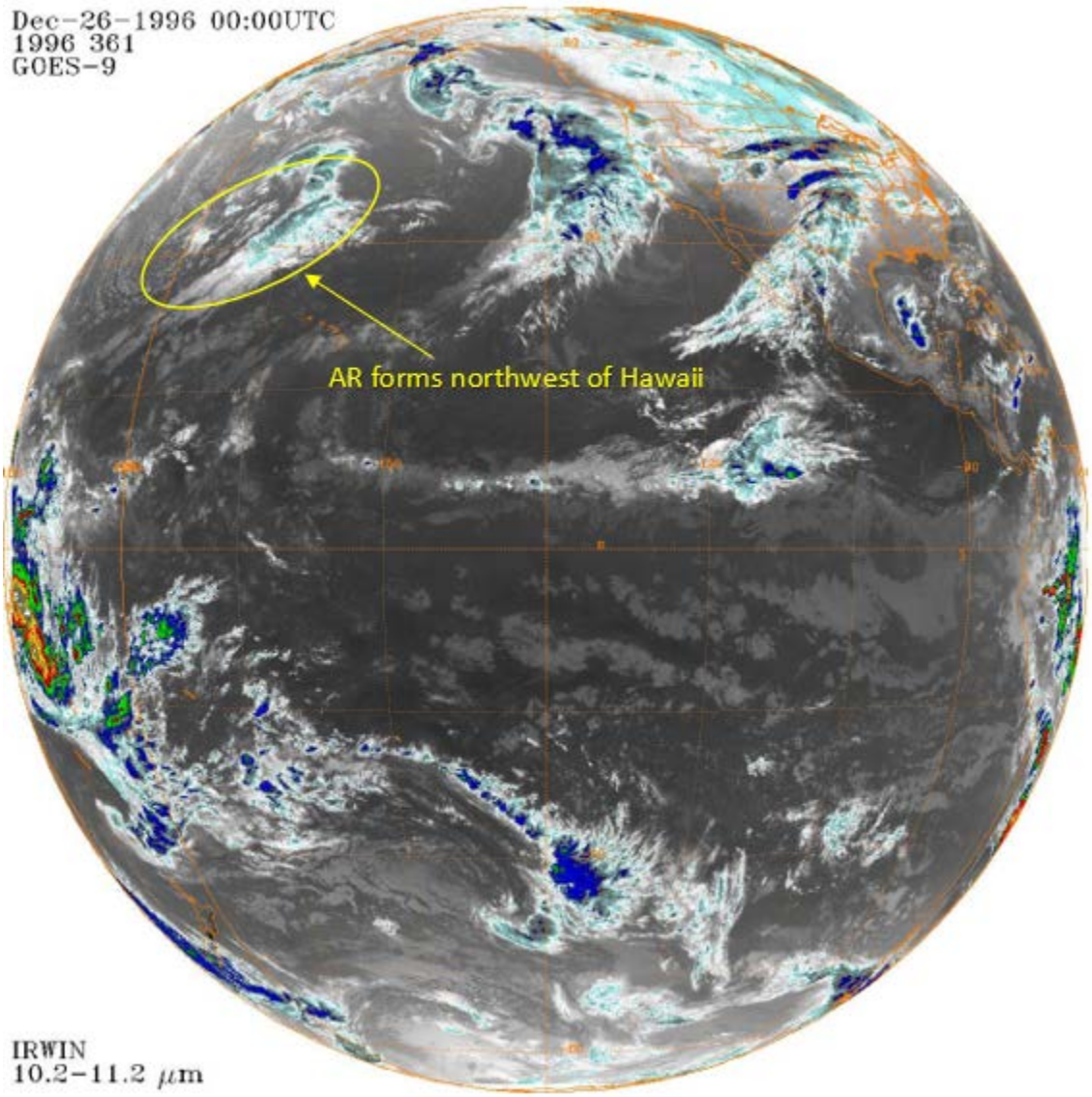

Above: GOES-09 (West) 0000 UTC 26 December 1996.

Figure 3. Case 1 GOES IR Imagery. Source: Knapp (2008).

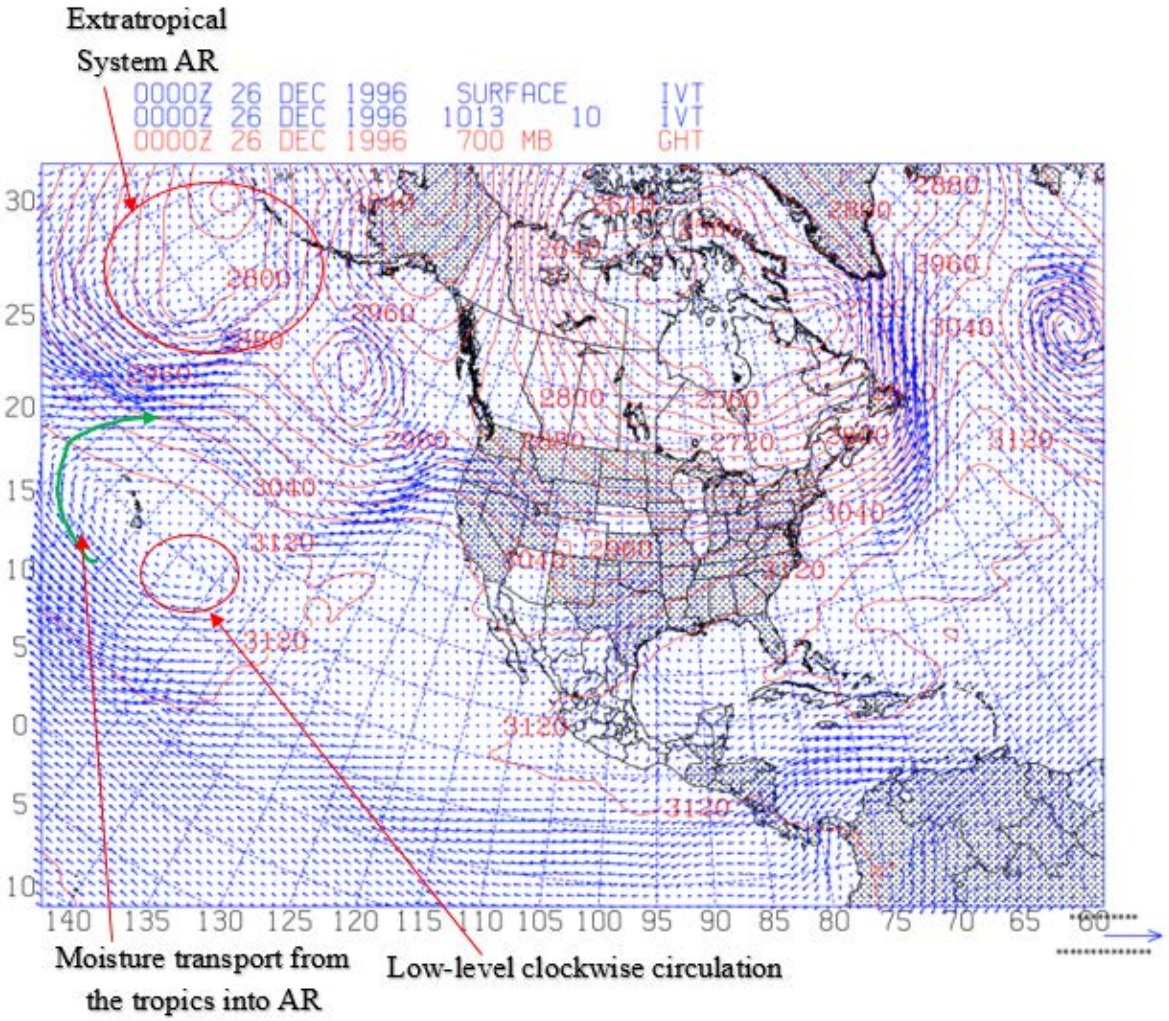

IVT plot for 0000 UTC 26 December 1996. Red lines 700 mb GHT and blue arrows are the IVT

Figure 4. Case 1 IVT and 700 mb GHT Plot.

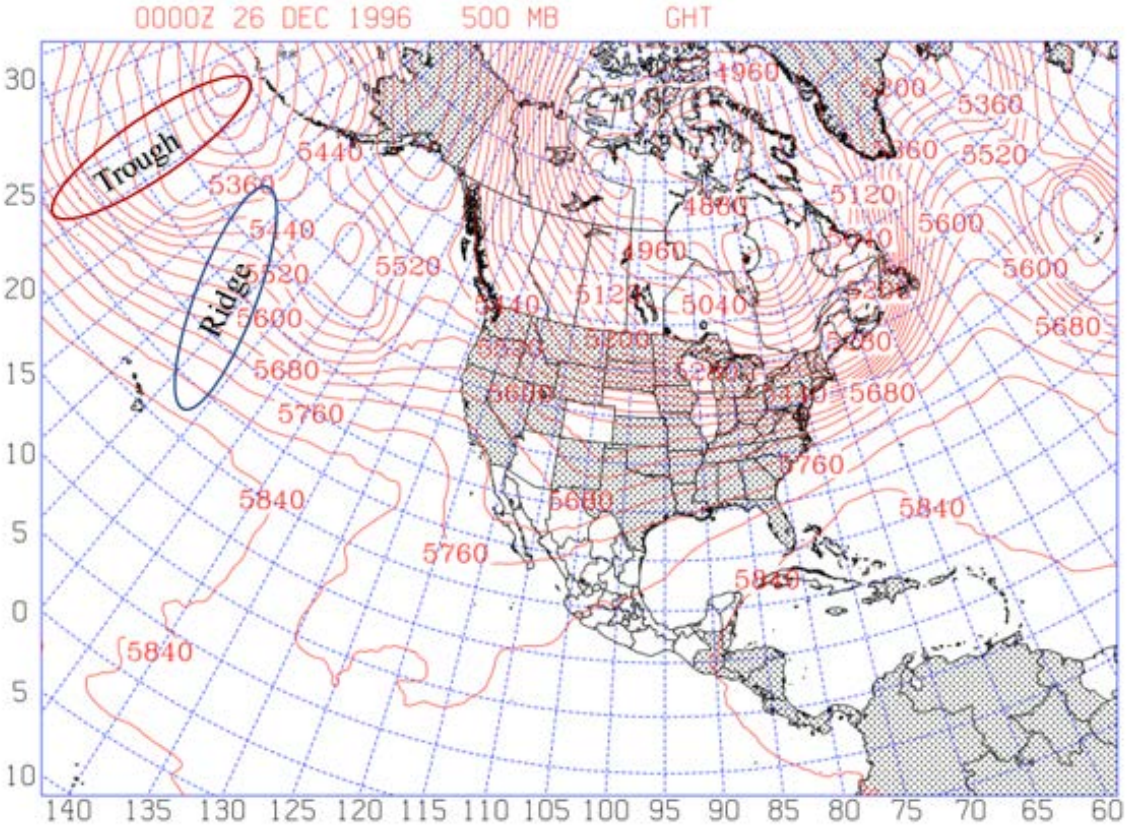

500 mb GHT plot for 0000 UTC 26 December 1996. 500 mb GHT are represented by the red lines in meters

Figure 5. Case 1 500 mb GHT Plot.

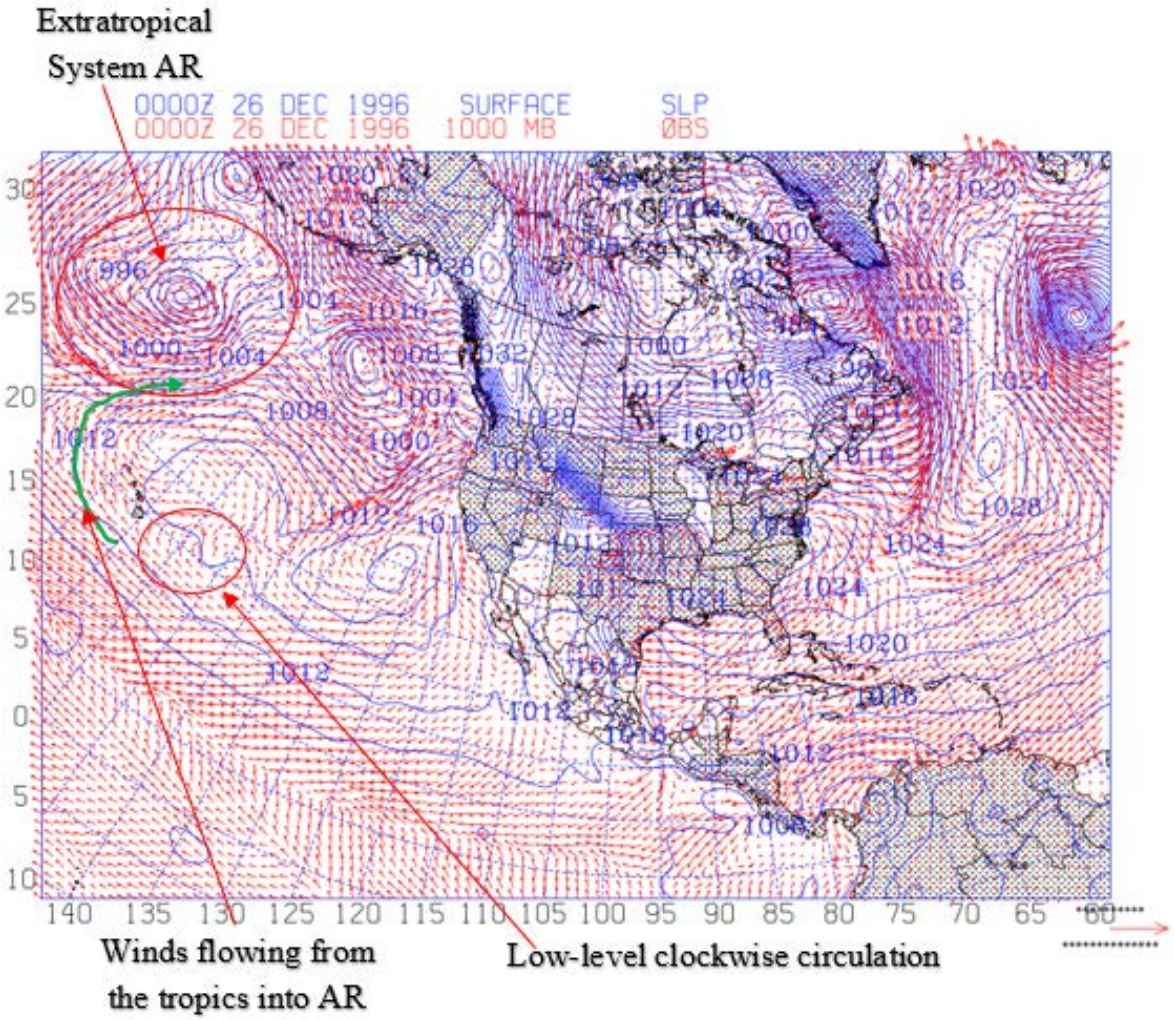

SLP and 1000 mb winds plot for 0000 UTC 26 December 1996. SLP are represented by the blue lines in mb and the red arrows represent wind vectors.

Figure 6. Case 1 SLP and 1000 mb Winds Plot.

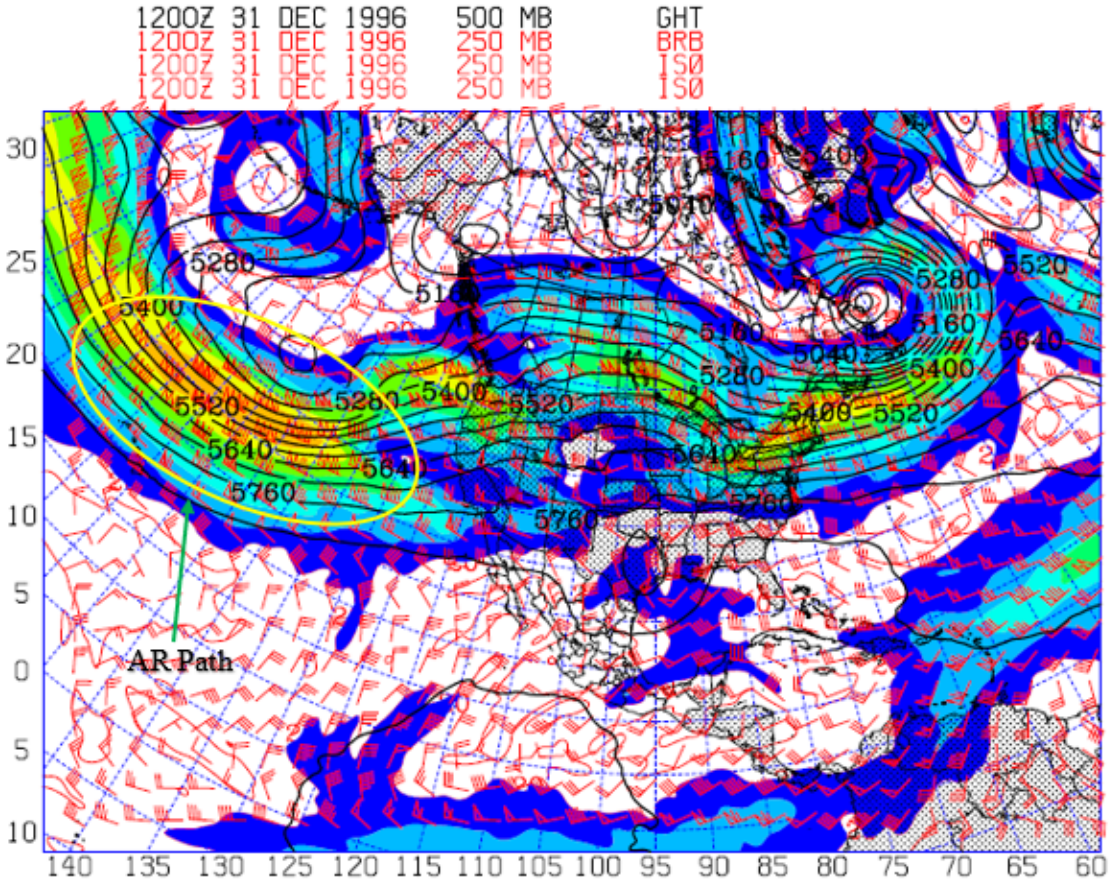

The 500 mb Geopotential Height contours are shown in black, the 250 mb jet stream is shown with the color fill, and the 250 mb wind is shown with red barbs, 1200 UTC 31 December 1996.

Figure 7. Case 1 Upper Air Chart.

B. CASE 2

Case 2 took place from 06 February 2007 – 11 February 1997. This event is very similar in structure and progression to Case 1, but much weaker. The maximum daily rainfall occurred on February 11 and was only around 1.5 inches in Auburn, CA (Figure 8) compared to over 4 inches in Case 1. Consequently, floods were not observed during this event, and snow levels were much lower in the Sierra Nevada Mountains compared to Case 1. Tahoe City CA observed new snow during this event (Figure 9).

Figure 10 is an IR image for 06 February 2007 and shows a low-pressure system developing north west of Hawaii just like Case 1. The system is somewhat further west in this case than Case 1. Another notable difference is that this case has considerably less clouds to the southeast of the system, which suggests that the moisture transport may be less at this stage than was observed in Case 1.

The integrated water vapor transport (IVT) and 700 mb GHT (Figure 11) confirm the weaker and less organized moisture transport in this case. The strongest transport occurs to the southeast of the developing system but is in a broad swath southeast of the 700 mb trough with no single well-defined strong plume. Again, the IVT displays a clockwise circulation east of Hawaii with westerly transport south of Hawaii contributing water vapor transport into the AR extratropical cyclone similar to Case 1. The anticyclonic circulation is also notably weaker at this time than the previous case.

The overall synoptic pattern at 500 mb is similar to that of Case 1 as shown in Figure 12. There is a broad trough in the region of the developing extratropical cyclone and a ridge east of the AR extratropical cyclone. The primary difference with Case 1 is the trough and ridge are displaced about 5-10 degrees west of their position in Case 1. Consequently, the ridge is north of Hawaii in this case and not east as seen in Case 1.

Figure 13 shows the winds at 1000 mb and sea-level pressure associated with the upper-level trough and ridge. The low-pressure is evident to the northwest of Hawaii near 175 W that is driving the initial AR development. As in Case 1, there is a low-level high-pressure system near Hawaii. However, in this case, the high-pressure center is almost due east of Hawaii with the surface ridge axis extending west across the Hawaiian Islands. The

anticyclonic circulation around this system produces easterly flow south of Hawaii that curves northward to the west of Hawaii and into the developing AR.

Figure 14 shows the 250 mb polar jet stream. In this event, the cloud plume found in the AR correlates with the jet stream. The jet maximum windspeeds were lower in comparison to Case 1, and the lower windspeed supports the less developed cloud plume found in Case 2.

Climatological Data for AUBURN, CA - February 2007

Click column heading to sort ascending, click again to sort descending.

Date	Temperature				HDD	CDD	Precipitation	New Snow	Snow Depth
	Maximum	Minimum	Average	Departure					
2007-02-01	54	35	44.5	-3.0	20	0	0.00	0.0	0
2007-02-02	M	35	M	M	M	M	0.00	0.0	0
2007-02-03	53	38	45.5	-2.3	19	0	0.00	0.0	0
2007-02-04	M	M	M	M	M	M	M	0.0	0
2007-02-05	M	M	M	M	M	M	0.00	0.0	0
2007-02-06	74	44	59.0	10.8	6	0	0.00	0.0	0
2007-02-07	M	48	M	M	M	M	M	M	0
2007-02-08	55	48	51.5	3.1	13	0	0.00	M	0
2007-02-09	57	51	54.0	5.4	11	0	1.02	0.0	0
2007-02-10	53	51	52.0	3.3	13	0	1.38	0.0	0
2007-02-11	M	M	M	M	M	M	M	0.0	0
2007-02-12	57	40	48.5	-0.5	16	0	3.11A	0.0	0
2007-02-13	61	38	49.5	0.4	15	0	0.56	0.0	0
2007-02-14	54	38	46.0	-3.3	19	0	0.00	0.0	0
2007-02-15	68	44	56.0	6.6	9	0	0.00	0.0	0
2007-02-16	M	44	M	M	M	M	0.00	0.0	0
2007-02-17	M	M	M	M	M	M	M	0.0	0
2007-02-18	M	M	M	M	M	M	M	0.0	0
2007-02-19	72	38	55.0	5.0	10	0	0.00	0.0	0
2007-02-20	72	38	55.0	4.9	10	0	0.00	0.0	0
2007-02-21	73	38	55.5	5.2	9	0	M	5.0	0
2007-02-22	48	36	42.0	-8.4	23	0	0.50	3.2	0
2007-02-23	50	36	43.0	-7.5	22	0	0.92	0.0	0
2007-02-24	M	M	M	M	M	M	M	0.0	0
2007-02-25	51	27	39.0	-11.8	26	0	1.03	T	0
2007-02-26	45	33	39.0	-11.9	26	0	0.39	0.0	0
2007-02-27	48	32	40.0	-11.1	25	0	0.64	0.0	0
2007-02-28	M	M	M	M	M	M	M	0.0	0
Sum	1045	832	-	-	292	0	6.44	8.2	-
Average	58.1	39.6	48.6	-0.8	-	-	-	-	0.0
Normal	58.4	40.3	49.4	-	438	0	6.28	0.2	-

Figure 8. NWS Forecast Office Report for Auburn, CA, February 2007.
Source: NWS Sacramento CA (2007)

Climatological Data for TAHOE CITY, CA - February 2007

Click column heading to sort ascending, click again to sort descending.

Date	Temperature				HDD	CDD	Precipitation	New Snow	Snow Depth
	Maximum	Minimum	Average	Departure					
2007-02-01	40	17	28.5	-1.0	36	0	0.00	0.0	T
2007-02-02	41	16	28.5	-1.1	36	0	0.00	0.0	T
2007-02-03	40	20	30.0	0.4	35	0	0.00	0.0	T
2007-02-04	43	M	M	M	M	M	0.00	0.0	T
2007-02-05	53	27	40.0	10.3	25	0	0.00	0.0	0
2007-02-06	44	M	M	M	M	M	0.00	0.0	0
2007-02-07	55	29	42.0	12.2	23	0	0.00	0.0	0
2007-02-08	43	33	38.0	8.2	27	0	0.18	T	T
2007-02-09	44	32	38.0	8.1	27	0	0.71	0.5	1
2007-02-10	39	33	36.0	6.0	29	0	0.79	0.0	0
2007-02-11	42	31	36.5	6.5	28	0	1.50	4.0	4
2007-02-12	38	28	33.0	2.9	32	0	0.03	T	3
2007-02-13	40	19	29.5	-0.7	35	0	0.09	T	3
2007-02-14	38	18	28.0	-2.3	37	0	0.00	0.0	2
2007-02-15	40	23	31.5	1.1	33	0	0.00	0.0	2
2007-02-16	49	27	38.0	7.5	27	0	0.00	0.0	1
2007-02-17	48	31	39.5	8.9	25	0	0.05	0.0	1
2007-02-18	52	30	41.0	10.3	24	0	0.00	0.0	0
2007-02-19	48	22	35.0	4.2	30	0	T	0.0	0
2007-02-20	38	21	29.5	-1.4	35	0	0.00	0.0	0
2007-02-21	46	33	39.5	8.4	25	0	0.00	0.0	0
2007-02-22	44	29	36.5	5.3	28	0	0.11	2.0	2
2007-02-23	M	17	M	M	M	M	0.65	10.0	12
2007-02-24	35	11	23.0	-8.5	42	0	T	T	9
2007-02-25	37	25	31.0	-0.6	34	0	0.71	15.0	20
2007-02-26	29	23	26.0	-5.8	39	0	0.81	12.0	28
2007-02-27	29	16	22.5	-9.4	42	0	1.72	20.0	42
2007-02-28	29	16	22.5	-9.5	42	0	0.13	2.0	37
Sum	1124	627	-	-	796	0	7.48	65.5	-
Average	41.6	24.1	32.9	2.4	-	-	-	-	6.0
Normal	40.7	20.3	30.5	-	966	0	5.69	40.7	-

Figure 9. NWS Forecast Office Report for Tahoe City, CA, February 2007. Source: NWS Reno NV (2007).

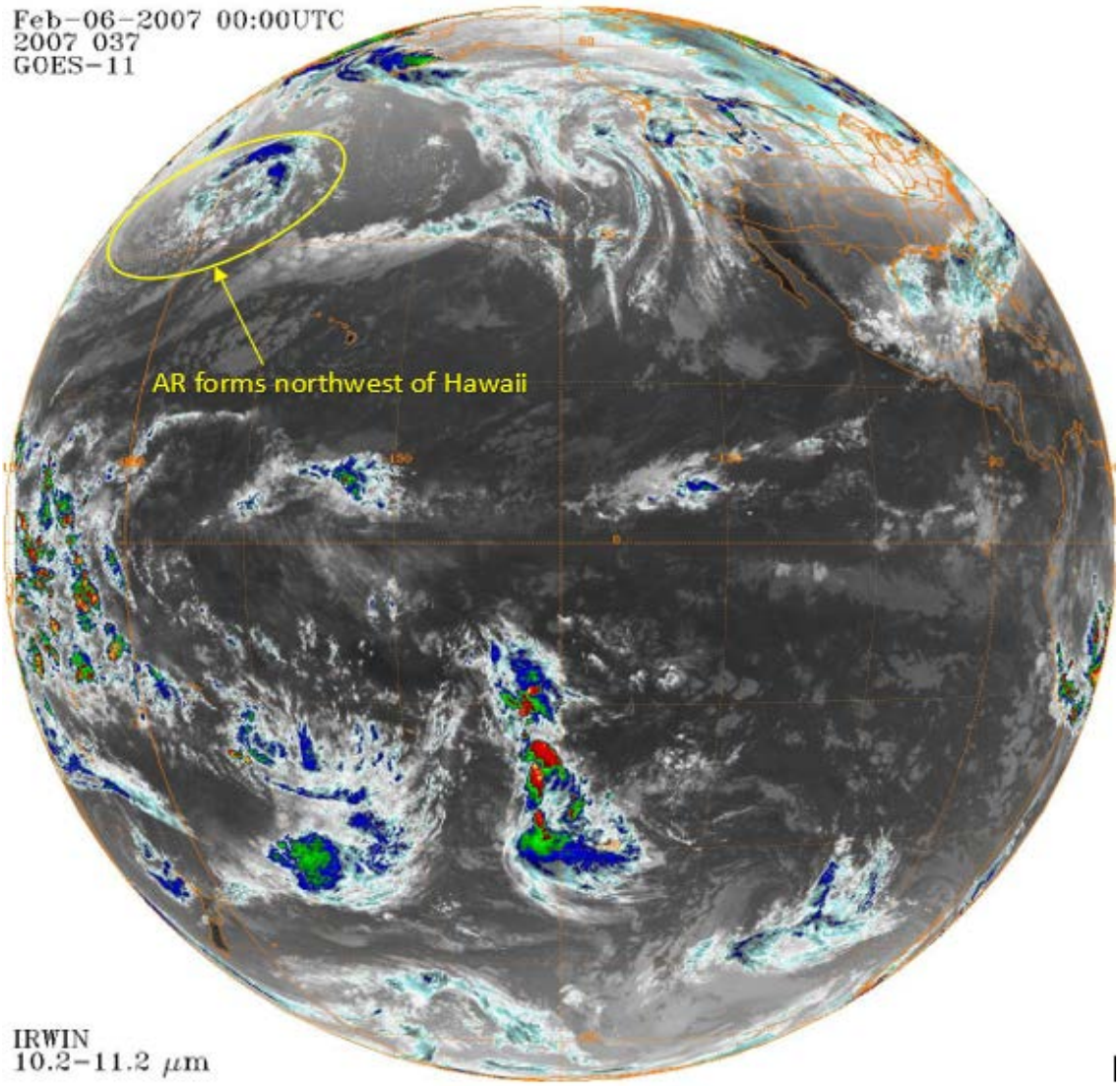

Above: GOES-11 (West) 0000 UTC 06 February 2007.

Figure 10. Case 2 GOES IR Imagery. Source: Knapp (2008).

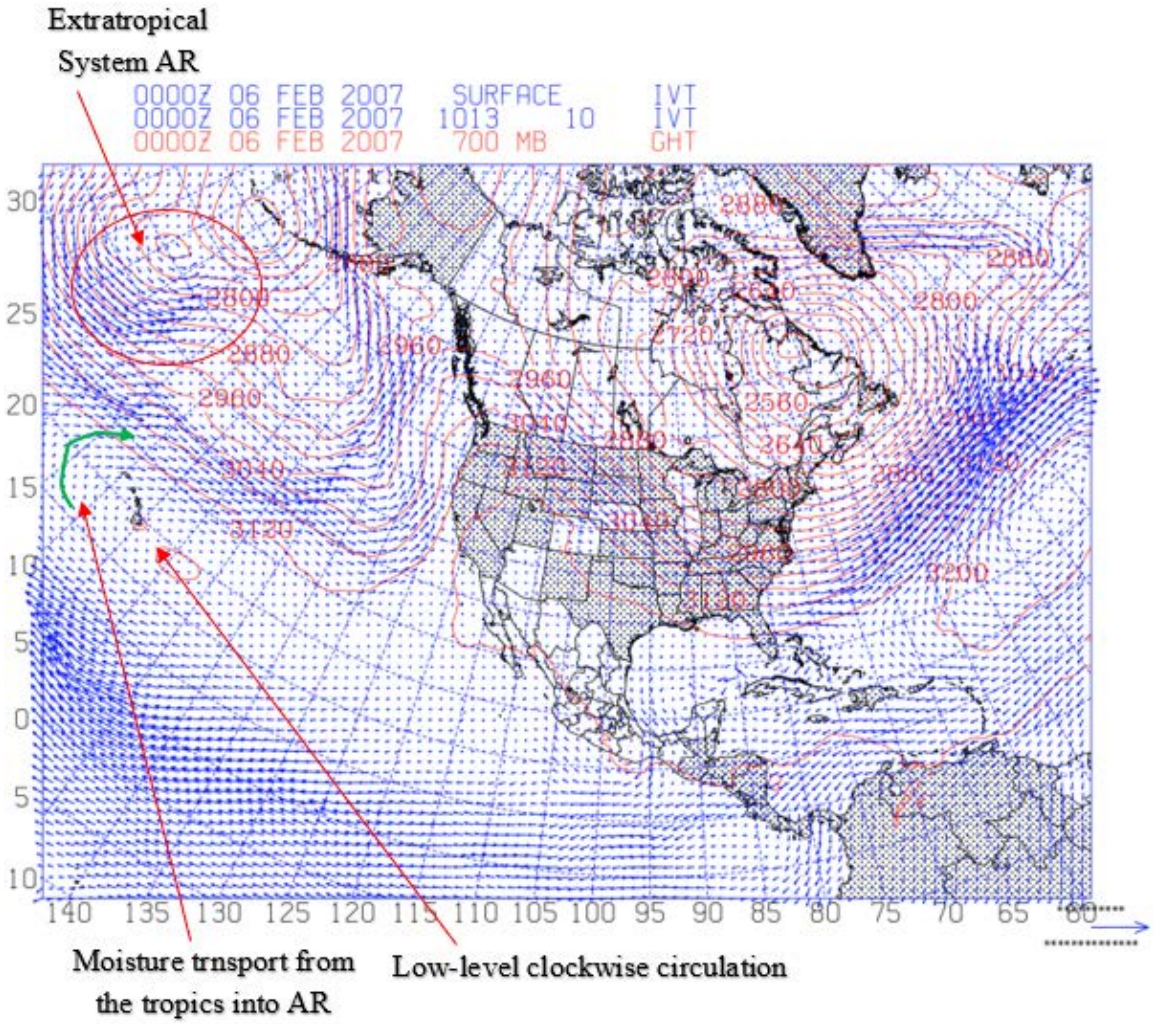

IVT plot for 0000 UTC 06 February 2007. Red lines 700 mb GHT and blue vectors are the IVT

Figure 11. Case 2 IVT and 700 mb GHT Plot.

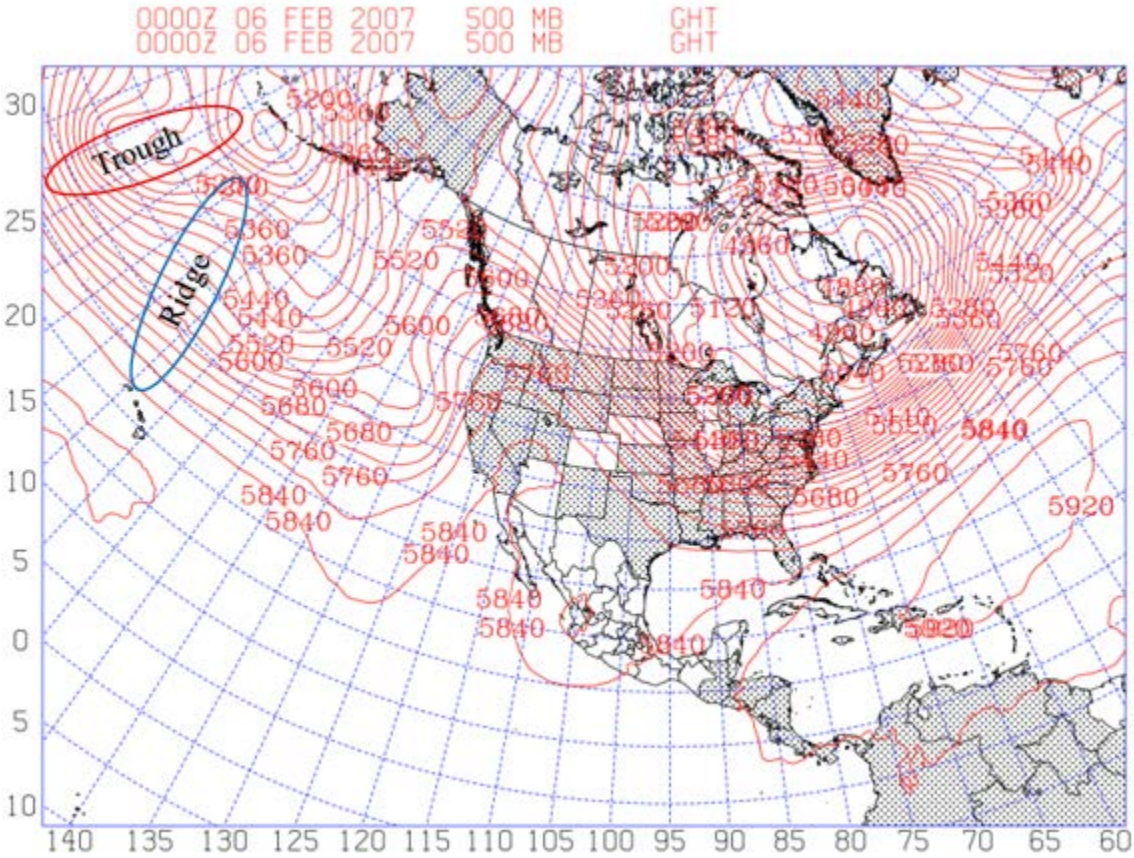

500 mb GHT plot for 0000 UTC 06 February 2007. 500 mb GHT are represented by the red lines in meters

Figure 12. Case 2 500 mb GHT Plot.

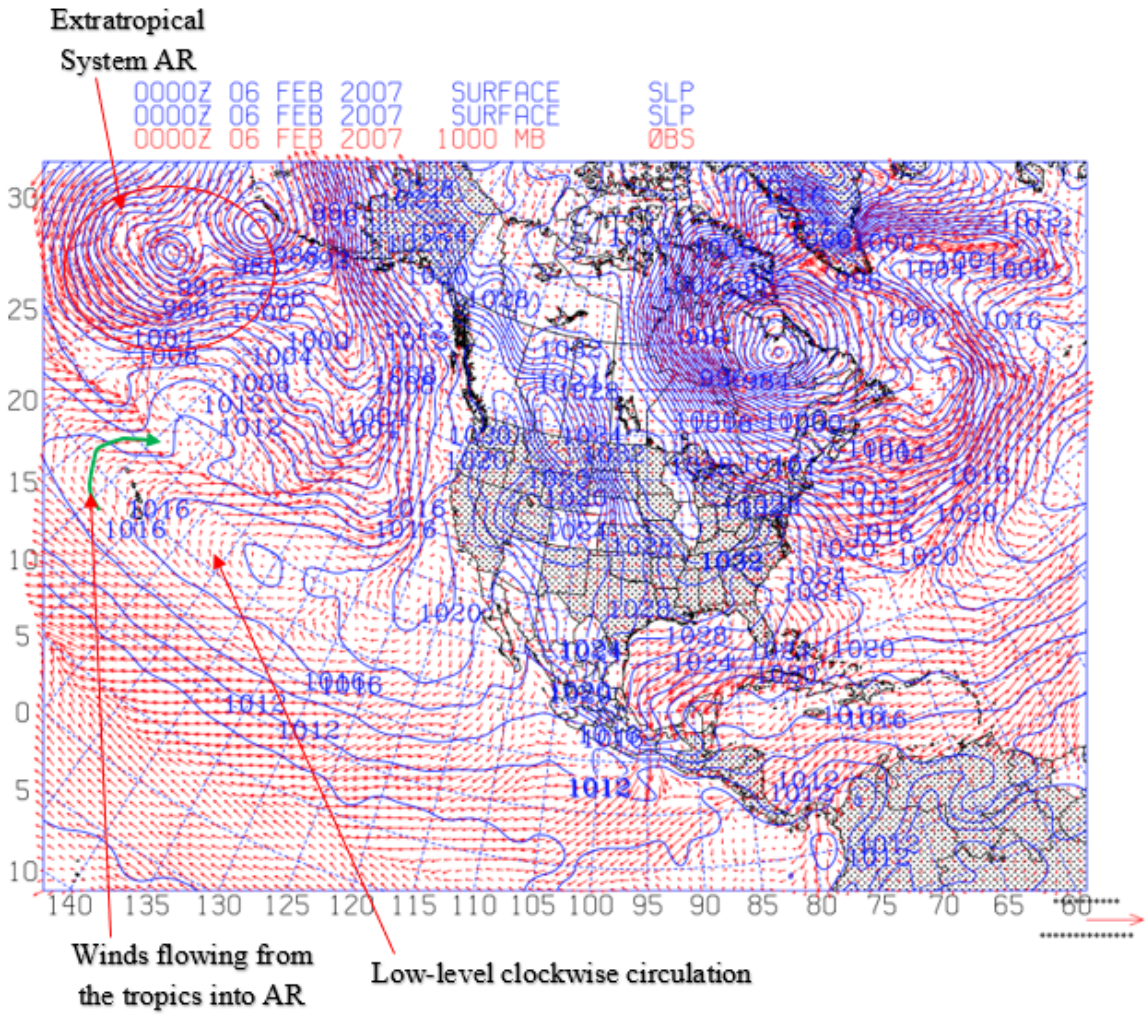

SLP and 1000 mb winds plot for 0000 UTC 06 February 2007. SLP are represented by the blue lines in mb and the red arrows represent wind vectors.

Figure 13. Case 2 SLP and 1000 mb Winds Plot.

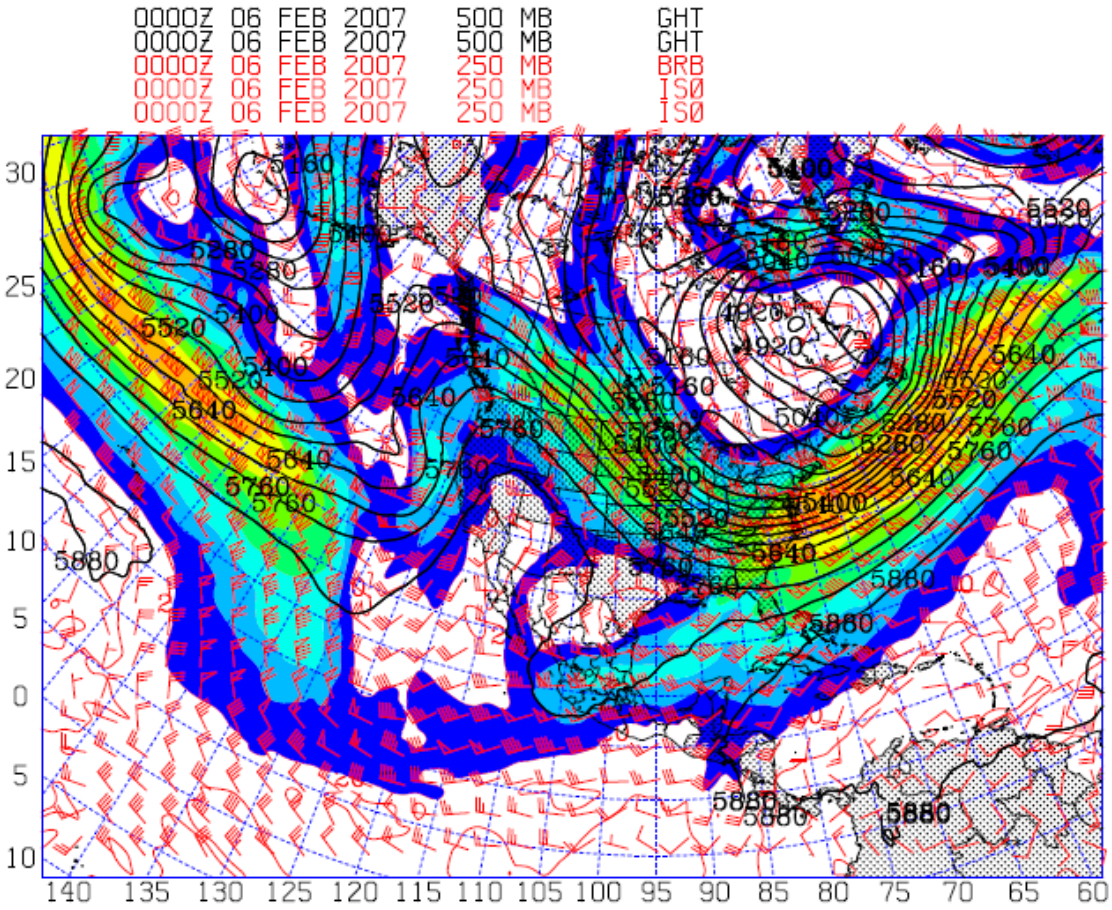

The 500 mb Geopotential Height contours are shown in black, the 250 mb jet stream is shown with the color fill, and the 250 mb wind is shown with red barbs, 1200 UTC 06 February 2007.

Figure 14. Case 2 Upper Air Chart

C. CASE 3

Case 3 took place from 08 February 2019 – 14 February 2019, although data for VISUAL was only available through 1800z 13 February 2019. Daily rainfall totals for Tahoe City (Figure 15) and Blue Canyon (Figure 16) and show maximum rainfall on February 13 and 14, respectively. The amount of precipitation exceeded 3 inches per day for both locations. Heavy rain and snow fell throughout the state, and floods were observed. Tahoe City CA and Blue Canyon CA observed rain/snow mix during this event (Figures 15 and 16) indicating that this was a colder system than was found in the previous cases.

The synoptic structure for this event is much different from Cases 1 and 2 as the system formed much further south just north of Hawaii. Figure 17 shows infrared (IR) satellite imagery of an extratropical cyclone developing on Feb. 8, 2019 northeast of Hawaii unlike Cases 1 and 2. A large plume of clouds extends southwestward to the south of Hawaii suggesting the initial development of the AR in this case.

The IVT and 700 mb geopotential heights (Figure 18) confirm the pattern seen in the satellite image. A 700 mb low and cyclonic IVT circulation is located north of Hawaii around 25 N 155 W with relatively strong vapor transport to the south and east of this feature. As in the other cases, the IVT displays a clockwise circulation southeast of Hawaii and water vapor transport curving up into the extratropical cyclone along 150 W. However, water vapor transport ahead of the extratropical cyclone does not extend very far east at this time. This is due to an upper-level long-wave ridge over the Eastern Pacific.

The upper-level long-wave ridge is clearly seen in Figure 19, which shows a ridge at the 500 mb level sandwiched by two troughs. This ridge is very high amplitude and extends from Alaska to the east of Hawaii. In the two previous cases, the upper level ridges were much lower amplitude with the ridge crest 1000s of kilometers south of Alaska. The two troughs occur up and downstream from the high amplitude ridge. The upstream trough is associated with the developing cyclone north of Hawaii that initiates the AR. The downstream trough is along the west coast of the United States with a weak cyclonic system evident in the satellite image (Figure 17) just off the coast.

Figure 20 shows winds at 1000 mb and sea-level pressure. The low-pressure system and cyclonic circulation seen in the satellite imagery are clearly evident at the surface. High pressure occurs to the east near 30 N 130 W that is producing a broad region of easterly to southeasterly flow toward the low north of Hawaii. This broad region of easterly flow however had little impact on the integrated vapor transport, which is very weak over this region in Figure 20. Of more significance is the low-level surface ridge axis that extends out of the main high-pressure center to just east of Hawaii. Air flow around this surface ridging is southerly into the extratropical cyclone along 150 W and easterly flow on its southern flank along 15 N. This low-level anticyclonic circulation is consistent with the water vapor transport in this area seen in Figure 18.

Figure 21 shows the 250 mb polar jet stream. A jet wind maxima is found to correlate with the cloud plume found southeast of Hawaii in the IR image Figure 15. However, the jet windspeed maxima is too low to support the extensive cloud plume found in the IR image Figure 17.

Climatological Data for TAHOE CITY, CA - February 2019

Click column heading to sort ascending, click again to sort descending.

Date	Temperature				HDD	CDD	Precipitation	New Snow	Snow Depth
	Maximum	Minimum	Average	Departure					
2019-02-01	50	30	40.0	10.5	25	0	0.00	0.0	13
2019-02-02	45	33	39.0	9.4	26	0	0.88	0.0	12
2019-02-03	39	27	33.0	3.4	32	0	0.85	8.5	22
2019-02-04	35	25	30.0	0.4	35	0	1.45	13.5	32
2019-02-05	29	14	21.5	-8.2	43	0	1.71	23.0	51
2019-02-06	25	15	20.0	-9.7	45	0	0.11	1.0	44
2019-02-07	27	7	17.0	-12.8	48	0	T	T	41
2019-02-08	32	9	20.5	-9.3	44	0	0.00	0.0	38
2019-02-09	30	22	26.0	-3.9	39	0	0.17	2.0	38
2019-02-10	28	15	21.5	-8.5	43	0	2.34	27.0	58
2019-02-11	25	1	13.0	-17.0	52	0	0.17	0.0	52
2019-02-12	34	8	21.0	-9.1	44	0	0.00	0.0	51
2019-02-13	38	23	30.5	0.3	34	0	0.77	1.0	45
2019-02-14	43	33	38.0	7.7	27	0	3.21	T	41
2019-02-15	40	19	29.5	-0.9	35	0	1.65	22.0	57
2019-02-16	41	20	30.5	0.0	34	0	0.85	11.0	65
2019-02-17	30	15	22.5	-8.1	42	0	0.59	8.5	67
2019-02-18	27	3	15.0	-15.7	50	0	0.33	3.5	63
2019-02-19	25	2	13.5	-17.3	51	0	0.00	0.0	58
2019-02-20	31	8	19.5	-11.4	45	0	0.02	0.5	57
2019-02-21	29	6	17.5	-13.6	47	0	0.05	1.0	56
2019-02-22	25	4	14.5	-16.7	50	0	T	T	55
2019-02-23	31	7	19.0	-12.3	46	0	0.00	0.0	54
2019-02-24	37	22	29.5	-2.0	35	0	0.02	0.5	53
2019-02-25	40	28	34.0	2.4	31	0	T	T	51
2019-02-26	40	29	34.5	2.7	30	0	1.05	13.0	64
2019-02-27	36	30	33.0	1.1	32	0	0.85	6.0	64
2019-02-28	40	31	35.5	3.5	29	0	0.29	0.5	56
Sum	952	486	-	-	1094	0	17.36	142.5	-
Average	34.0	17.4	25.7	-4.8	-	-	-	-	48.5
Normal	40.7	20.3	30.5	-	966	0	5.69	40.7	-

Figure 15. NWS Forecast Office Report for Tahoe City, CA, February 2019. Source: NWS Reno, NV (2019)

Climatological Data for BLUE CANYON AP, CA - February 2019

Click column heading to sort ascending, click again to sort descending.

Date	Temperature				HDD	CDD	Precipitation
	Maximum	Minimum	Average	Departure			
2019-02-01	44	37	40.5	1.3	24	0	0.30
2019-02-02	41	31	36.0	-3.2	29	0	2.31
2019-02-03	35	29	32.0	-7.1	33	0	1.90
2019-02-04	30	19	24.5	-14.6	40	0	1.31
2019-02-05	24	18	21.0	-18.1	44	0	0.39
2019-02-06	25	20	22.5	-16.5	42	0	T
2019-02-07	28	20	24.0	-15.0	41	0	0.00
2019-02-08	30	22	26.0	-13.0	39	0	0.10
2019-02-09	29	24	26.5	-12.5	38	0	1.11
2019-02-10	24	18	21.0	-18.0	44	0	0.20
2019-02-11	29	17	23.0	-16.0	42	0	0.00
2019-02-12	40	25	32.5	-6.5	32	0	0.06
2019-02-13	43	30	36.5	-2.5	28	0	3.81
2019-02-14	44	27	35.5	-3.6	29	0	2.18
2019-02-15	28	23	25.5	-13.6	39	0	1.16
2019-02-16	27	23	25.0	-14.2	40	0	0.92
2019-02-17	26	21	23.5	-15.7	41	0	0.38
2019-02-18	31	18	24.5	-14.8	40	0	0.00
2019-02-19	36	17	26.5	-12.8	38	0	T
2019-02-20	29	21	25.0	-14.4	40	0	0.29
2019-02-21	29	20	24.5	-15.0	40	0	0.00
2019-02-22	37	18	27.5	-12.0	37	0	T
2019-02-23	35	25	30.0	-9.6	35	0	0.01
2019-02-24	35	29	32.0	-7.7	33	0	0.01
2019-02-25	36	30	33.0	-6.8	32	0	1.42
2019-02-26	33	31	32.0	-7.9	33	0	1.61
2019-02-27	38	31	34.5	-5.5	30	0	2.37
2019-02-28	35	30	32.5	-7.6	32	0	0.53
Sum	921	674	-	-	1015	0	22.37
Average	32.9	24.1	28.5	-10.8	-	-	-
Normal	44.4	34.2	39.3	-	719	0	10.56

Figure 16. NWS Forecast Office Report for Blue Canyon, CA, February 2019. Source: NWS Reno, NV (2019)

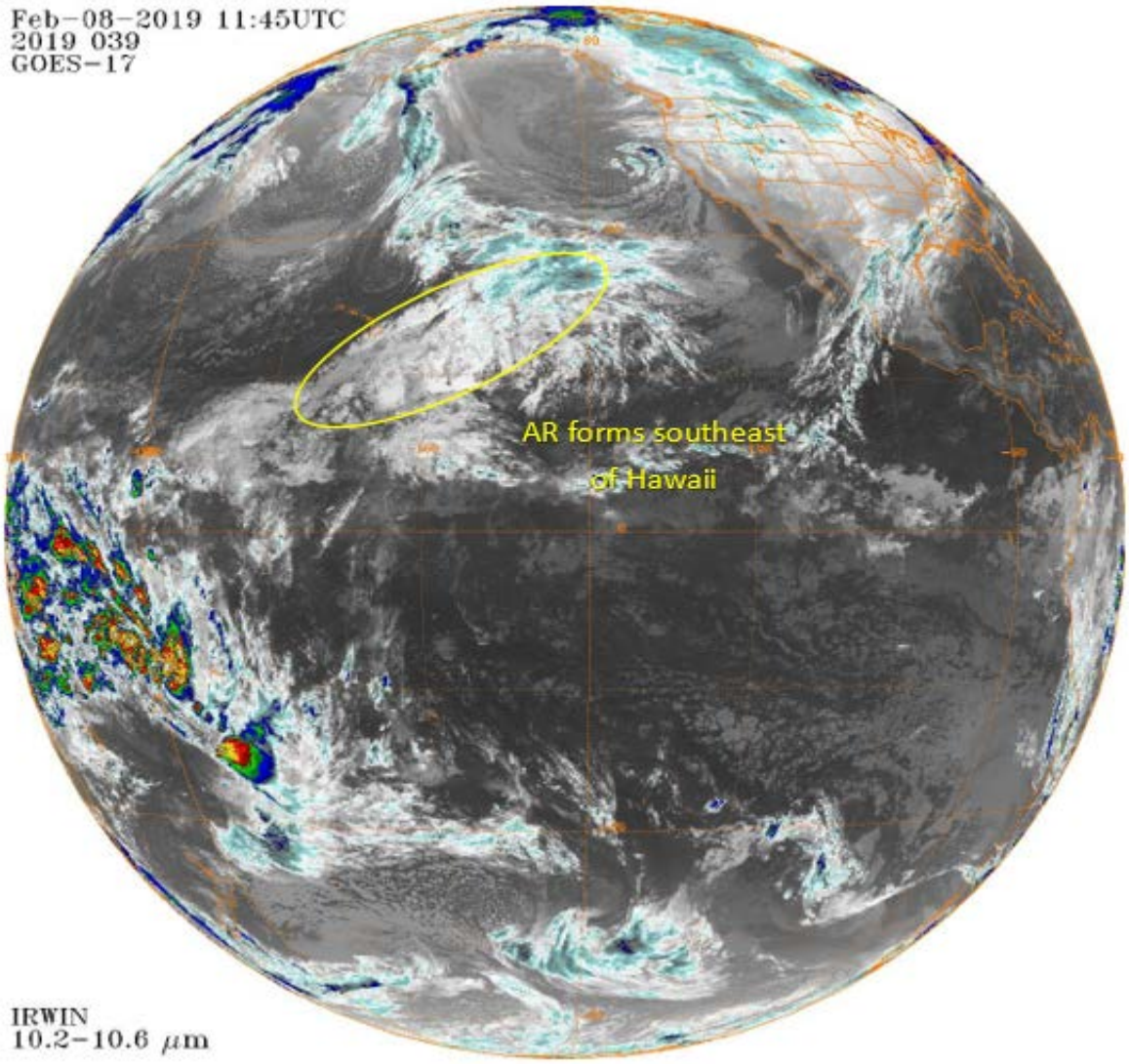

Above: GOES-17 (West) 1145 UTC 08 February 2019.

Figure 17. Case 3 GOES IR Imagery. Source: Knapp (2008)

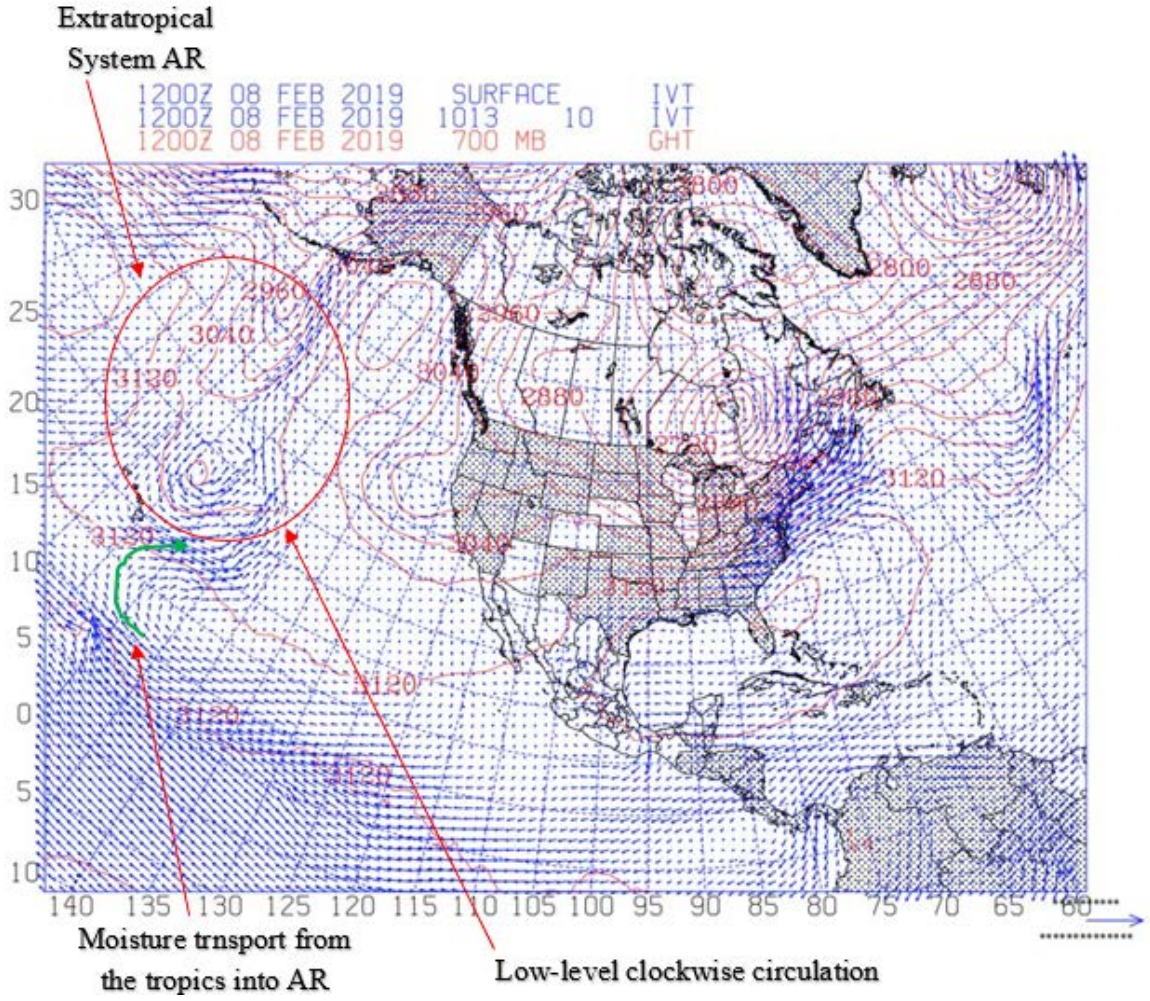

IVT plot for 1200 UTC 08 February 2019. Red lines 700 mb GHT and blue arrows are the IVT

Figure 18. Case 3 IVT and 700 mb GHT Plot.

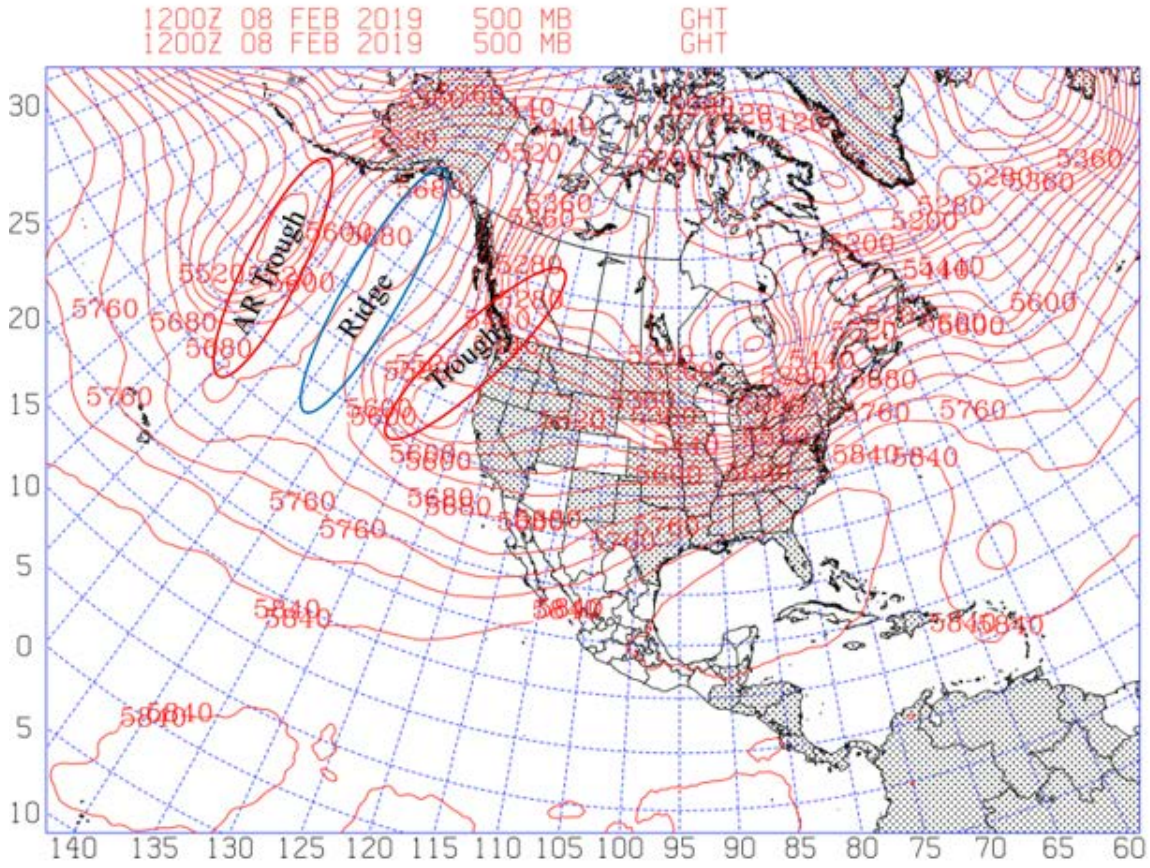

500 mb GHT plot for 1200 UTC 08 February 2019. 500 mb GHT are represented by the red lines in meters

Figure 19. Case 3 500 mb GHT Plot

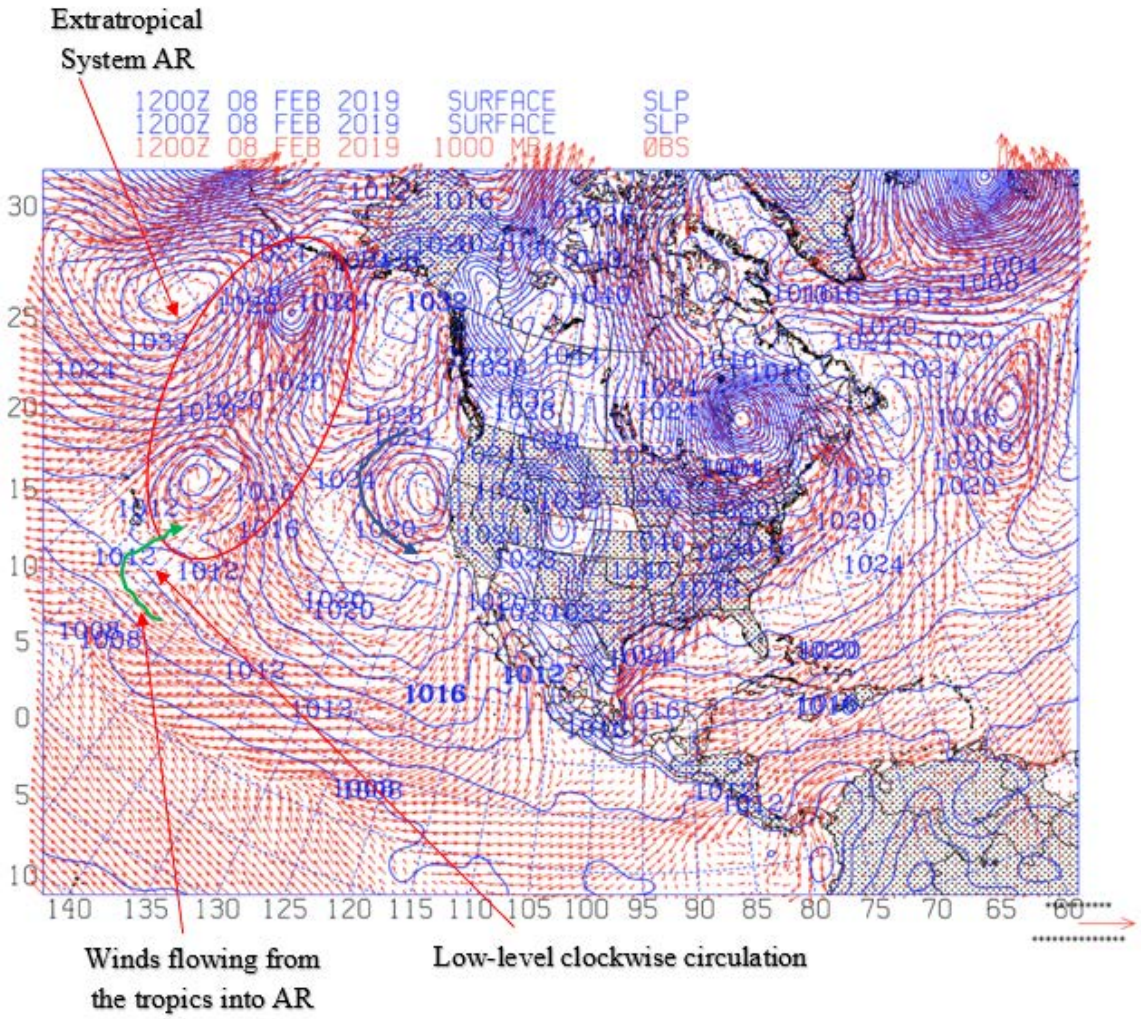

SLP and 1000 mb winds plot for 1200 UTC 08 February 2019. SLP are represented by the blue lines in mb and the red arrows represent wind vectors.

Figure 20. Case 3 SLP and 1000 mb Winds Plot.

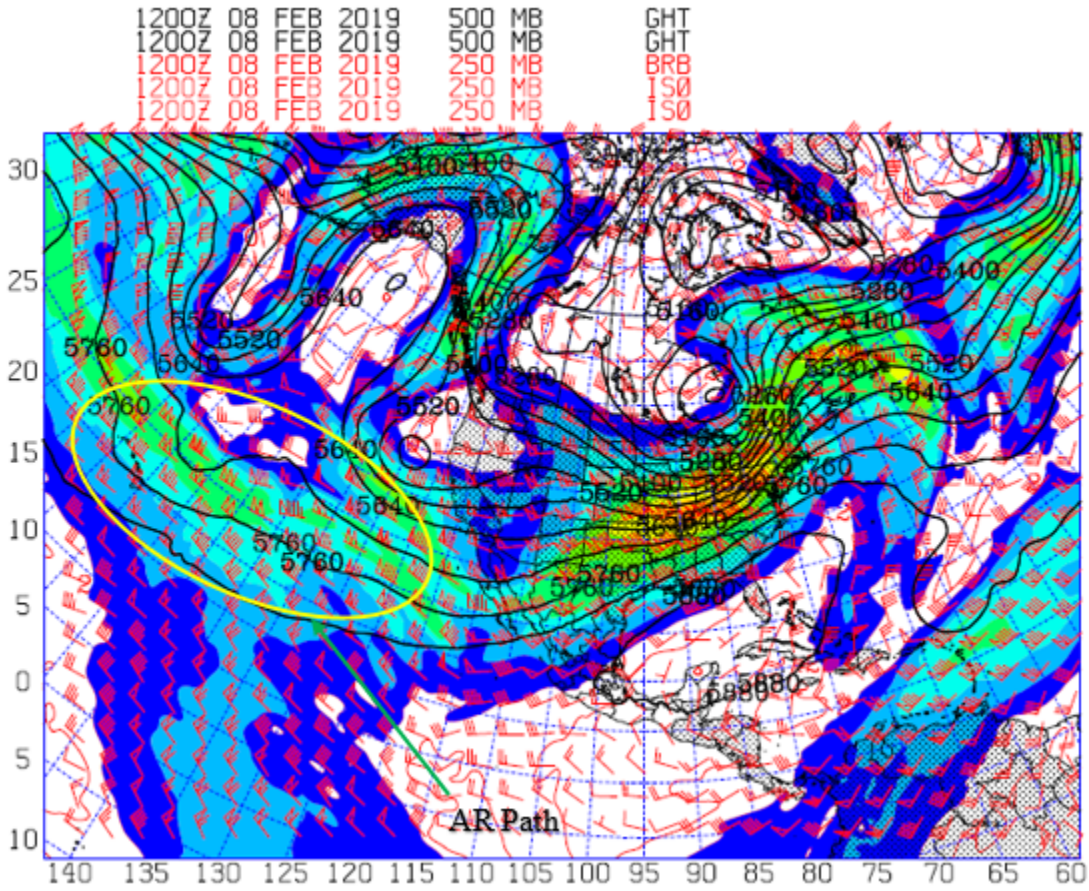

The 500 mb Geopotential Height contours are shown in black, the 250 mb jet stream is shown with the color fill, and the 250 mb wind is shown with red barbs, 1200 UTC 08 February 2019.

Figure 21. Case 3 Upper Air Chart.

D. CASE 4

Case four took place from 27 November 2019 – 02 December 2019. As we will see, the synoptic structure for this event was more similar to Case 3 than Cases 1 and 2. Daily rainfall totals for Tahoe City (Figure 22) and Big Sur (Figure 23) show maximum precipitation occurred on December 2, exceeding 6 inches along the coast at Big Sur with lower values of 2.7 inches in the Sierra's at Tahoe City. As in Case 3, this system was colder compared to Cases 1 and 2, producing snow at Tahoe City (Figure 22). Most of the precipitation occurred in central California along the coast as seen by the nearly 7 inches at Big Sur (Figure 23).

Infrared (IR) satellite imagery (Figure 24) shows a broad low-pressure system to the northwest of Hawaii similar to the other cases. The main cloud plume is almost in a north south orientation indicating a very high amplitude trough and ridge system similar to Case 3. The main difference with Case 3 is that the trough associated with the AR is further west with the base of the trough in position to the northwest of Hawaii similar to Cases 1 and 2.

The high amplitude long wave trough/ridge is evident in Figure 25 showing the IVT and 700 mb geopotential height. The water vapor transport occurs in a narrow plume along 160 W just east of an elongated 700 mb trough. No closed cyclonic circulation is seen in Figure 25, but cyclonic turning does occur near the base of the trough to feed the AR. As will be seen in the results, this north-south AR will evolve into a more east-west orientation when it reaches the U.S. west coast. The IVT (Figure 25) displays a large clockwise circulation northeast of Hawaii centered near 35 N 130 W, which is 100s of kilometers further northeast compared to the three previous cases. However, on the southwest side of this circulation near Hawaii, water vapor is clearly being transported from the east into the north-south vapor plume. This water vapor transport is strong into the broad trough, but as in Case 3, there is no eastward water vapor transport ahead of the trough at this time.

The primary long wave pattern seen at 700 mb and the satellite imagery is confirmed by the 500 mb geopotential height analysis (Figure 26). An elongated trough to

the northwest of Hawaii, a highly amplified ridge to the northeast, and a trough just off the coast of North America are seen in Figure 26. This high amplitude structure with the ridge extending north into Alaska is very similar to Case 3, except the wave is shifted about 10 degrees to the west. One difference between this case and the previous case is that the 500 mb ridge is not as sharp in this case, which may help it to flatten allowing the north-south AR to become more east-west.

Figure 27 is sea-level pressure and 1000 mb winds and confirms the presence of both the elongated low-pressure system northwest of Hawaii as well as a low-level high-pressure system to the northeast. The elongated low-pressure system consists of multiple weak low-pressure centers that produce a region strong south winds on its east side where the large integrated water vapor transport occurs in the north-south AR. Air flow around the high-pressure system that also extends in a north-south direction along 145 W produces east winds that turn to the north into the elongated extratropical cyclone on its southwestern flank near Hawaii. However, a second separate low-level clockwise circulation (high-pressure system) will later contribute to water vapor transport as the AR reaches the west Coast, which will be analyzed in the results.

Figure 28 shows the 250 mb polar jet stream, which correlates to the cloud plume found in the IR images. The jet maxima windspeeds found in the 250 mb flow support cloud development in the AR by providing strong downstream (northward in this case) transport of water vapor.

Climatological Data for TAHOE CITY, CA - December 2019

Click column heading to sort ascending, click again to sort descending.

Date	Temperature				HDD	CDD	Precipitation	New Snow	Snow Depth
	Maximum	Minimum	Average	Departure					
2019-12-01	38	14	26.0	-5.7	39	0	0.88	1.0	11
2019-12-02	39	31	35.0	3.5	30	0	2.72	3.0	12
2019-12-03	36	30	33.0	1.7	32	0	0.35	0.0	11
2019-12-04	45	29	37.0	5.9	28	0	0.01	0.0	10
2019-12-05	36	28	32.0	1.1	33	0	0.15	0.0	9
2019-12-06	42	25	33.5	2.7	31	0	0.00	0.0	M
2019-12-07	48	28	38.0	7.4	27	0	0.69	M	M
2019-12-08	41	31	36.0	5.6	29	0	1.16	2.0	10
2019-12-09	40	23	31.5	1.2	33	0	0.05	1.0	9
2019-12-10	40	23	31.5	1.3	33	0	0.00	0.0	8
2019-12-11	41	29	35.0	5.0	30	0	T	0.0	7
2019-12-12	43	32	37.5	7.6	27	0	0.40	0.0	7
2019-12-13	45	32	38.5	8.7	26	0	0.11	0.0	5
2019-12-14	38	27	32.5	2.8	32	0	0.91	T	5
2019-12-15	36	13	24.5	-5.1	40	0	0.21	4.0	9
2019-12-16	33	11	22.0	-7.6	43	0	0.00	0.0	8
2019-12-17	37	13	25.0	-4.5	40	0	0.00	0.0	7
2019-12-18	37	12	24.5	-4.9	40	0	0.00	0.0	7
2019-12-19	38	27	32.5	3.1	32	0	0.00	0.0	6
2019-12-20	44	24	34.0	4.7	31	0	0.00	0.0	5
2019-12-21	50	25	37.5	8.2	27	0	0.00	0.0	4
2019-12-22	50	40	45.0	15.7	20	0	0.00	0.0	3
2019-12-23	46	27	36.5	7.2	28	0	0.55	6.0	9
2019-12-24	34	12	23.0	-6.2	42	0	0.17	2.5	11
2019-12-25	33	15	24.0	-5.2	41	0	T	0.0	11
2019-12-26	33	20	26.5	-2.7	38	0	0.00	0.0	10
2019-12-27	33	12	22.5	-6.7	42	0	0.00	0.0	10
2019-12-28	35	14	24.5	-4.7	40	0	0.00	0.0	10
2019-12-29	40	17	28.5	-0.7	36	0	0.00	0.0	9
2019-12-30	40	27	33.5	4.3	31	0	0.03	T	8
2019-12-31	39	26	32.5	3.3	32	0	0.00	0.0	8
Sum	1230	717	-	-	1033	0	8.39	19.5	-
Average	39.7	23.1	31.4	1.5	-	-	-	-	8.2
Normal	39.6	20.2	29.9	-	1088	0	5.97	38.2	-

Figure 22. NWS Forecast Office Report for Tahoe City, CA, November 2019. Source: NWS Reno, NV (2019).

Climatological Data for BIG SUR STATION, CA - December 2019

Click column heading to sort ascending, click again to sort descending.

Date	Temperature				HDD	CDD	Precipitation
	Maximum	Minimum	Average	Departure			
2019-12-01	55	M	M	M	M	M	2.10
2019-12-02	57	52	54.5	2.9	10	0	6.80
2019-12-03	63	49	56.0	4.5	9	0	0.06
2019-12-04	59	53	56.0	4.6	9	0	1.71
2019-12-05	59	50	54.5	3.2	10	0	0.08
2019-12-06	62	54	58.0	6.8	7	0	0.06
2019-12-07	59	56	57.5	6.4	7	0	0.67
2019-12-08	57	55	56.0	4.9	9	0	1.20
2019-12-09	59	44	51.5	0.5	13	0	0.00
2019-12-10	59	44	51.5	0.6	13	0	0.00
2019-12-11	62	49	55.5	4.6	9	0	0.00
2019-12-12	67	54	60.5	9.7	4	0	0.00
2019-12-13	67	52	59.5	8.7	5	0	0.00
2019-12-14	63	48	55.5	4.8	9	0	0.00
2019-12-15	56	42	49.0	-1.7	16	0	0.18
2019-12-16	56	39	47.5	-3.2	17	0	0.00
2019-12-17	60	42	51.0	0.3	14	0	0.00
2019-12-18	56	48	52.0	1.4	13	0	1.26
2019-12-19	58	43	50.5	-0.1	14	0	0.23
2019-12-20	63	47	55.0	4.4	10	0	0.00
2019-12-21	58	49	53.5	2.9	11	0	0.00
2019-12-22	58	52	55.0	4.4	10	0	1.08
2019-12-23	57	43	50.0	-0.7	15	0	0.02
2019-12-24	54	38	46.0	-4.7	19	0	0.00
2019-12-25	51	42	46.5	-4.2	18	0	0.85
2019-12-26	55	42	48.5	-2.2	16	0	0.95
2019-12-27	56	33	44.5	-6.2	20	0	0.00
2019-12-28	58	37	47.5	-3.2	17	0	0.00
2019-12-29	M	M	M	M	M	M	S
2019-12-30	59	39	49.0	-1.8	16	0	0.62A
2019-12-31	60	40	50.0	-0.8	15	0	0.00
Sum	1763	1336	-	-	355	0	17.87
Average	58.8	46.1	52.5	1.6	-	-	-
Normal	59.9	41.9	50.9	-	437	0	8.63

Figure 23. NWS Forecast Office Report for Big Sur, CA, November 2019. Source: NWS Monterey, CA (2019)

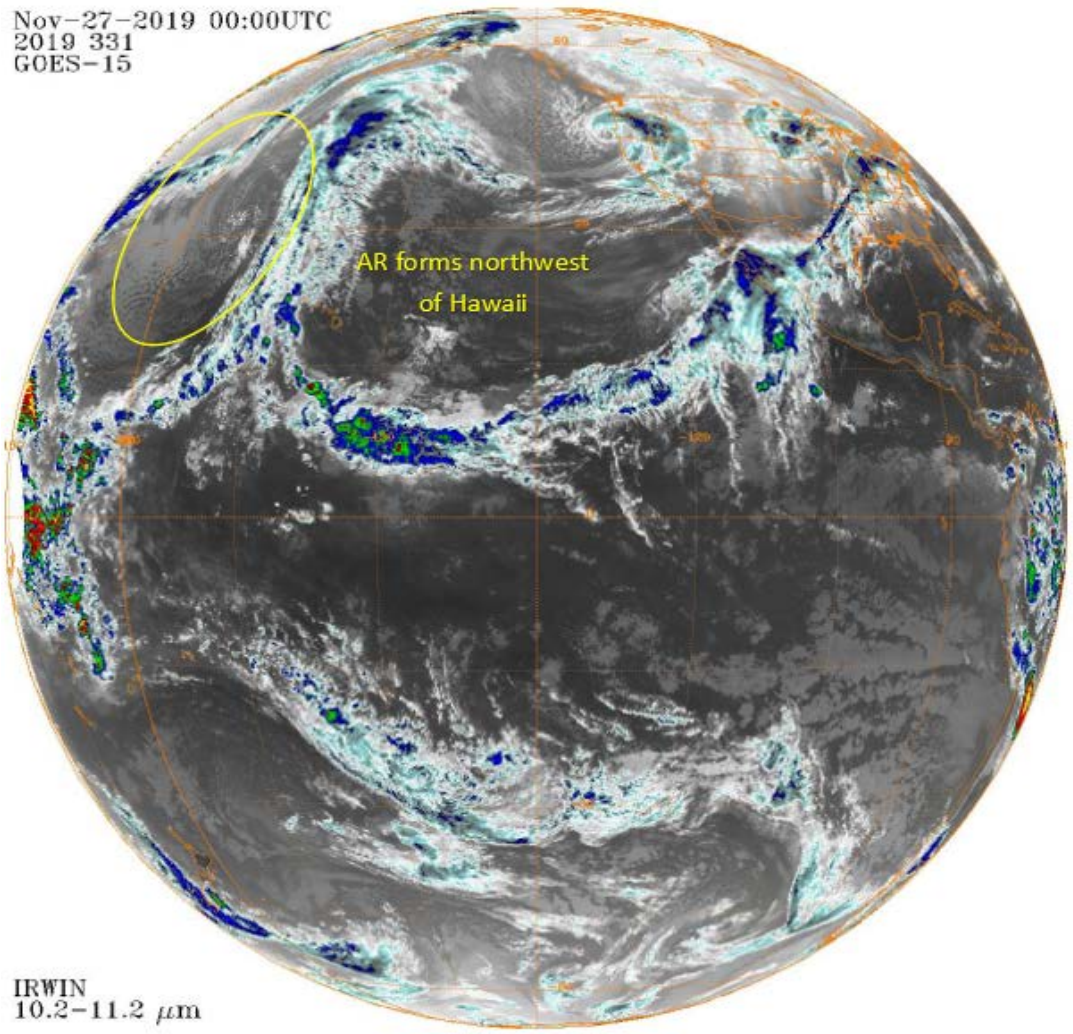

Above: GOES-15 (West) 0000 UTC 27 November 2019.

Figure 24. Case 4 GOES IR Imagery. Source: Knapp (2008)

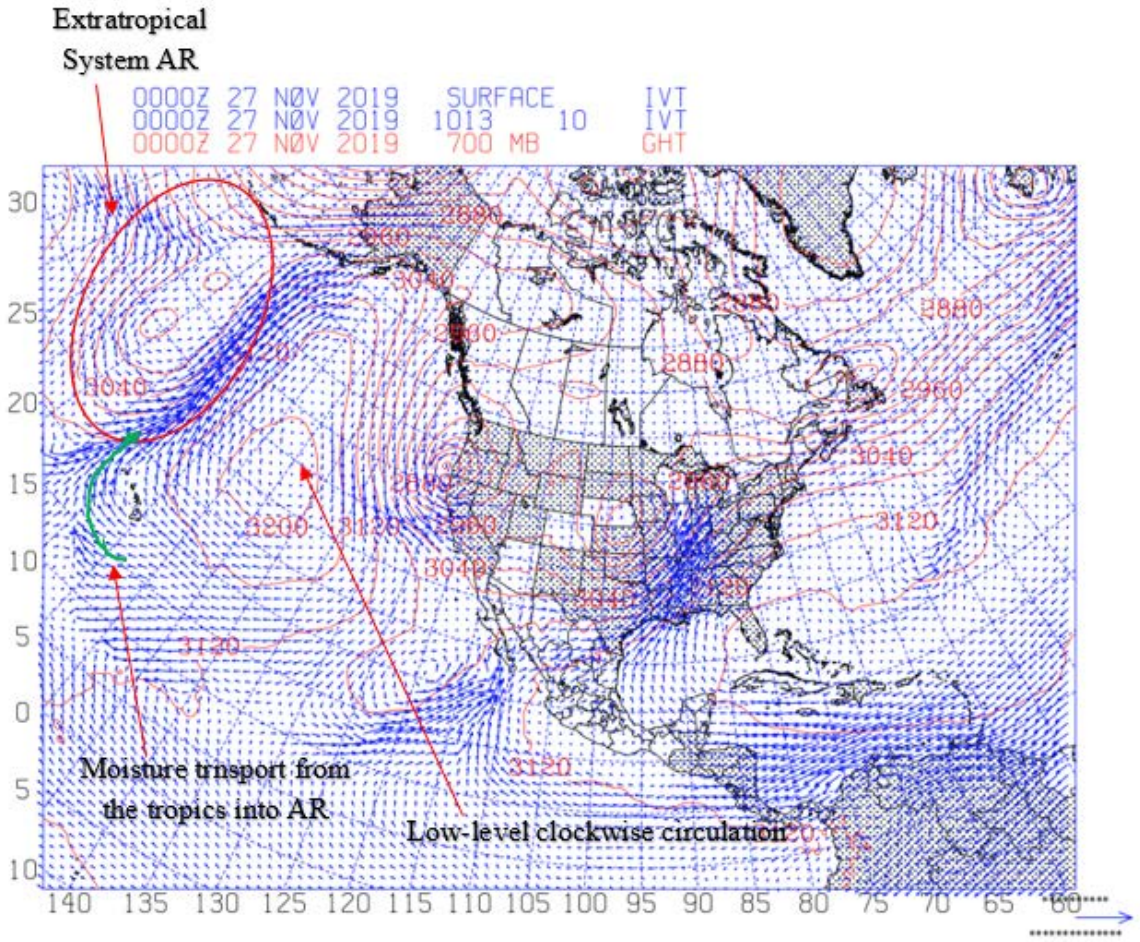

IVT plot for 0000 UTC 27 November 2019. Red lines 700 mb GHT and blue arrows are the IVT

Figure 25. Case 4 IVT and 700 mb GHT Plot.

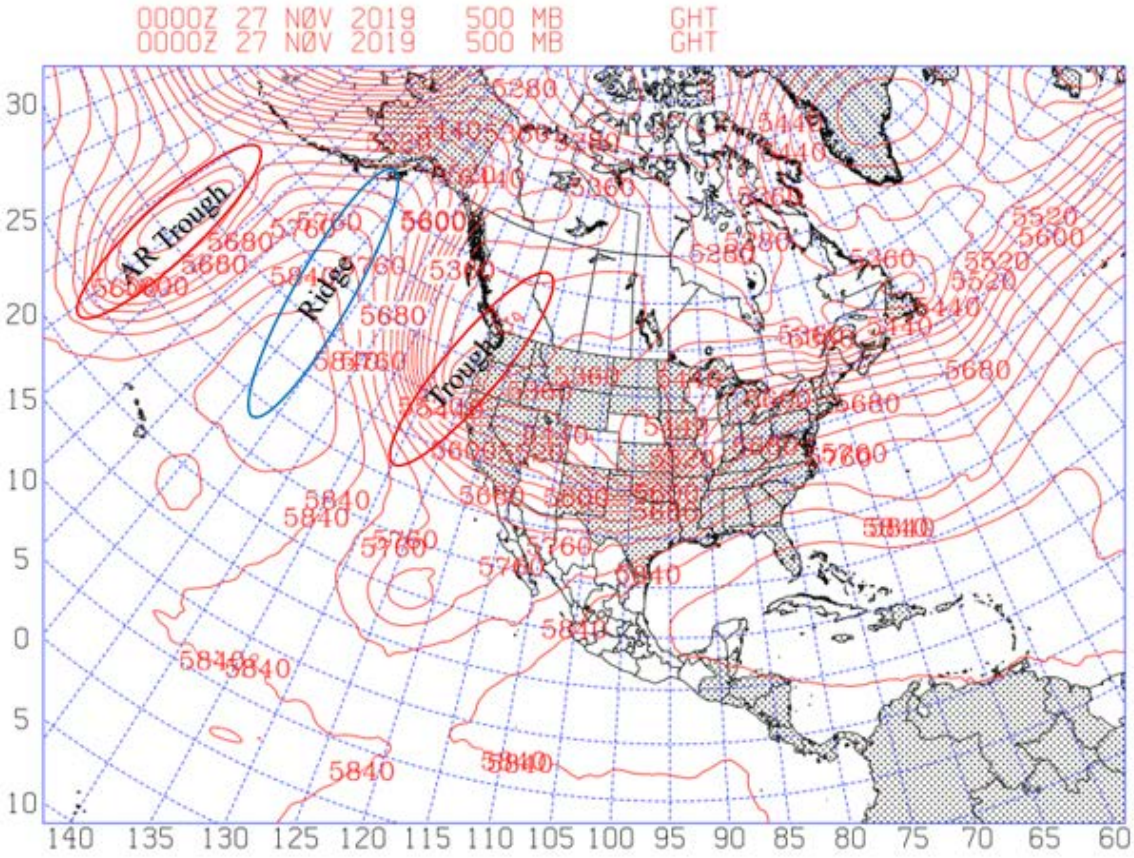

500 mb GHT plot for 0000 UTC 27 November 2019. 500 mb GHT are represented by the red lines in meters

Figure 26. Case 4 500 mb GHT Plot.

\

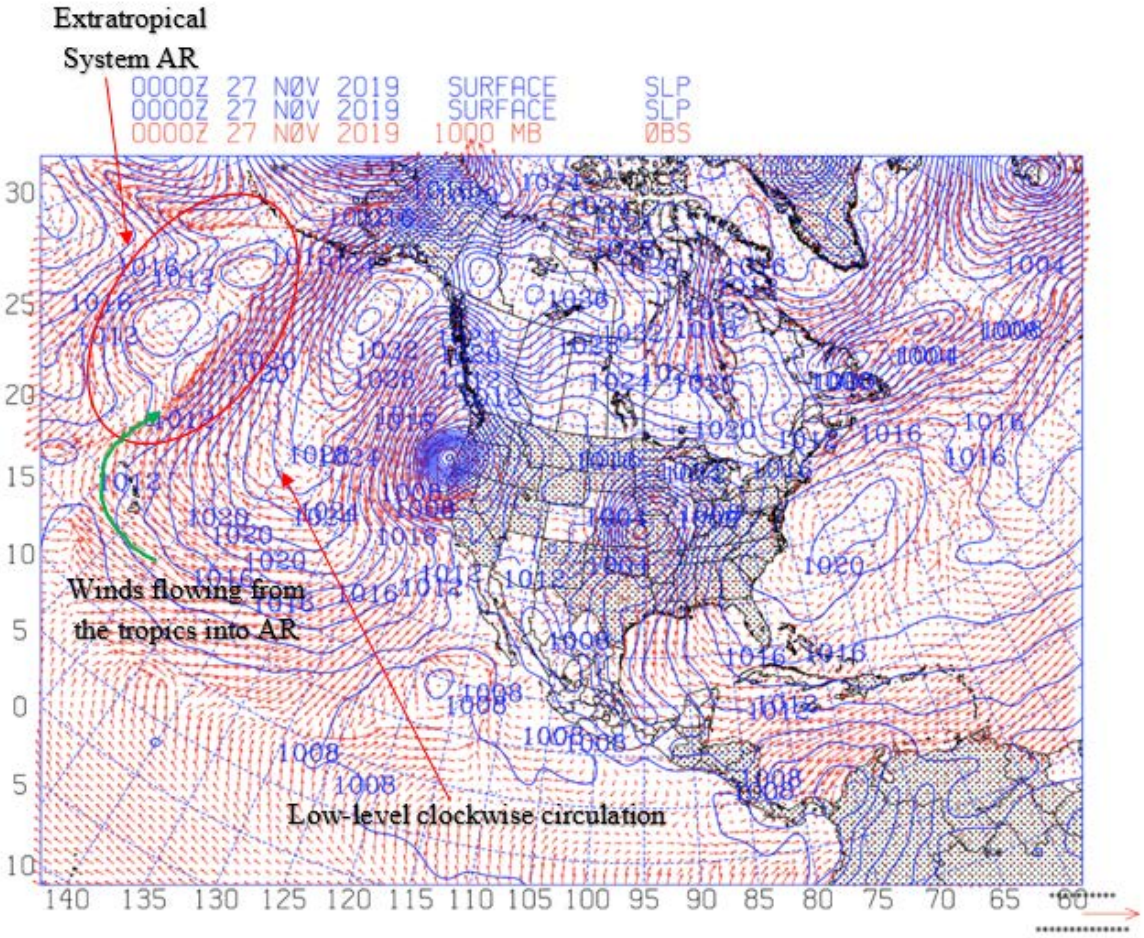

SLP and 1000 mb winds plot for 0000 UTC 27 November 2019. SLP are represented by the blue lines in mb and the red arrows represent wind vectors.

Figure 27. Case 4 SLP and 1000 mb Winds Plot.

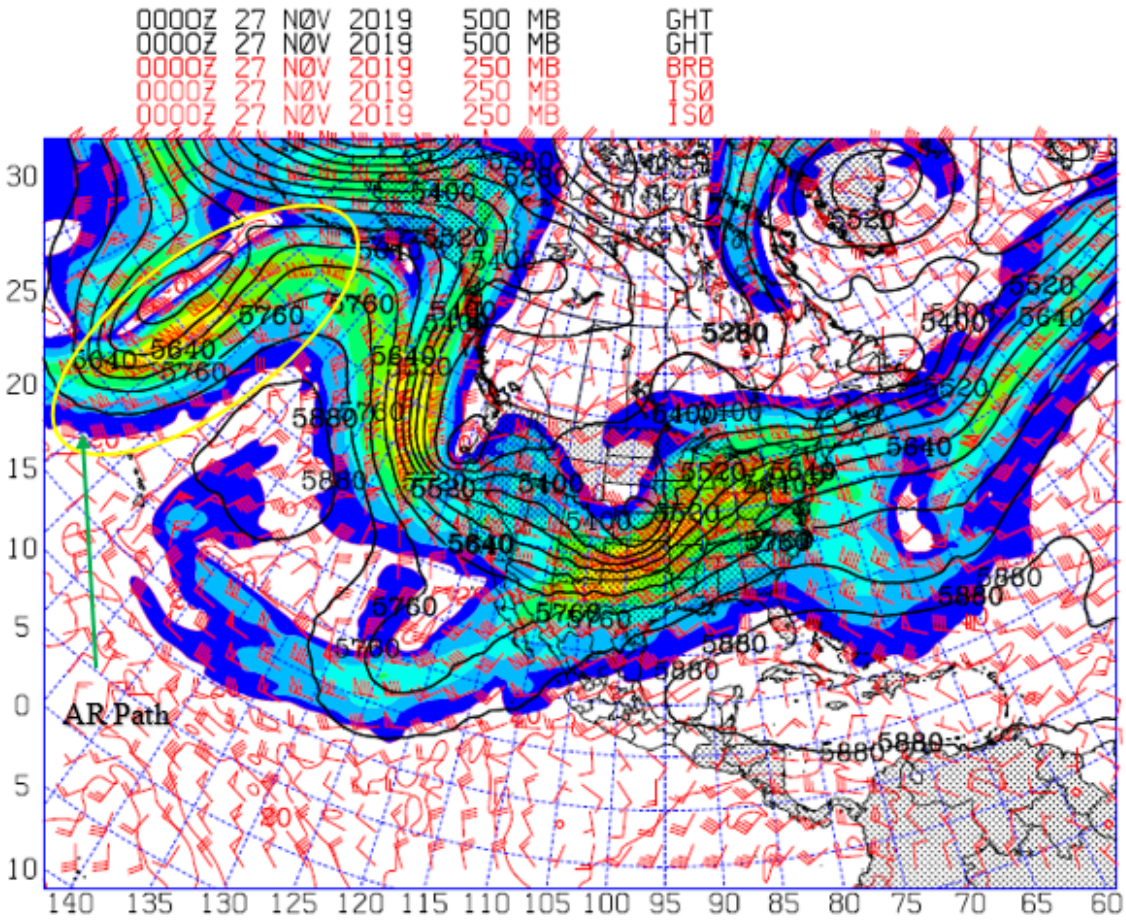

The 500 mb Geopotential Height contours are shown in black, the 250 mb jet stream is shown with the color fill, and the 250 mb wind is shown with red barbs, 0000UTC 27 November 2019

Figure 28. Case 4 Upper Air Chart.

E. CASE STUDY SUMMARY

All four case studies displayed some common characteristics as well as some distinct differences. One common characteristic seen in the integrated water vapor transport was a clockwise (anticyclonic) circulation that occurred east of the developing AR, east and north of the Hawaiian Islands. This clockwise circulation was a surface high-pressure system that occurred below a 500 mb ridge. In all cases, the high-pressure system produced easterly then southerly winds along its southwest flank to produce water vapor transport into the AR extratropical cyclone. It appears that this high-pressure system is a contributor in providing water vapor transport from the tropics into the AR extratropical cyclone. The primary difference between these cases was the initial synoptic scale patterns they displayed. Cases 1 and 2 were similar with a more zonal flow pattern that produced a developing cyclone northwest of Hawaii and weak downstream upper-level ridging. Cases 3 and 4 were similar in that they occurred under a highly amplified wave pattern with a deep trough that spawns the initial AR and a strong downstream ridge that extended north into Alaska. While these initial synoptic patterns were different between the cases, they evolved over 5-7 days to produce an AR across central California that is oriented in a southwest to northeast direction. This evolution will be analyzed in the results to assess the role that the high-pressure associated water vapor transport contributes to the AR evolution and associated rainfall.

IV. RESULTS

The four cases above were chosen to exhibit the interaction of a low-level high-pressure system and an extratropical cyclone that forms near Hawaii. The results in this section describe the evolution of the extratropical cyclone and associated AR from its inception to just after it made landfall on the west Coast of the United States. The results show that AR's from these extratropical cyclones: 1) result from the interaction of the surface high and low-pressure system centers to form major (Pineapple Express) AR events; 2) are fed moisture from the high-pressure system to the east; and 3) have different relative sources of moisture that impact on observed downstream precipitation. Understanding these aspects of the formation and evolution of ARs will help better predict their occurrence and impacts over the United States west coast.

A. CASE 1

Figure 29 shows the GOES IR imagery at specific times in the evolution of the 1996–1997 AR event. Beginning at 0000 UTC 26 December 1996 (Figure 29 upper left) an AR extratropical cyclone forms northwest of Hawaii. On 0000 UTC 28 December 1996 (Figure 29 upper left), the AR extratropical cyclone has migrated eastward and the main cloud plume is taking a noticeable classic Pineapple Express shape as it elongates eastward. The cloud plume stretches from the northeast to the southwest from 140 W past the Hawaiian Islands to the International Date Line. From 1200 UTC 31 December 1996 (Figure 29 bottom left) to 0000 UTC 02 January 1997 (Figure 29 bottom right) the AR extends into the eastern Pacific and then makes landfall in California. The low-pressure that supports the AR makes landfall further north in British Columbia. However, for the next three days, the AR is maintained across California with the cloud plume stretching from California to Hawaii, and continuous rain throughout the three-day period in Northern California.

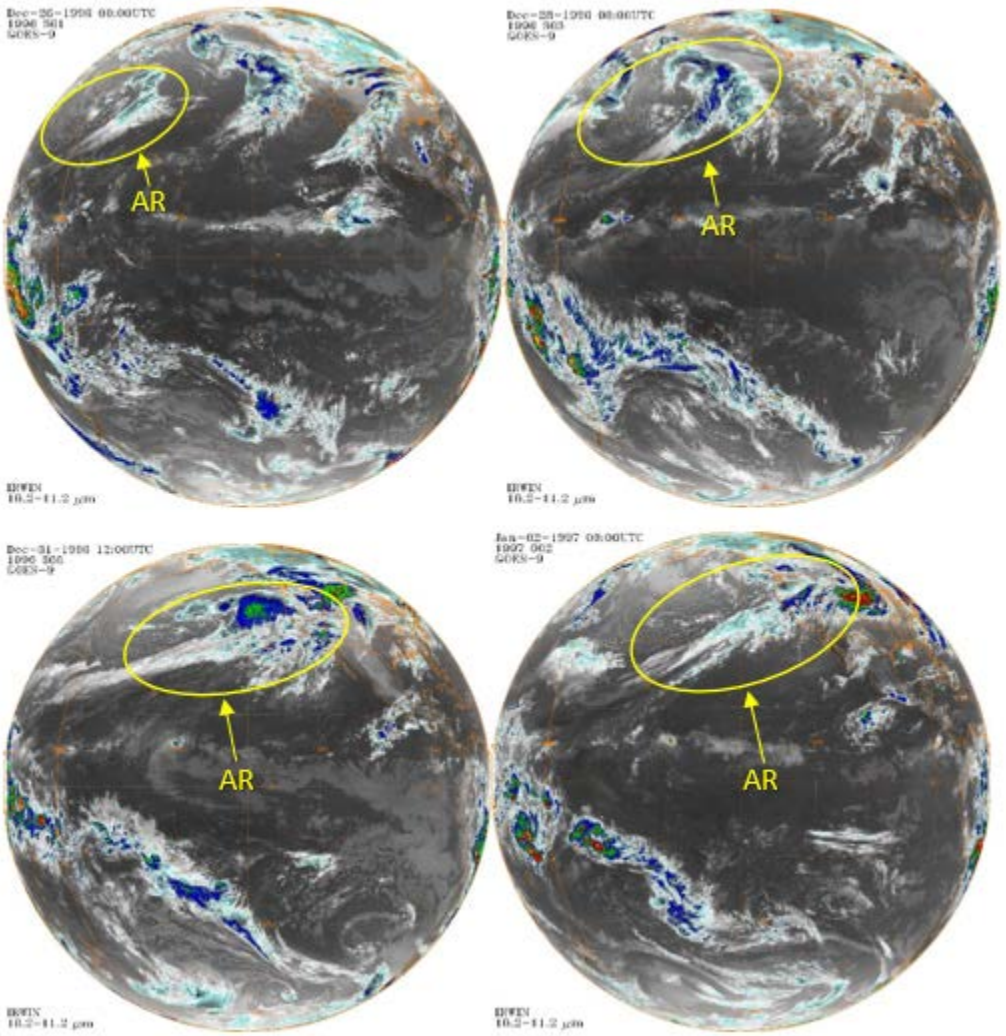

Upper-left: 0000UTC 26 December 1996; upper-right: 0000UTC 28 December 1996; lower-left: 1200 UTC 31 December 1996; lower-right: 0000 UTC 02 January 1997.

Figure 29. Case 1 AR IR Satellite Evolution. Source: Knapp (2008).

To demonstrate the evolution of the 1996–1997 AR event, we examine the IVT and 700 mb GHT at specific times over its lifecycle (Figure 30). Starting at 0000 UTC 26 December 1996 (Figure 30 upper left), an IVT clockwise circulation is visible east of Hawaii along with a 700 mb GHT low-level trough (extratropical cyclone) and relatively strong moisture transport northwest of Hawaii. Both the IVT clockwise circulation to the southeast of the AR and the 700 mb GHT trough migrate with each other eastward to the west coast of the United States. Additionally, the IVT that defines the AR intensifies as the 700 mb trough migrates eastward as seen in Figure 30 (upper right) eventually extending

to the U.S. west coast in Figure 30 (bottom left). On the western side of the clockwise circulation to the east, the water vapor transport source appears to come from 10–15 N and continues this pattern throughout the evolution. Although this transport from the south is much weaker than the transport in the main AR, it is a persistent source of moisture into the AR. Water vapor may have already been pushed to California before the main AR event arrived. Next the 500 mb GHT, SLP, and 1000 mb winds will be analyzed to confirm the clockwise IVT circulation is due to a surface high-pressure system. TQV will be analyzed to confirm the pre-existence of water vapor ahead of the AR.

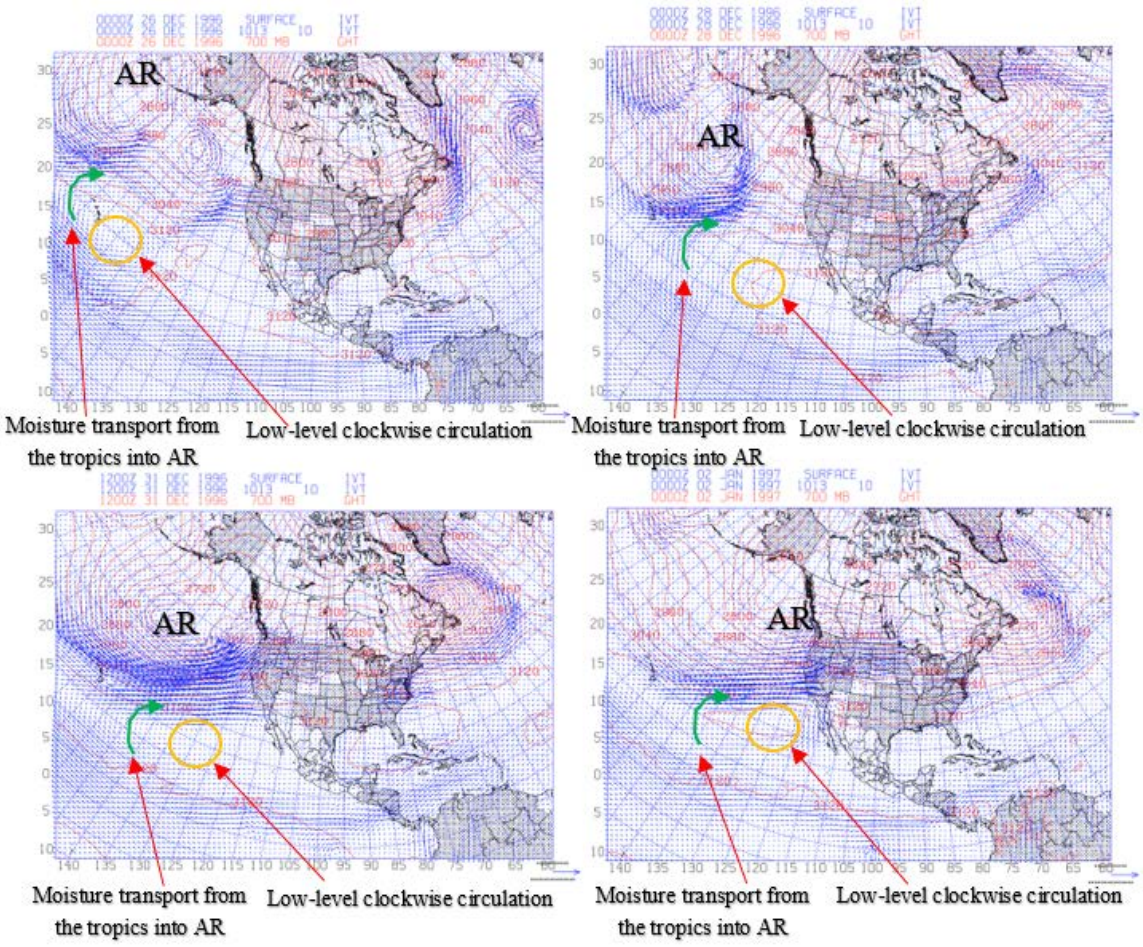

Upper-left: 0000UTC 26 December 1996; upper-right: 0000UTC 28 December 1996; lower-left: 1200 UTC 31 December 1996; lower-right: 0000 UTC 02 January 1997. Red lines are 700 mb GHT and blue arrows are the IVT

Figure 30. Case 1 IVT and 700 mb GHT Plot Evolution.

Figure 31 is 500 mb GHT at specific times in the evolution of the 1996–1997 AR event. By analyzing the 500 mb GHT, it can be confirmed that clockwise circulation found in the IVT is associated with an upper level ridge (high-pressure system). Also, it can be confirmed that both the 500 mb trough (extratropical cyclone) and 500 mb ridge are progressing together throughout the evolution.

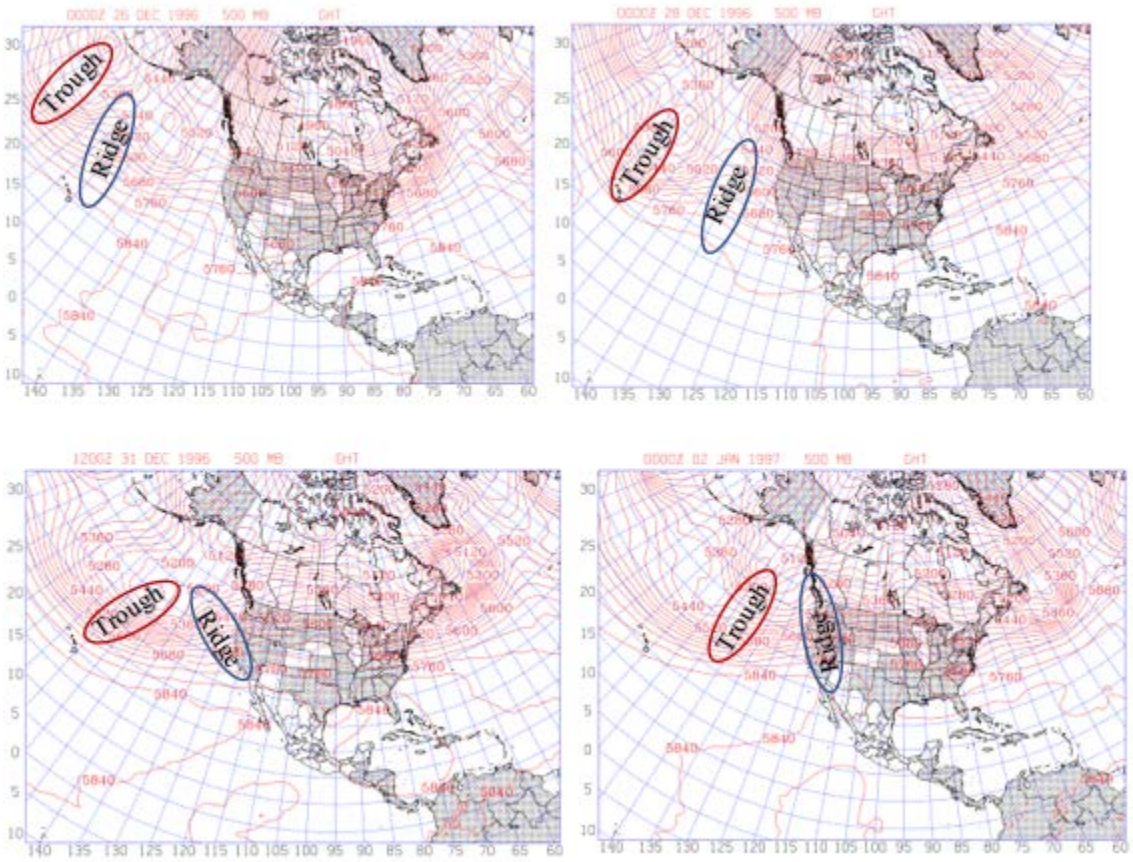

Upper-left: 0000UTC 26 December 1996; upper-right: 0000UTC 28 December 1996; lower-left: 1200 UTC 31 December 1996; lower-right: 0000 UTC 02 January 1997. 500 mb GHT are represented by the red lines in meters

Figure 31. Case 1 500 mb GHT Plot Evolution.

Figure 32 is SLP and 1000 mb winds at specific times in the evolution of the 1996–1997 AR event. Both the SLP and 1000 mb winds were analyzed to further confirm the existence of a low-level high-pressure system to the east of the AR and the interaction between the extratropical cyclone associated with the AR and this low-level high-pressure system. The sequence of sea-level pressure plots show that an extratropical cyclone developed northwest of Hawaii Figure 32 (upper left), tracked east and intensified Figure 32 (upper right), then became a very strong system north of Hawaii by 1200UTC 31 December (Figure 32 bottom left), and finally weakening as it reached the west coast (Figure 32 bottom right). The strong cyclonic flow around this system produced the very high IVT just to the southeast of the low. In all plots, the SLP also displays a low-level high-pressure system associated with the low-level clockwise circulation found in the IVT. The 1000 mb winds are highly correlated with IVT vectors indicating that the low-level flow around the high dominates the moisture transport in this feature. Further analysis indicates that the low-level winds from the high-pressure system and the extratropical cyclone produce confluence into the AR suggesting that the high-pressure may be important in concentrating the moisture into a defined AR plume. Finally, the low-level high-pressure system is tapping southern regions of the Pacific Ocean where water vapor is higher and may be important in the overall moisture content of the AR.

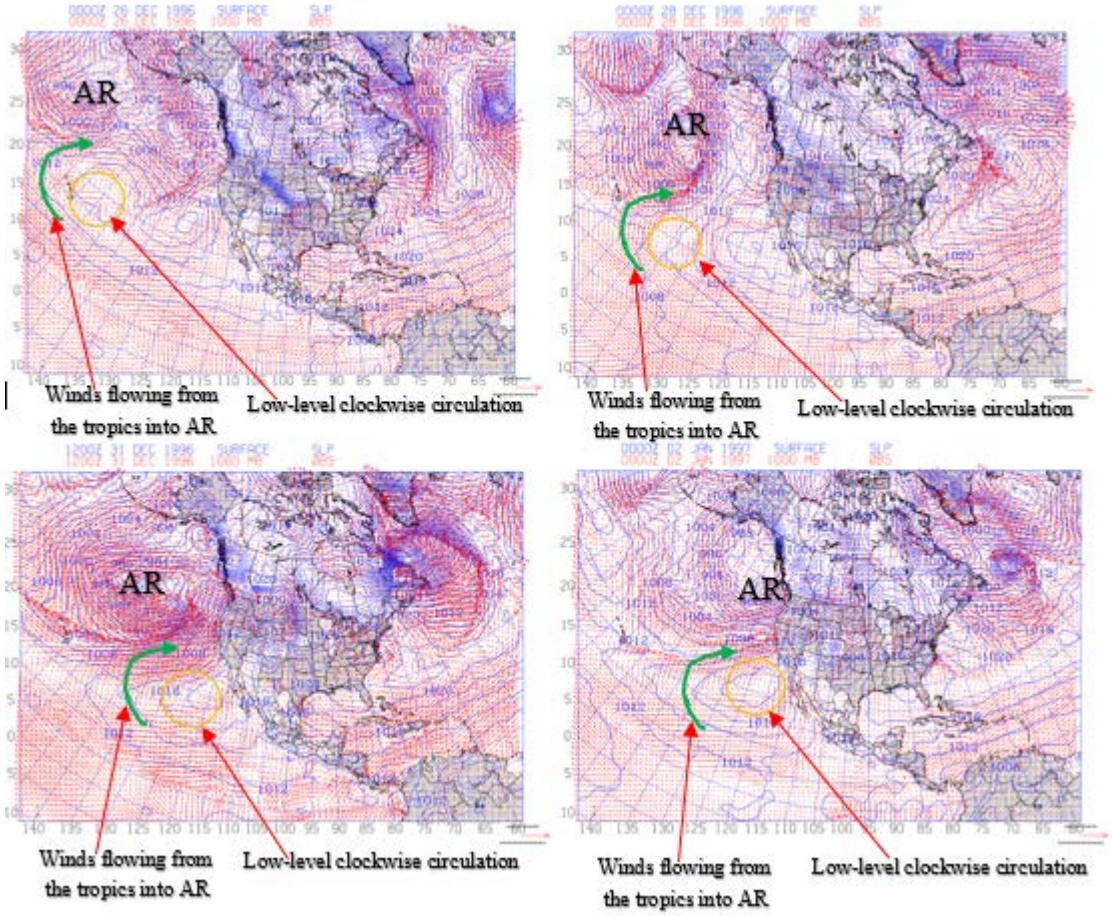

Upper-left: 0000UTC 26 December 1996; upper-right: 0000UTC 28 December 1996; lower-left: 1200 UTC 31 December 1996; lower-right: 0000 UTC 02 January 1997. SLP are represented by the blue lines in mb and the red arrows represent wind vectors.

Figure 32. Case 1 SLP and 1000 mb Winds Plot.

Figure 33 shows the total column water vapor (TQV) and 700 mb GHT at specific times in the evolution of the 1996–1997 AR event. Starting 26 December 1996 Figure 34 (upper left) values of four g/kg TQV are near Hawaii, but off the west coast of the United States TQV values are less than two g/kg. By 28 December 1996 (Figure 33 upper right), a sliver of TQV greater than two g/kg migrates into Southern California from 135 W to 115 W. This is well ahead of the main AR extratropical cyclone located 43 N 155 W at this time. Values greater than four g/kg are beginning to be transported northeastward with the extratropical cyclone in the AR. On 31 December 1996 (Figure 33 bottom left), values greater than two g/kg TQV penetrate western United States into the Rocky Mountains. Values greater than four g/kg TQV spread throughout the southern flank of the extratropical cyclone as the AR develops. This corresponded with the 31 December 1996 cloud plume found on the IR satellite image. It is interesting to note that a separate plume of four g/kg TQV occurs south of the extratropical cyclone and main AR. This plume extends to Southern California at this time. By 02 January 1997 (Figure 33 bottom right), values greater than four g/kg TQV occur over all of California as the southern and northern plumes seem to have combined. Upon further analysis, it appears that values greater than two g/kg TQV were being transported into California prior to the AR arriving. Comparing the 28 December 1996 IVT (Figure 30 upper right) and the 28 December 1996 TQV (Figure 33 upper left), the high-pressure system identified in the (IVT Figure 30) is transporting water vapor into that region. It must be noted that on 26 December 1996, a previous low-pressure system went through California and may have contributed to the deposit of water vapor in that region. Nevertheless, there was higher than normal water vapor in the region prior to the storm's arrival. This may have helped contribute to heavy rainfall observed in Northern California.

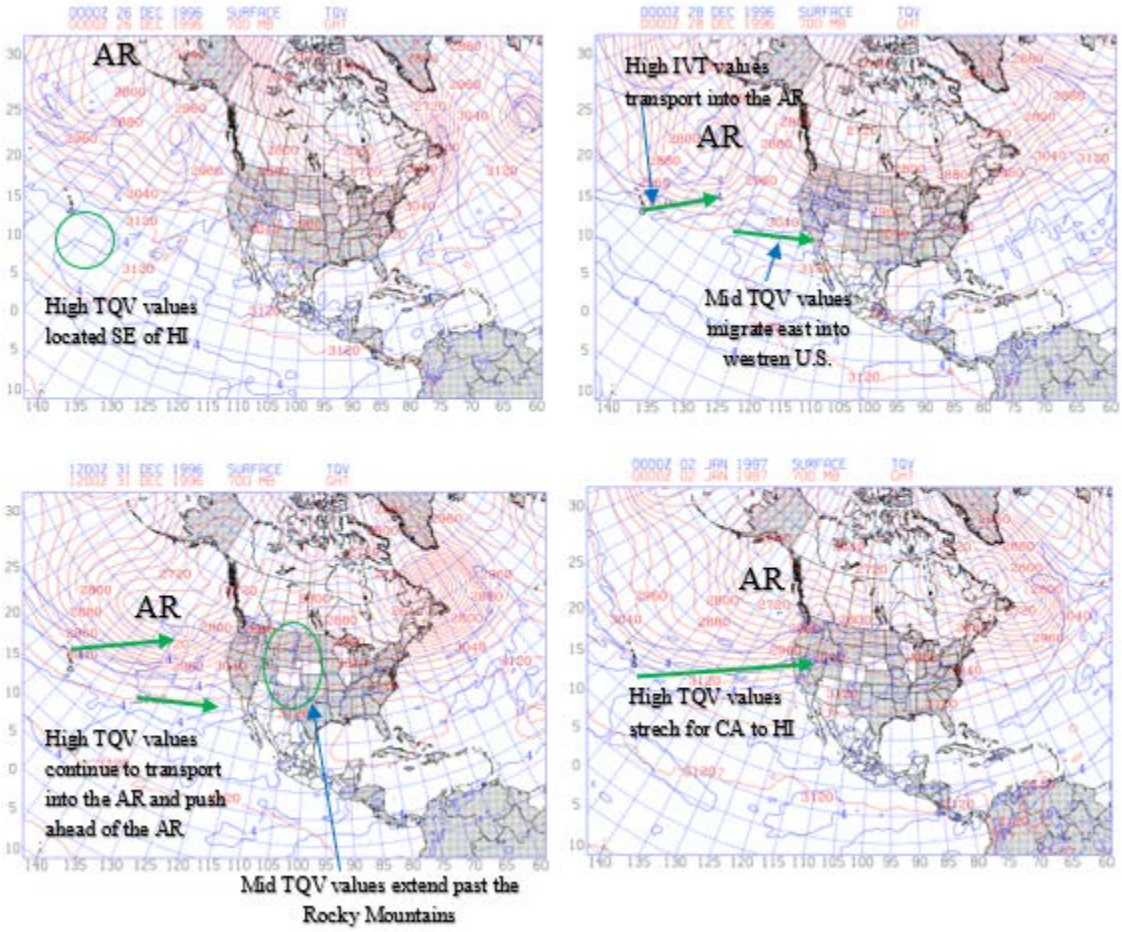

Upper-left: 0000UTC 26 December 1996; upper-right: 0000UTC 28 December 1996; lower-left: 1200 UTC 31 December 1996; lower-right: 0000 UTC 02 January 1997. Blue lines represent TQV and red lines represent 700 mb GHT

Figure 33. Case 1 TQV and 700 mb GHT Plot Evolution.

Figure 34 shows upper air jet stream at 250 mb and 500 GHT at specific times in the evolution of the 1996–1997 AR event. Throughout the event, the strong jet windspeeds correspond to the cloud plume found in the IR image (Figure 29).

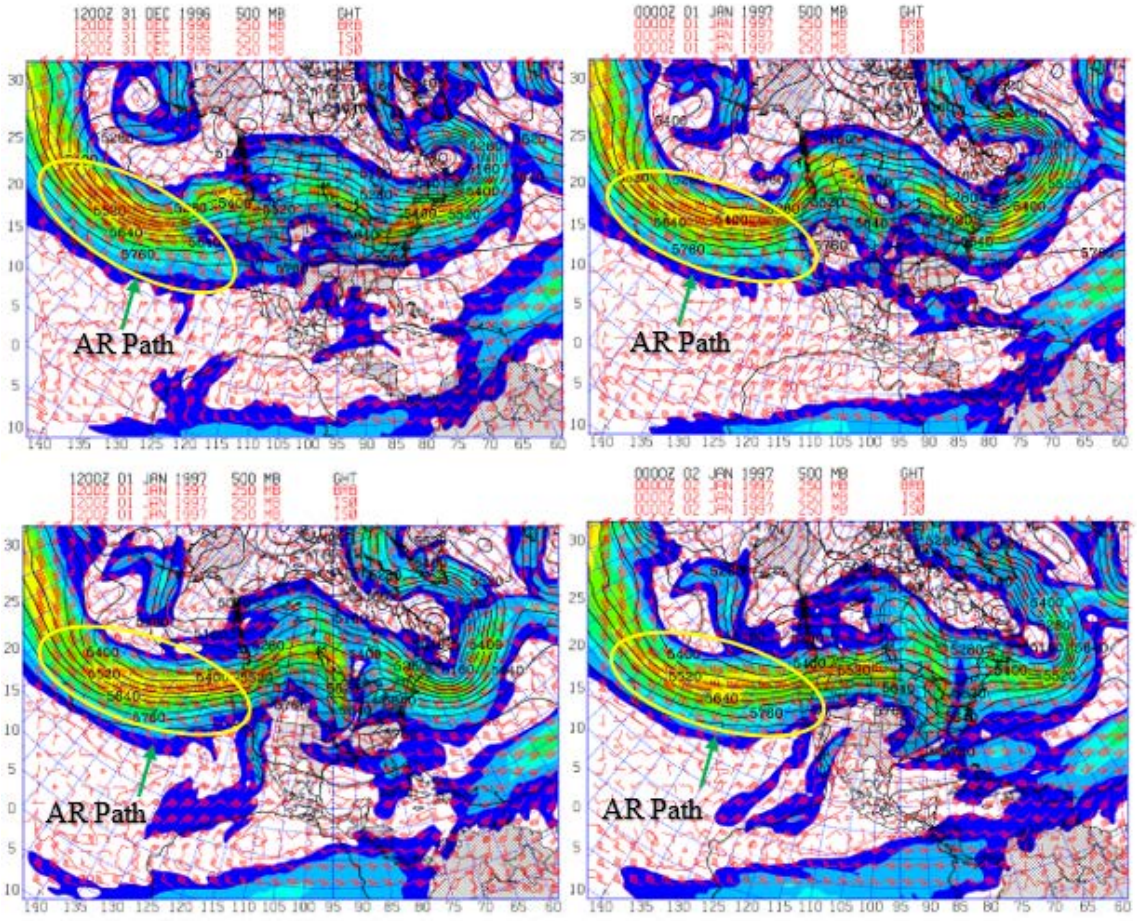

The 500 mb GHT is shown in black contours, the 250 mb wind is shown with red barbs, and the 250 mb jet stream is shown with a color fill. Upper-left: 1200 UTC 31 December 1996; upper-right: 0000 UTC 01 January 1997; lower-left: 1200 UTC 01 January 1997 lower-right: 0000 UTC 02 January

Figure 34. Case 1 Upper-Air Chart Evolution.

To illustrate the source of moisture during the period of heavy rainfall, backward trajectories were constructed. Figure 35 shows the trajectory ending at 700 mb on 1200 UTC 02 January 1997, when heavy rain was occurring. This trajectory is traced back over the previous 48 hours to identify where the parcel originated and how it traveled. The trajectory endpoint is a Blue Canyon California, and 48 hours prior the trajectory originated

near Hawaii. This trajectory corresponds well with the IVT plume (Figure 30 bottom left) and cloud plume (Figure 29 bottom left) around 1200UTC 31 December. This trajectory supports the idea that low-level moisture near Hawaii is picked up in the AR to result in heavy precipitation 48 hours later over central California.

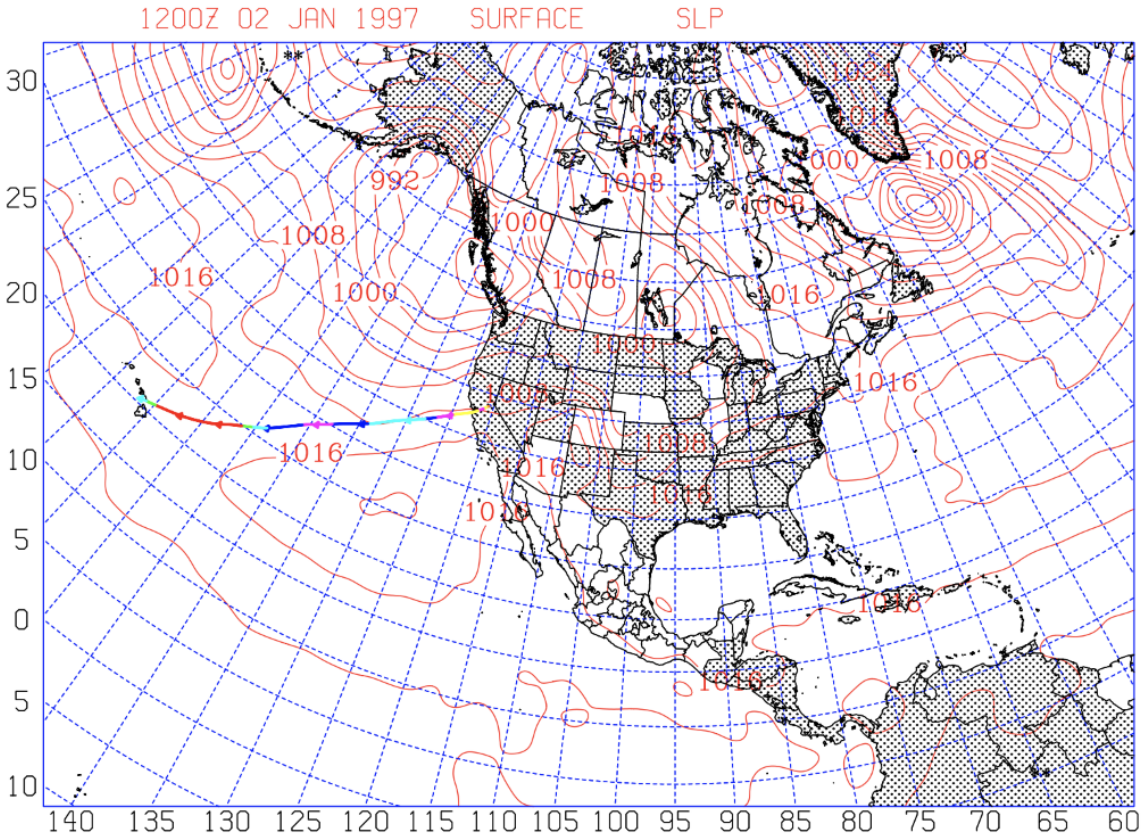

Figure 35. Case 1 700 mb Parcel Trajectory.

B. CASE 2

Figure 36 shows the GOES IR and visible (VIS) imagery at specific times in the evolution of the 2007 AR event. Beginning at 0000 UTC 06 February 2007 Figure 36 (upper left) an extratropical cyclone with associated AR has already formed northwest of Hawaii. By 0000 UTC 08 February 2007 (Figure 36 upper right), the extratropical cyclone with associated AR has migrated eastward and the main cloud plume has organized into a small noticeable classic Pineapple Express shape. Though the Case 2 AR cloud plume is smaller compared to Case 1, looking at the VIS image for 2100 UTC 09 February 2007 (Figure 36 bottom left) the cloud plume stretches from California to Hawaii. For the next three-four days precipitation falls continuously throughout in Northern California.

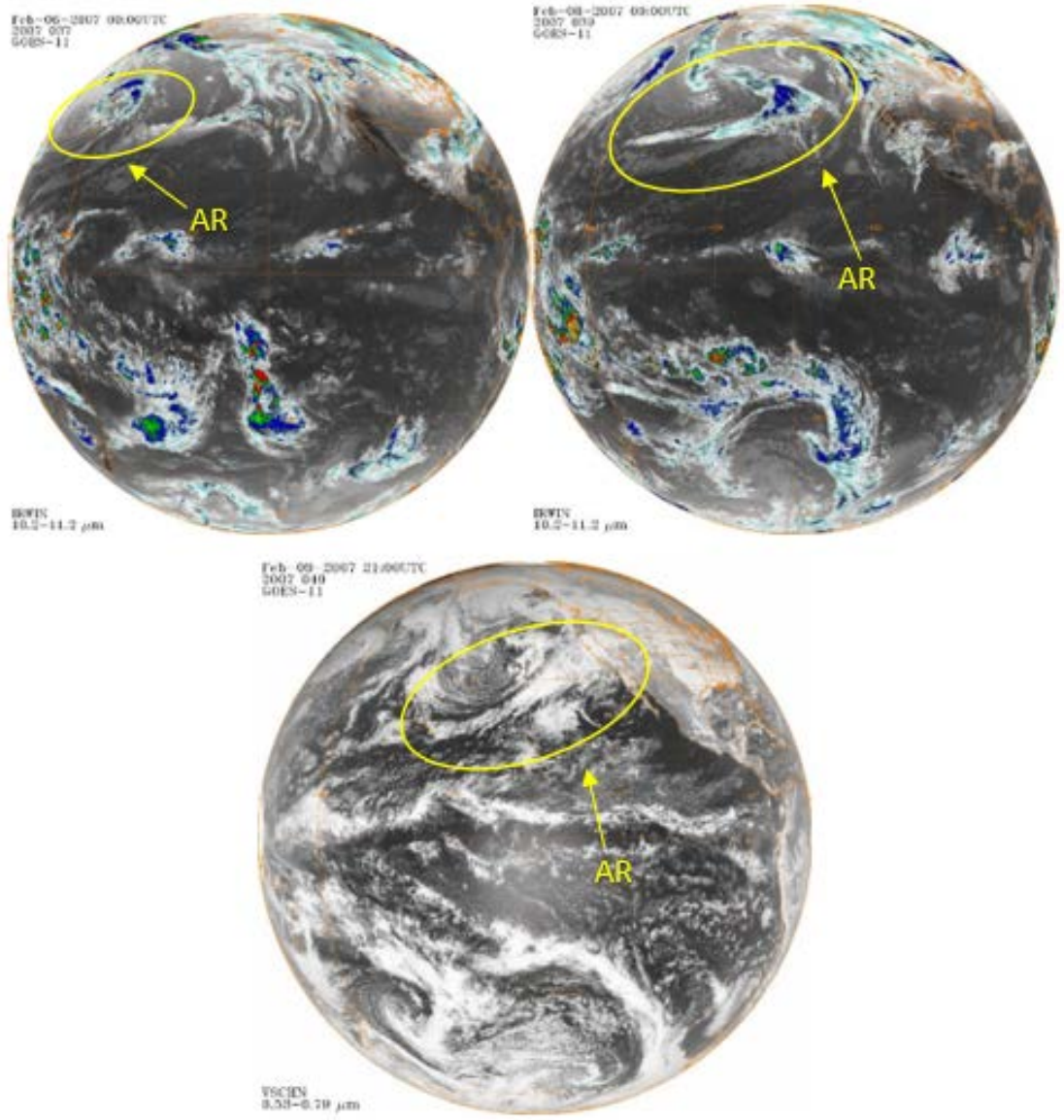

Upper-left: IR 0000UTC 06 February 2007; upper-right: IR 0000UTC 08 February 2007; bottom-center: VIS 2100 UTC 09 February.

Figure 36. Case 2 AR IR and VIS Satellite Evolution. Source: Knapp (2008).

Figure 37 shows the IVT and 700 mb GHT at specific times in the evolution of the 2007 AR event. Again, there is an IVT clockwise circulation east of Hawaii and a low-level 700 mb GHT trough (extra tropical cyclone) northwest of Hawaii at 0000 UTC 06 February 2007 (Figure 37 upper left). Both the IVT clockwise circulation and 700 mb GHT trough migrate with each other eastward toward the west coast of the United States as seen in Figure 37 (upper right and center). The IVT at 0000 UTC 08 February (Figure 37 upper right) occurs in a rather narrow plume southeast of the trough and is certainly weaker than what was observed in Case 1. Additionally, same as in Case 1, on the western side of the anticyclonic IVT circulation to the east, the IVT appears to transport water vapor into the AR. As the system translates to the coast (Figure 37 center), the IVT shows relatively strong water vapor transport ahead of the 700 mb GHT trough. Unlike Case 1, this IVT plume or AR extends more north-south and is not that strong as it extends back towards Hawaii. At 1200 UTC 10 February (Figure 37 center), the northward transport of water vapor into the AR associated with the high to the east is well-defined and almost as strong as the eastward transport from Hawaii. This suggests that in the later stages of this system the moisture transport around the high may be an important contribution to the overall moisture.

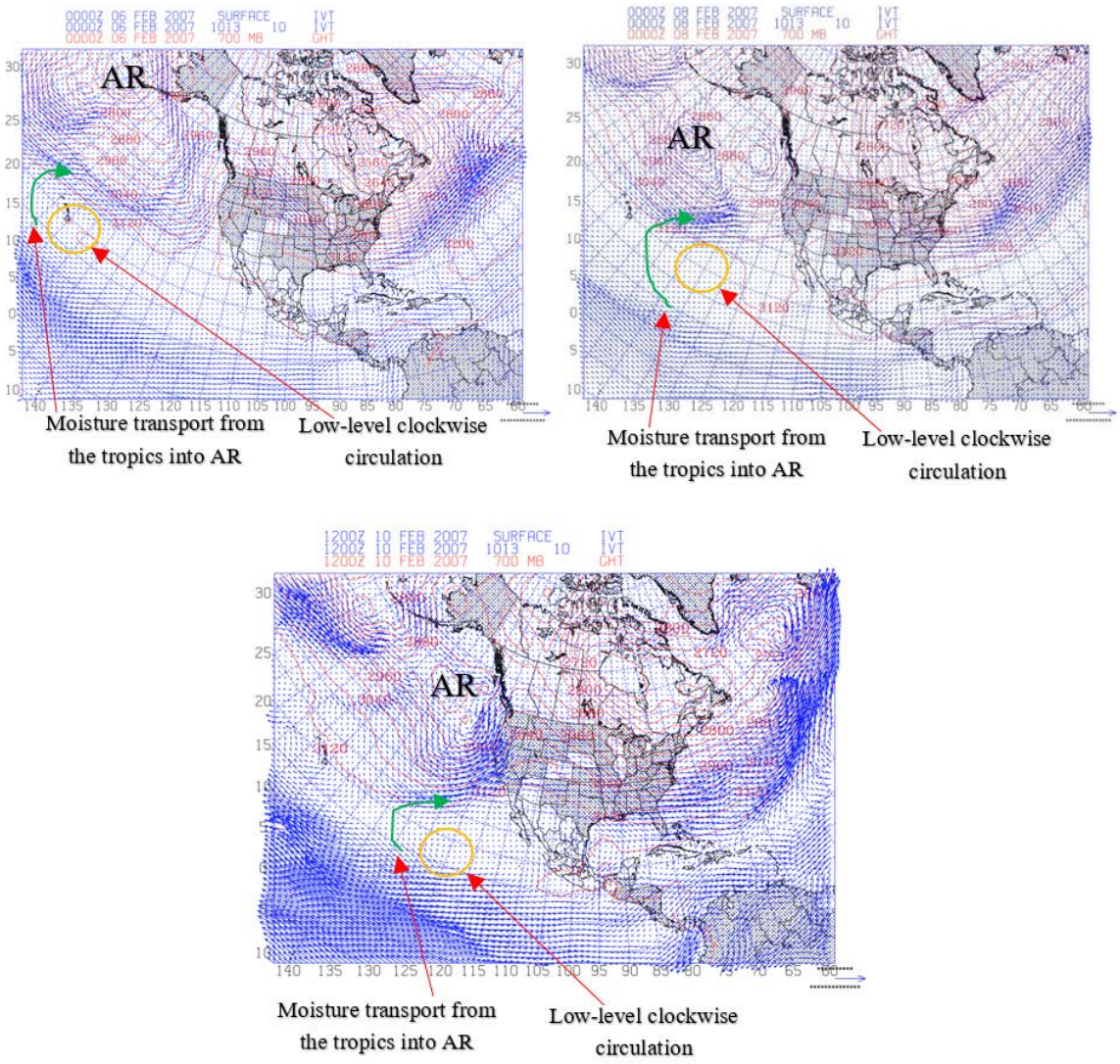

Upper-left: 0000UTC 06 February 2007; upper-right: 0000UTC 08 February 2007; bottom-center: 1200 UTC 10 February 2007. Red lines are 700 mb GHT and blue arrows are the IVT

Figure 37. Case 2 IVT and 700 mb GHT Plot Evolution.

Figure 38 shows the 500 mb GHT at specific times in the evolution of the AR event. The 500 mb GHT confirms that low-level clockwise circulation found in the IVT east of the AR is associated with an upper level ridge. Both the 500 mb trough and ridge progress together throughout the evolution of this event consistent with a progressive baroclinic wave. As the system makes landfall at 1200 UTC 10 February, the upper-level ridge is fairly amplified indicative of development of the low-level extratropical cyclone to the west.

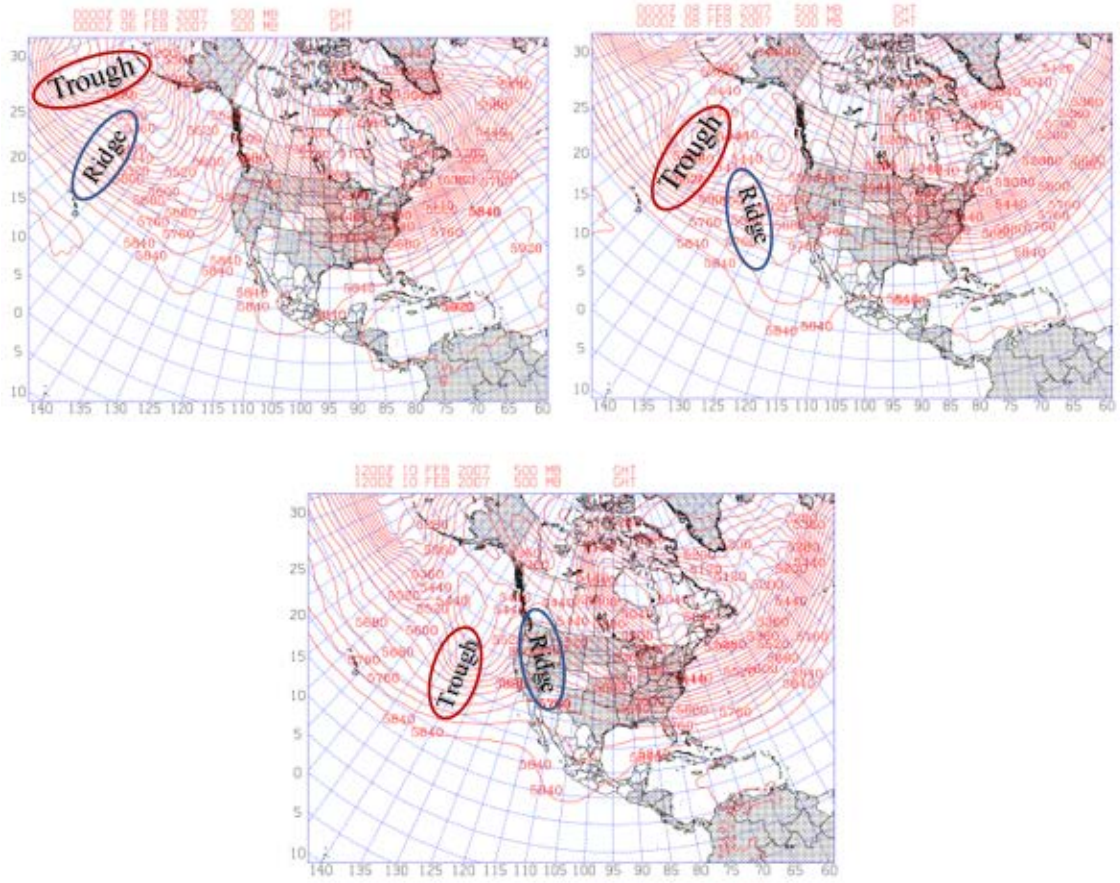

Upper-left: 0000UTC 06 February 2007; upper-right: 0000UTC 08 February 2007; bottom-center: 1200 UTC 10 February 2007. 500 mb GHT are represented by the red lines in meters.

Figure 38. Case 2 500 mb GHT Plot Evolution

The SLP and 1000 mb winds (Figure 39) are shown at specific times in the evolution of the 2007 AR event to illustrate the development and evolution of the surface low and high. Both the SLP and 1000 mb winds show the development and intensification of a surface cyclone associated with the AR. The cyclone started out as a weak frontal wave on 0000 UTC 06 February to the northwest of Hawaii (Figure 39 upper left). This wave amplified as it moved north of Hawaii on 0000 UTC 08 February (Figure 39 upper right) and then intensified strongly as it approached the west coast on 1200 UTC February (Figure 39 center). As the low developed, a low-level high-pressure system became more distinct to the southeast of the low center. The anticyclonic circulation around the high produced pronounced southerly flow into the AR on the southeast side of the extratropical cyclone. In all plots, the SLP and winds display a low-level high-pressure system and anticyclonic winds associated with the low-level clockwise circulation found in the IVT. The fact that the 1000 mb winds are highly correlated with IVT vectors indicates the dominance of the low-level flow in producing the moisture transport. Again, as in Case 1, the low-level winds from both the high-pressure system and the extratropical cyclone interact with each other to feed the AR. In Case 2 the position of the low-level high-pressure system indicates water vapor transport from southern regions of the Pacific into the east side of the extratropical cyclone. This synoptic feature was similar to Case 1. The TQV will be analyzed to confirm the pre-existence of high concentrations of water vapor ahead of the extratropical cyclone that feeds into the AR.

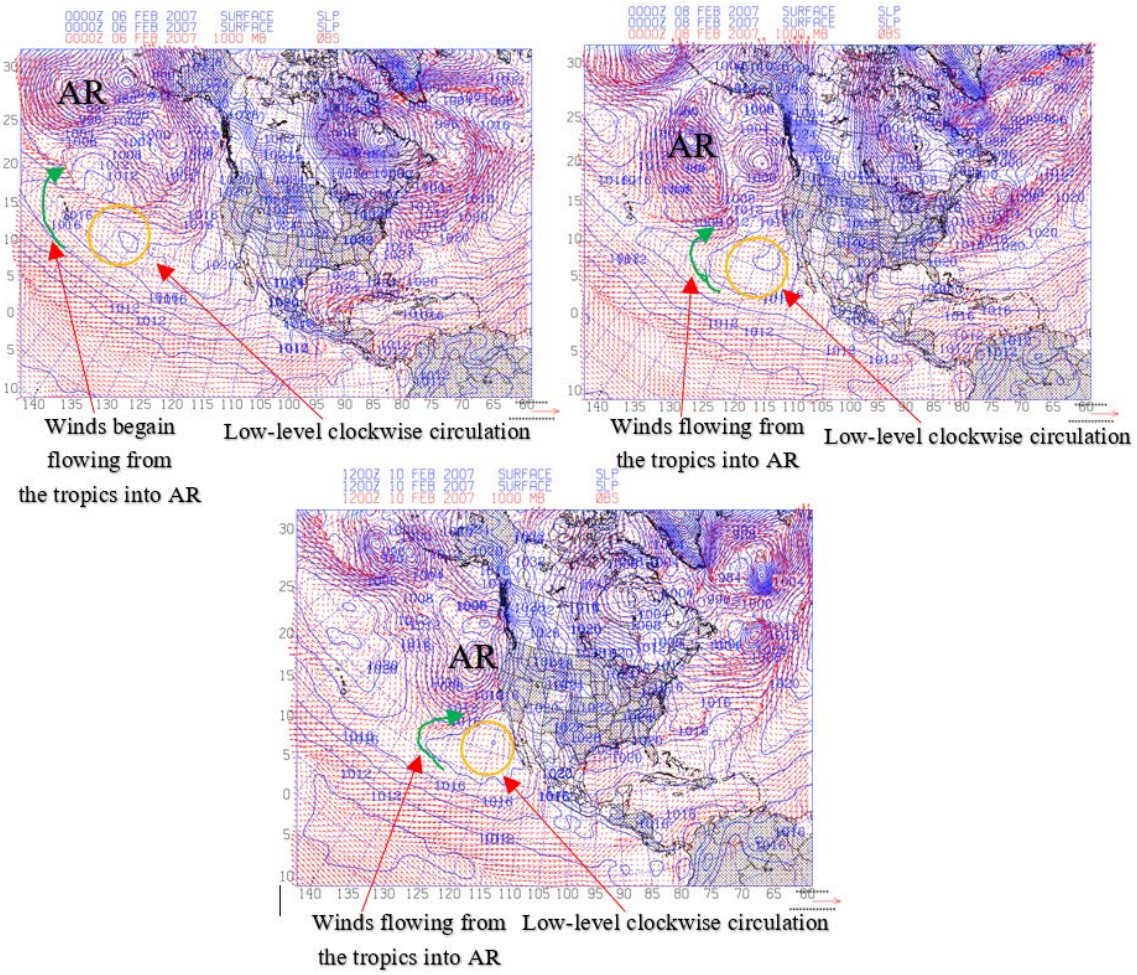

Upper-left: 0000UTC 06 February 2007; upper-right: 0000UTC 08 February 2007; bottom-center: 1200 UTC 10 February 2007. SLP are represented by the blue lines in mb and the red arrows represent wind vectors.

Figure 39. Case 2 SLP and 1000 mb Winds Plot.

Figure 40 shows the total column water vapor (TQV) and 700 mb GHT over the evolution of the 2007 AR event. Starting on 06 February 2007 (Figure 40 upper left) values of four g/kg TQV stay well below Hawaii and never migrate north through the evolution. However, TQV values greater than two g/kg are off the coast of the western United States, well ahead of the AR and extratropical cyclone. By 08 February 2007 (Figure 40 upper right), TQV greater than two g/kg migrates into California. This is well ahead of the main AR and extratropical cyclone. This maybe aided by both the low-level high-pressure system to the east of the main extratropical cyclone and an initial weak extratropical

cyclone east of the main AR. Additionally, TQV values greater than two g/kg begin to be drawn into the main extratropical cyclone associated with the AR. On 10 February 2007 (Figure 40 center), TQV values greater than two g/kg penetrate the western United States into the Rocky Mountains. This corresponded with the 09 February 2007 cloud plume found on the VIS satellite image. As in Case 1, it appears that values greater than two g/kg TQV were being transported into California prior to the AR extratropical cyclone arriving. Comparing the 08 February 2007 IVT (Figure 37 upper right) and the 08 February 2007 TQV (Figure 40 upper right), the clockwise circulation identified in the IVT is transporting water vapor closer to California.

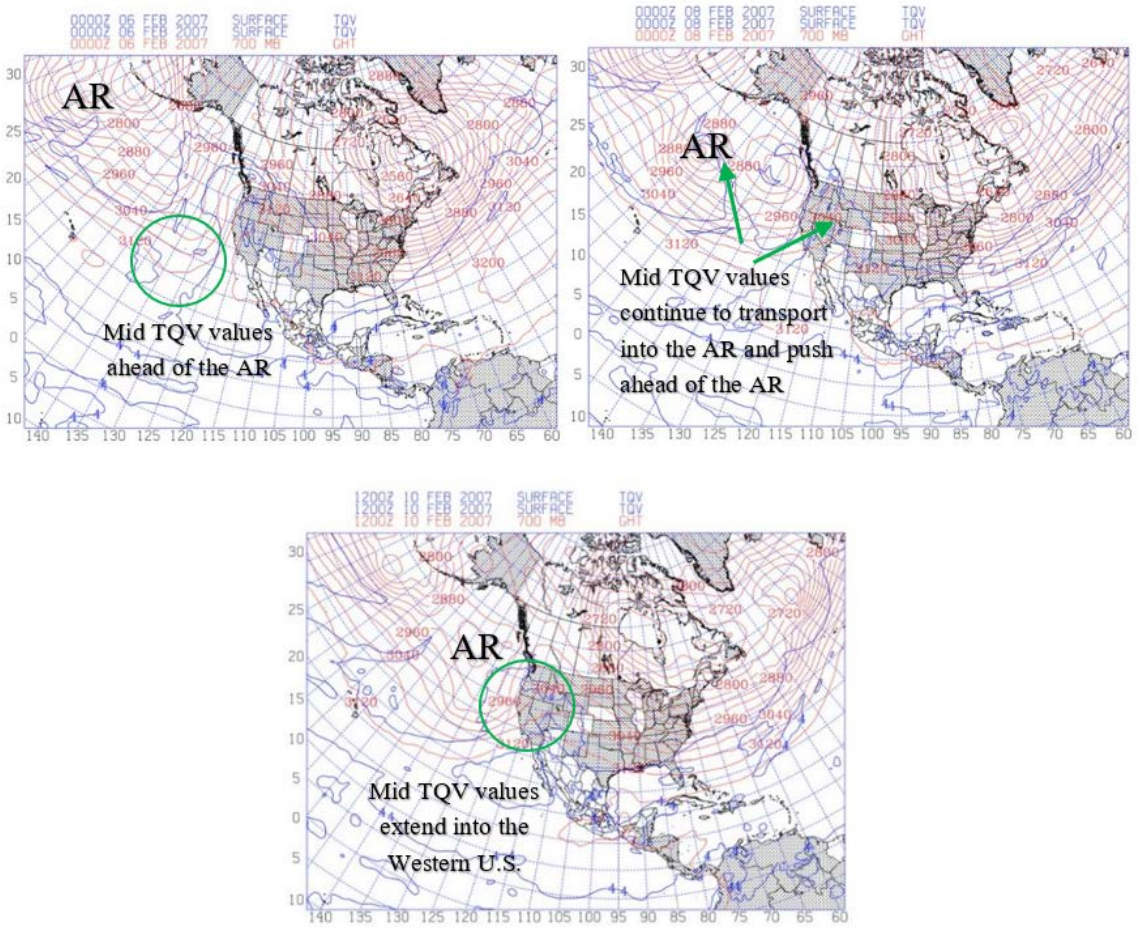

Upper-left: 0000UTC 06 February 2007; upper-right: 0000UTC 08 February 2007; lower-center: 1200 UTC 10 February 2007.

Figure 40. Case 2 TQV and 700 mb GHT Plot Evolution.

Figure 41 shows upper air jet stream at 250 mb and 500 GHT at specific times in the evolution of the 2007 AR event. Throughout the event the jet maximum windspeeds would weaken and correspond to diminishing size of the cloud plume found in the IR and visible images.

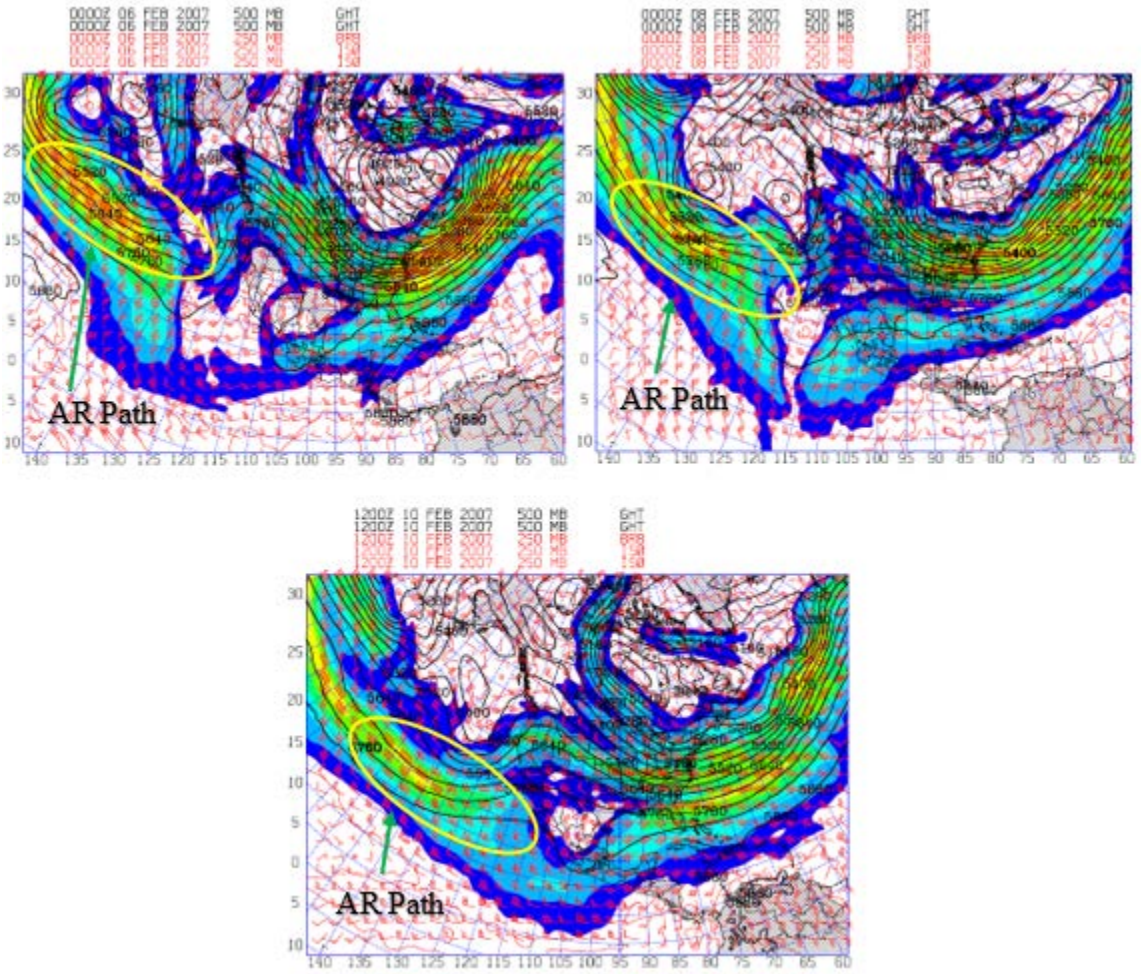

The 500 mb GHT is shown in black contours, the 250 mb wind is shown with red barbs, and the 250 mb jet stream is shown with a color fill. Upper-left: 0000 UTC 06 February 2007; upper-right: 0000 UTC 08 February 2007; bottom: 1200 UTC 10 February 2007.

Figure 41. Case 2 Upper-Air Chart Evolution.

Figure 42 shows the air parcel trajectory ending at 700 mb on 1200 UTC 10 February 2007 over the Central California precipitation region. This trajectory traces the air parcel back the previous 48 hours to identify where the parcel originated and how it

traveled. The trajectory endpoint is a Blue Canyon California, and 48 hours prior the trajectory traced back to 33 N 144 W. This trajectory indicates that the moisture source for the Central California precipitation originated north of Hawaii where the moisture was drawn up into the developing extratropical system. Its eastward movement is consistent with the eastward track of the developing low suggesting that the AR moisture plume may be very much associated with the warm conveyor belt of the main extratropical cyclone. While the satellite image on 2100 UTC 09 February indicates a cloud band that extends back toward Hawaii, the trajectory seems to show that air does not actually move along this cloud band but more typically tracks its movement eastward as the system evolves. Dacre (et al 2015) suggest that AR's are footprints or trails of moisture left behind a moving system and the trajectory in this case seems to confirm that behavior.

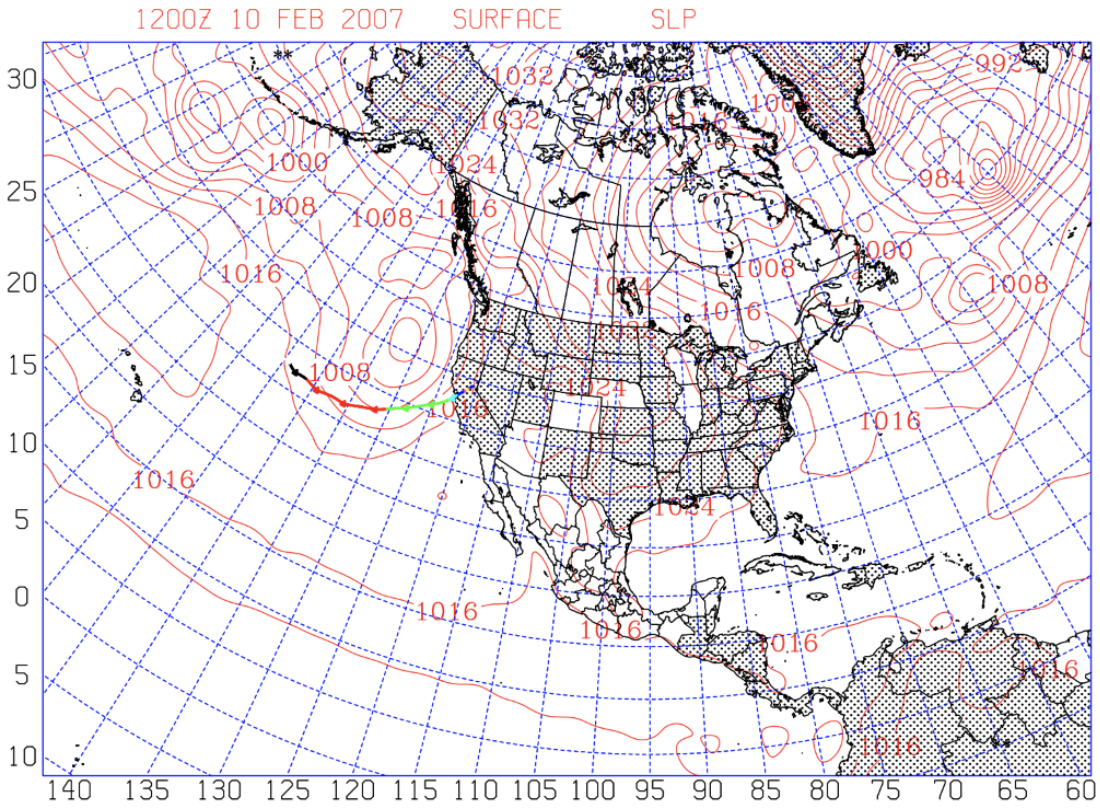

Figure 42. Case 2 700 mb Parcel Trajectory.

C. CASE 3

Figure 43 shows the GOES IR imagery over the evolution of the February 2019 AR event. Beginning at 1200 UTC 08 February 2019 (Figure 43 upper left) an extratropical cyclone forms northwest of Hawaii with a robust cloud plume that extends well to the south of Hawaii. There is a separate extratropical cyclone already affecting the United States west coast. On 1200 UTC 09 February 2019 (Figure 43 upper right), the extratropical cyclone with associated AR has moved eastward while the extratropical cyclone at the United States west coast has moved northward. On 1200 UTC 11 February 2019 (Figure 43 bottom right), the extratropical cyclone has migrated eastward and the cloud plume has grown. By 1200 UTC 13 February 2019 (Figure 43 bottom right), the AR has made landfall on the western continental United States and extends well to the southwest of Hawaii. The cloud evolution for this case shows that the primary moisture plume occurs further south than was seen in Cases 1 and 2.

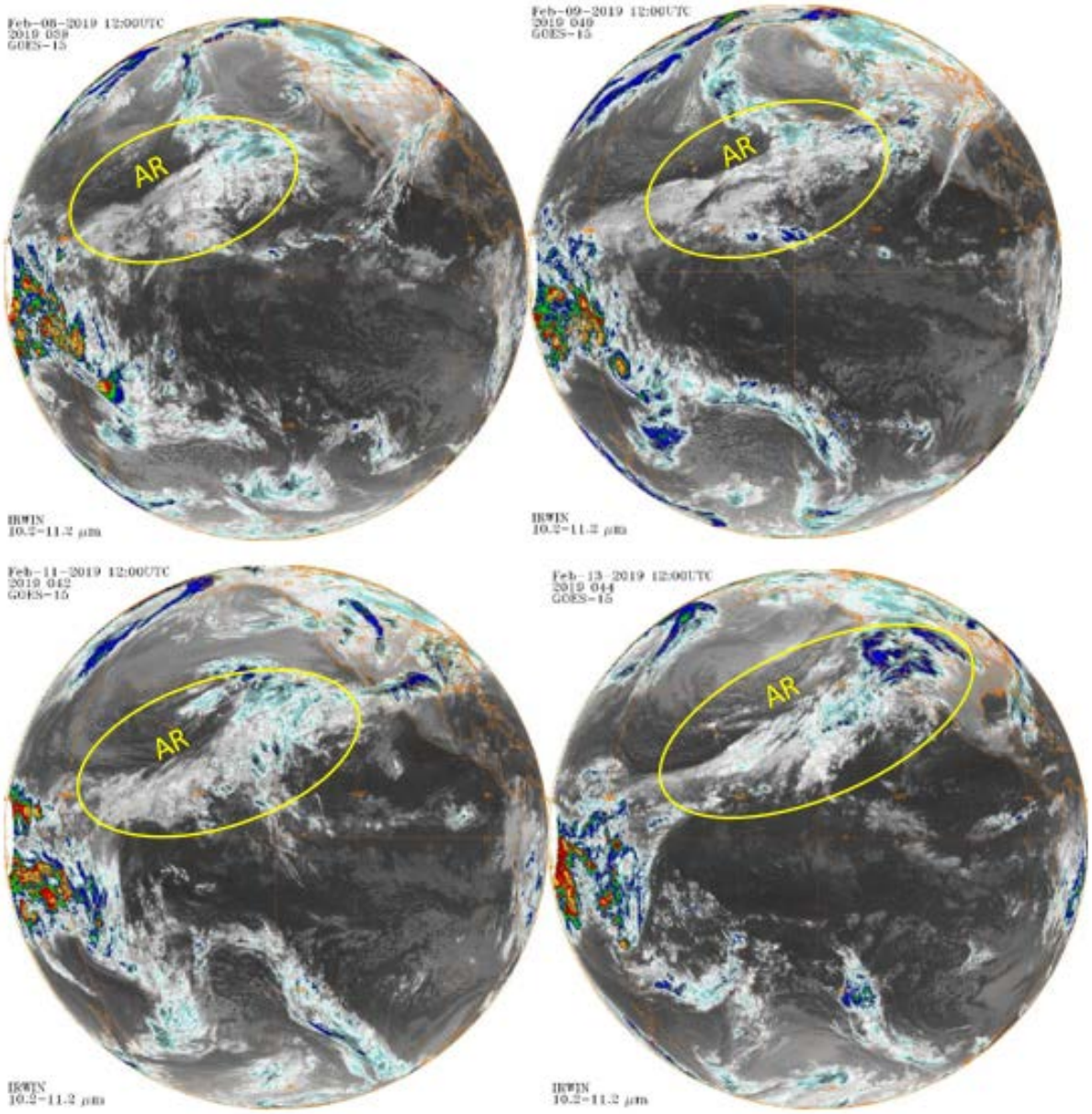

Upper-left: 1200 UTC 08 February 2019; upper-right: 1200 UTC 09 February 2019; lower-left: 1200 UTC 11 February 2019; lower-right: 1200 UTC 13 February 2019.

Figure 43. Case 3 AR IR Satellite Evolution. Source: Knapp (2008)

Figure 44 shows the IVT and 700 mb GHT at specific times in the evolution of the February 2019 AR event. Again at 1200 UTC 08 February (Figure 44 upper left), we have a clockwise motion east of Hawaii, and a low-level trough north of Hawaii with a developing AR moisture plume between these features. Both the clockwise circulation and trough migrate with each other eastward to the west coast of the United States. As both systems move eastward, the IVT moisture transport extends over a progressively longer distance from southwest of Hawaii all the way to United States. west coast. Again, the IVT shows transport of water vapor into the AR from the tropics on the western side of the clockwise circulation. In Case 3, IVT vectors east of the AR are weak and appears water vapor transport ahead of the AR isn't occurring. In the two previous cases, IVT vectors east of the AR were much stronger and water vapor transport ahead of the AR was occurring. However, on 11 February 2019, IVT vectors strengthen and appeared to push water vapor ahead of the AR.

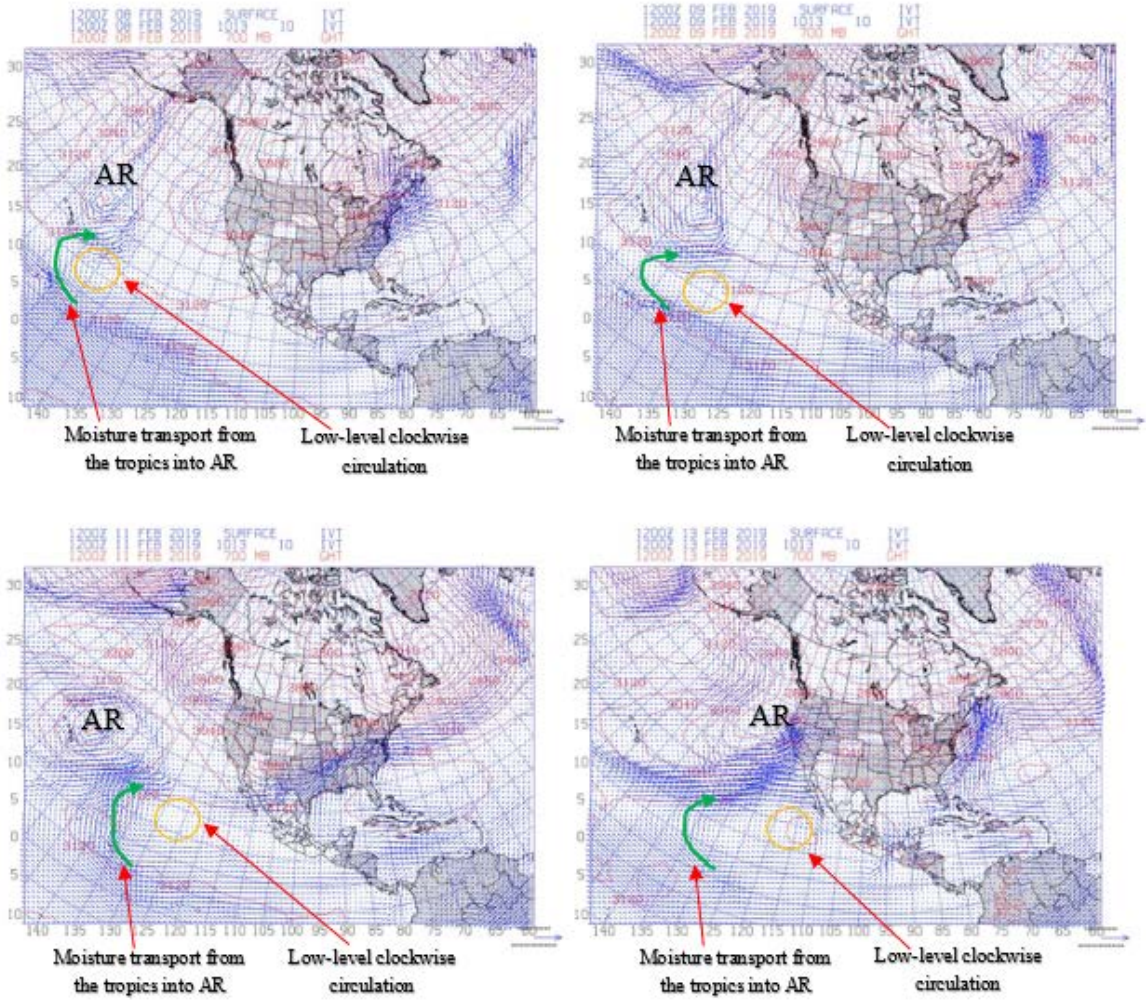

Upper-left: 1200UTC 08 February 2019; upper-right: 1200UTC 09 February 2019; bottom-left: 1200 UTC 11 February 2019; bottom-right: 1200 UTC 13 February 2019. Red lines are 700 mb GHT and blue arrows are the IVT

Figure 44. Case 3 IVT and 700 mb GHT Plot Evolution.

Figure 45 shows the 500 mb GHT at specific times in the evolution of the AR event. The evolution in this case is substantially different than found in the previous cases. In this case, there is a high amplitude ridge over the eastern Pacific (Figures 45 upper left and upper right), which breaks down as a trough coming out of Alaska and merges with the trough near Hawaii to undercut the ridge. This sets up a broad southwesterly flow by 1200 UTC 13 February (Figure 45 bottom right) from Hawaii to the west Coast. During this event, the major ridge over the eastern Pacific is associated with the clockwise circulation in the IVT vectors east of Hawaii on 1200 UTC 08 (Figure 45 upper left) and 09 February 2019 (Figure 45 upper right). By 1200 UTC 11 and 13 February 2019 (Figures 45bottom left and bottom right) the ridge in 500 mb GHT has migrated eastward and built over the western continental United States as the two upper-level troughs merge. Again, as in the first two cases, the low-level clockwise circulation found in the IVT is associated with an upper level ridge. In addition, the AR corresponds to the 500 mb trough as it develops and then progresses eastward toward the United States west coast.

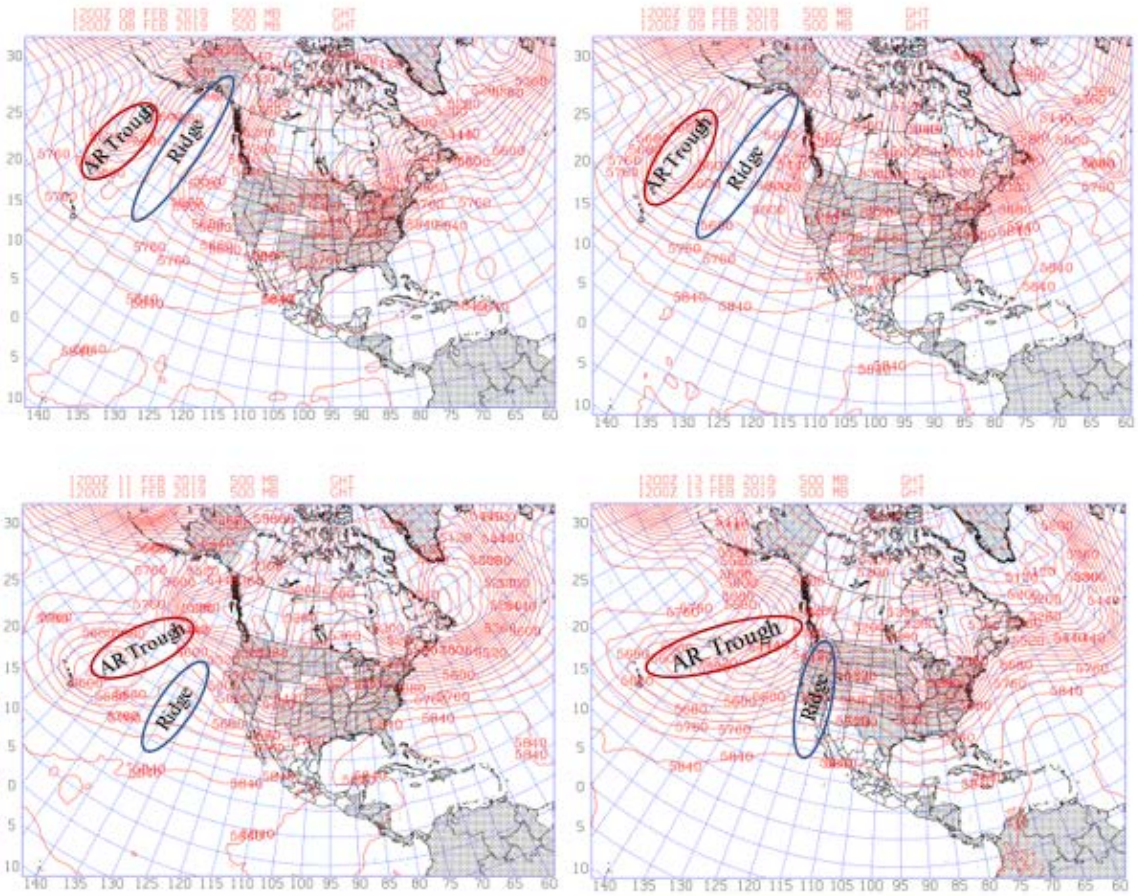

Upper-left: 1200UTC 08 February 2019; upper-right: 1200UTC 09 February 2019; bottom-left: 1200 UTC 11 February 2019; bottom-right: 1200 UTC 13 February 2019. 500 mb GHT are represented by the red lines in meters.

Figure 45. Case 3 500 mb GHT Plot Evolution.

The SLP and 1000 mb winds (Figure 46) at specific times in the evolution of the February 2019 AR event show a weak low-pressure system north of Hawaii that undergoes strong development late in the evolution as the upper-level troughs merge northeast of Hawaii. Both the SLP and 1000 mb winds confirm the existence of a low-level high-pressure system to the east of the low, which was initially weak as well. This high-pressure system strengthened as the low developed as seen in Figure 46 (bottom right). Although the AR developed slowly at first, interaction between the extratropical cyclone and low-level high-pressure system was evident throughout its lifecycle and became strong as the high strengthened by 13 February (Figure 46 bottom right). On 08 February 2019 (Figure 46 upper left), wind flow on the western side of the high-pressure system near Hawaii is flowing from the tropics into the AR, which correlates with the IVT analysis. The orientation of the current low-pressure system in California and the high-pressure system over Alaska is transporting colder air into the western United States. This wind flow and cold air is preventing warm moist from migrating ahead of the AR. This pattern remains in place until 11 February 2019 (Figure 46 bottom left) when the two troughs started to merge. The pressure gradient between the two systems has increased substantially by 13 February (Figure 46 bottom right) as the surface low and high develop. Winds are flowing from the tropics and into the AR and over California. This evolution was much different for the previous two cases. In the first two cases the low-level high-pressure system did not extend into the Alaska and the northern flank of the high in the first two case was able to transport warm moist air to California before the AR arrived.

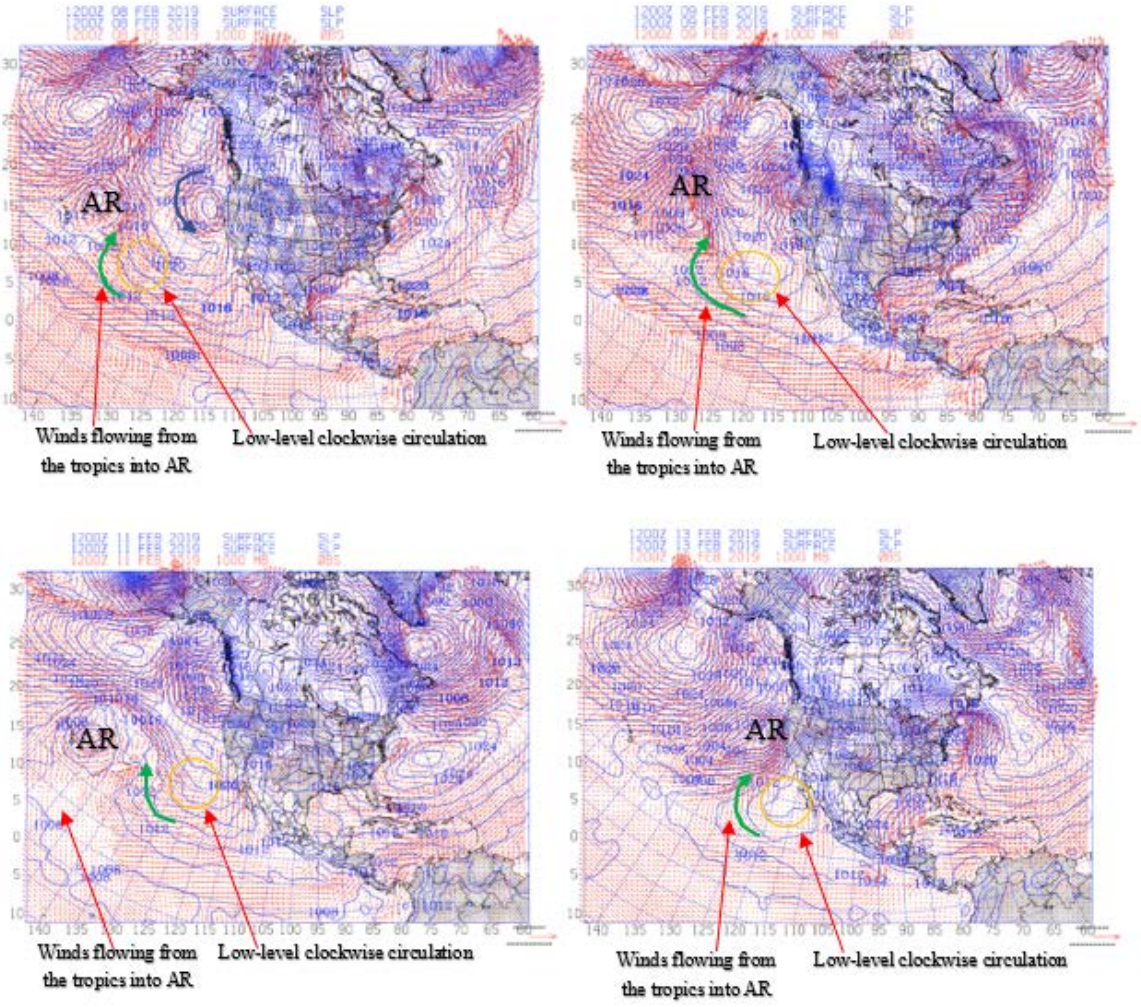

Upper-left: 1200UTC 08 February 2019; upper-right: 1200UTC 09 February 2019; bottom-left: 1200 UTC 11 February 2019; bottom-right: 1200 UTC 13 February 2019. SLP are represented by the blue lines in mb and the red arrows represent wind vectors.

Figure 46. Case 3 SLP and 1000 mb winds Plot.

Figure 47 shows the TQV and 700 mb GHT at the same times in the evolution of the February 2019 AR event. Starting 08 February 2019 (Figure 47 upper right) values of four g/kg TQV are north of Hawaii while values of two g/kg TQV are being drawn into the extratropical cyclone. On 09 February (Figure 47 upper right) values of four g/kg TQV have migrated eastward ahead of the extratropical cyclone associated with the AR. However, two g/kg TQV values are far southwest of California. In the previous two cases, two g/kg TQV values were migrating into the western United States well before the AR and extratropical cyclone arrived. The values maybe low due to the current low-pressure system over the western United States This system along with the high-pressure system to its west is transporting colder and drier air into the United States west coast region. By 13 February 2019 (Figure 47 upper right), the AR system has made landfall and high TQV values are being drawn into the AR system. This resulted in heavy precipitation through the western United States in the form of snow and rain.

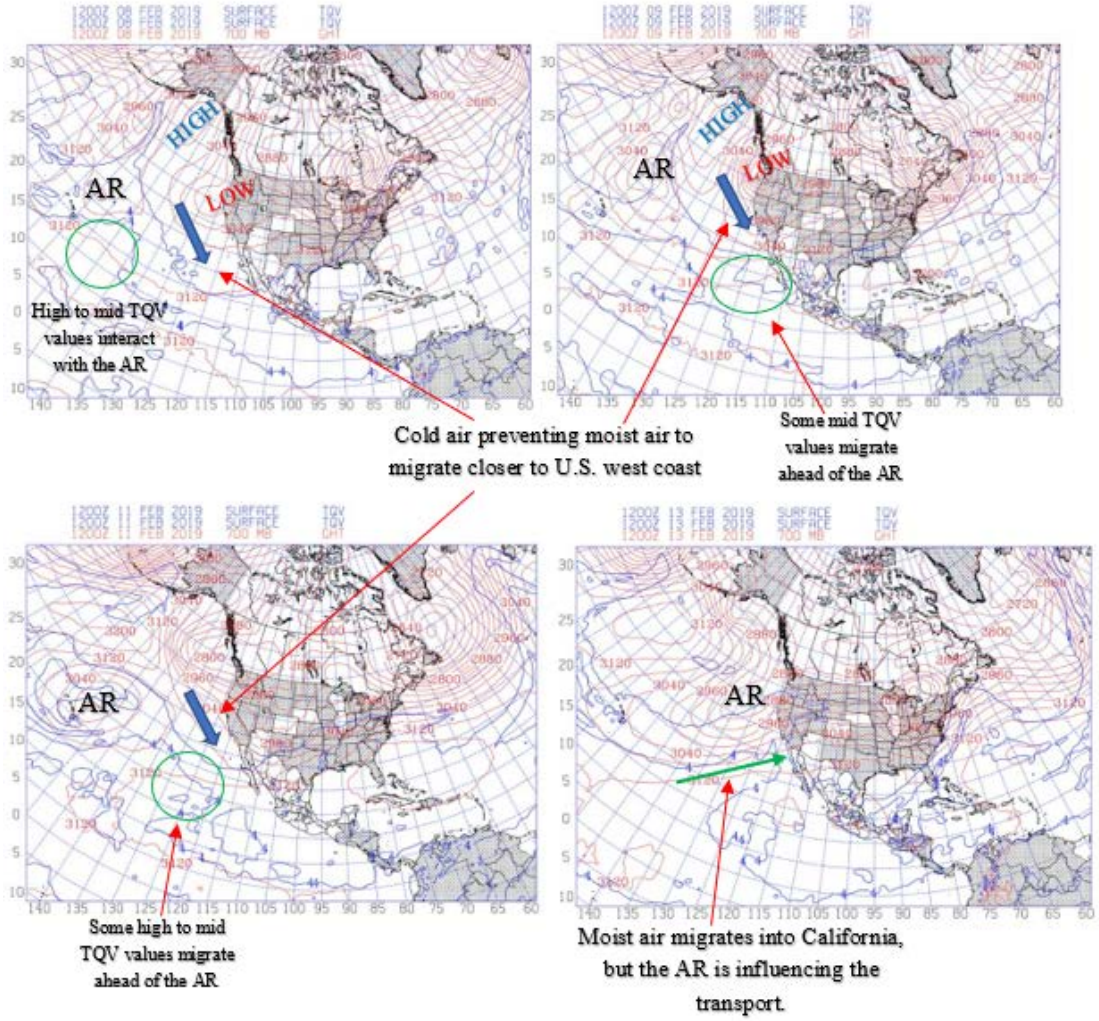

Upper-left: 1200UTC 08 February 2019; upper-right: 1200UTC 09 February 2019; bottom-left: 1200 UTC 11 February 2019; bottom-right: 1200 UTC 13 February 2019. Blue lines represent TQV and red lines represent 700 mb GHT.

Figure 47. Case 3 TQV and 700 mb GHT Plot Evolution.

Figure 48 shows upper air jet stream at 250 mb and 500 GHT at specific times in the evolution of the February 2019 AR event. Initially, jet max values were weak but throughout the event, jet max values would strengthen. The stronger jet max later in the evolution would support the massive cloud plume found in the IR images.

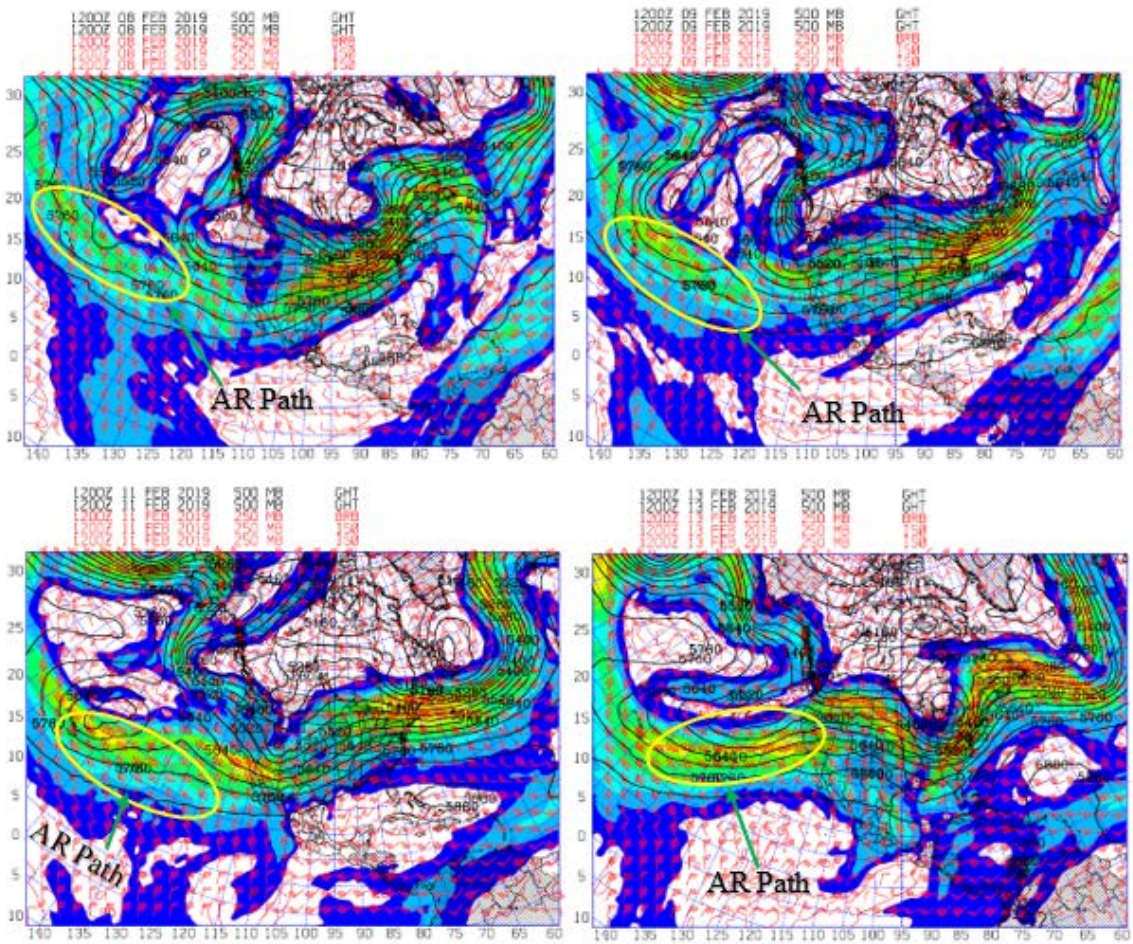

The 500 mb GPT is shown in black contours, the 250 mb wind is shown with red barbs, and the 250 mb jet stream is shown with a color fill. Upper-left: 1200 UTC 08 February 2019; upper-right: 1200 UTC 09 February 2019; lower-left: 1200 UTC 11 February 2019; lower-right: 1200 UTC 13 February 2019.

Figure 48. Case 3 Upper-Air Chart Evolution.

Figure 49 shows the trajectory ending at 700 mb on 1200 UTC 13 February 2019 over Central California. The trajectory endpoint is a Blue Canyon California, and 48 hours prior the trajectory traced back to 31 N 127 W. This trajectory shows that the moisture in this case originates much further east than the previous cases. The moist air is being drawn up from the south into the AR. This occurs even though the high-water vapor transport at 1200 UTC 13 February (Figure 44 bottom right) extends well to the west south of Hawaii. This northward transport appears to be due to the high-pressure to the east feeding moisture into the AR as it progresses eastward.

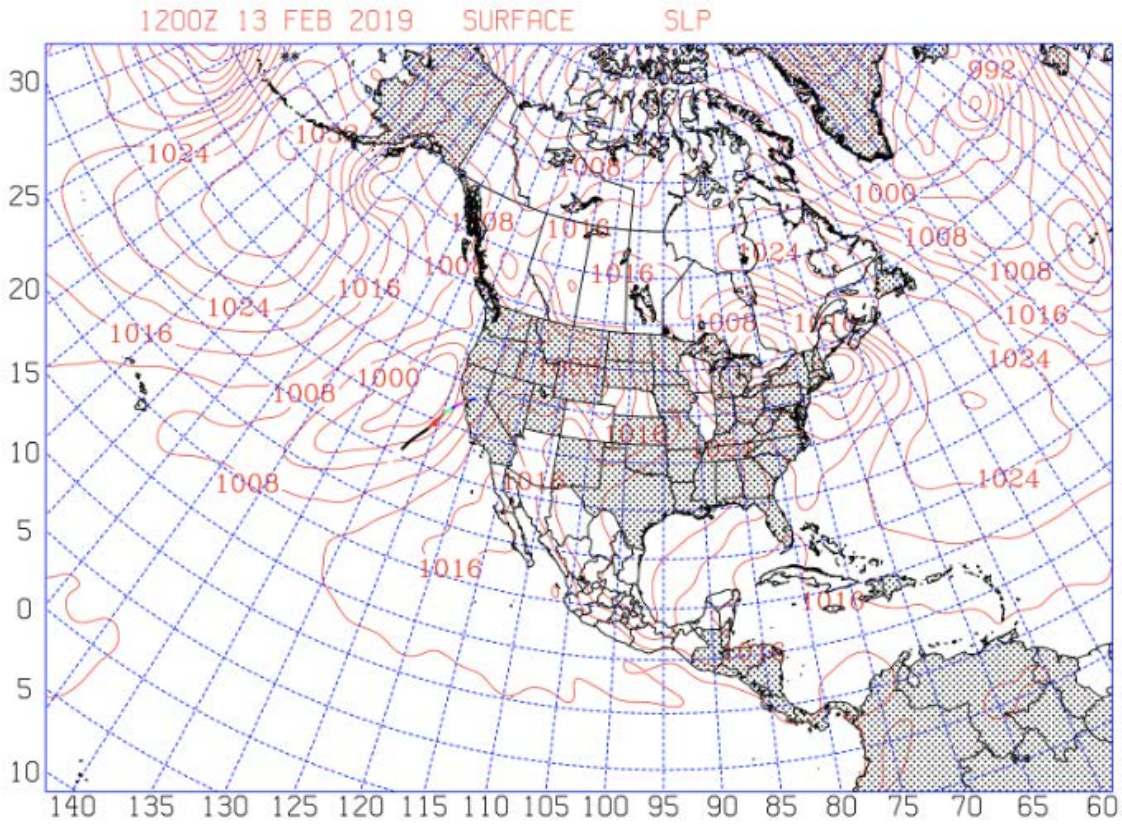

Figure 49. Case 3 700 mb Parcel Trajectory.

D. CASE 4

Figure 50 shows the GOES IR imagery at specific times in the evolution of the November-December 2019 AR event. Beginning at 0000 UTC 27 November 2019 an extratropical cyclone forms northwest of Hawaii that produces a north-south oriented AR (Figure 50 upper left). On 0000 UTC 29 November 2019 (Figure 50 upper right), the extratropical cyclone has migrated northeastward into the Gulf of Alaska, and the cloud plume and AR has dissipated. On 0000 UTC 01 December 2019 (Figure 50 bottom left), the cyclone begins to migrate southeastward and the main AR cloud plume is relatively narrow but has made landfall on the west coast of the United States and extends back towards Hawaii. By 0000 UTC 02 December 2019 (Figure 50 bottom right), the system's AR and cloud plume has grown, and heavy precipitation was observed primarily over the Central California Coast.

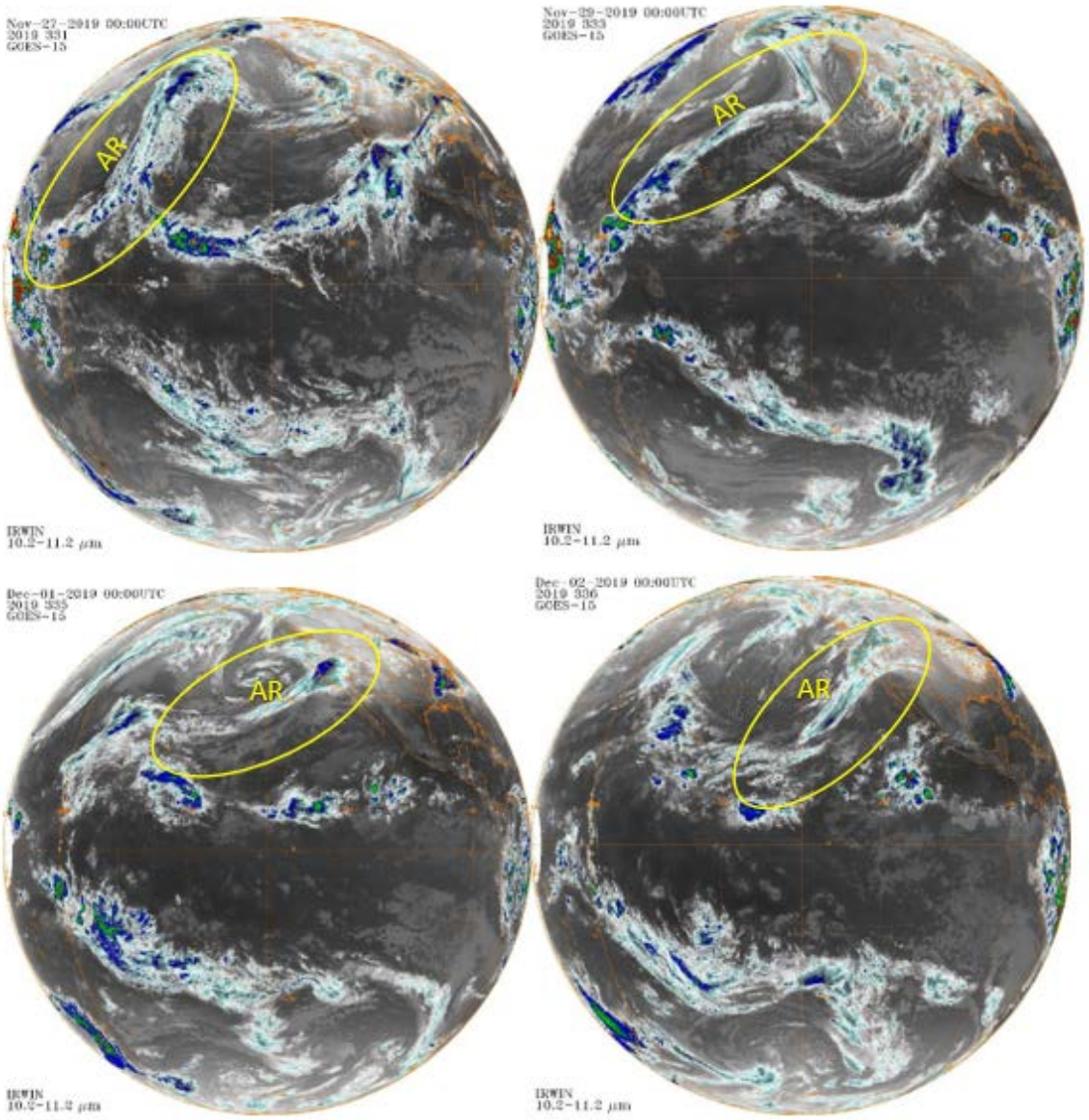

Upper-left: 0000 UTC 27 November 2019; upper-right: 0000 UTC 29 November 2019; lower-left: 0000 UTC 01 December 2019; lower-right: 0000 UTC 02 December 2019.

Figure 50. Case 4 AR IR Satellite Evolution. Source: Knapp (2008)

Figure 51 is the IVT and 700 mb GHT at specific times in the evolution of the November December 2019 AR. The AR evolution is quite different in this case as it starts out in north-south orientation and then transitions to the more typical southwest-northeast orientation. As in all the cases, on 0000 UTC 27 November 2019 a clockwise circulation is visible northeast of Hawaii and is feeding moisture into the AR associated with an extratropical cyclone to the west. In this case, the clockwise circulation is much further northeast from Hawaii than previous cases as there is a very high amplitude ridge over the eastern Pacific. On 0000 UTC 29 November 2019 (Figure 51 upper right) the ridge interacting with the AR begins to break down and the AR and associated cyclone migrate northeastward. As it moved northeast, the moisture transport in the AR weakened as well. Between 30 November and 01 December 2019 (Figure 51 bottom left), the ridge dissipates, and the trough and associated AR migrates southeastward into California. During this transition, it appears a low-level clockwise circulation originating in Mexico migrates westward and begins to interact with the AR. On 0000 UTC 02 December 2019 (Figure 51 bottom right) this new low-level clockwise circulation aids water vapor transport from the tropics into the AR as it migrates into California.

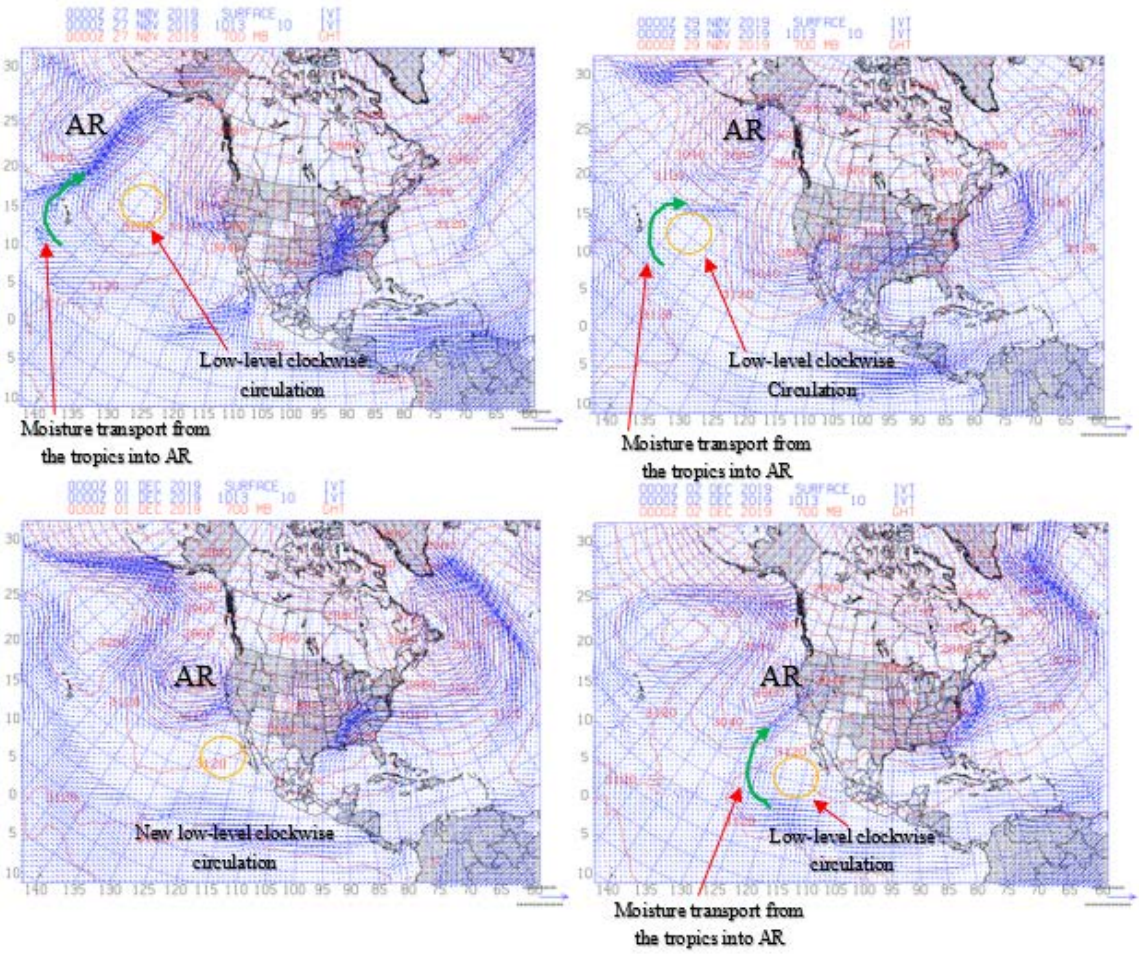

Upper-left: 0000 UTC 27 November 2019; upper-right: 0000 UTC 29 November 2019; lower-left: 0000 UTC 01 December 2019; lower-right: 0000 UTC 02 December 2019. Red lines are 700 mb GHT and blue arrows are the IVT

Figure 51. Case 4 IVT and 700 mb GHT Plot Evolution.

The 500 mb GHT is shown in Figure 52 through the evolution of the November December 2019 AR event. The upper-level evolution seen at 500 mb confirms the evolution found in the 700 mb heights and IVT. The initial trough is west of Hawaii with a high amplitude ridge to the northeast. The trough moves over the top of the ridge and then drops down west of California to set up southwesterly flow over the eastern Pacific (Figure 52 bottom right). As seen in the previous cases, the 500 mb GHT shows that the low-level clockwise circulation found in the IVT is associated with an upper level ridge. Initially, on 29 November 2019 (Figure 52 upper right), the ridge and clockwise IVT circulation is centered in the Gulf of Alaska. By 01 December 2019 (Figure 52 bottom left) the ridge is over the western United States and extends south off the coast of Mexico, where a new anticyclonic IVT circulation develops. On 02 December 2019 (Figure 52 bottom right) the ridge over the western United States builds into the mid United States but still appears to support the low-level high-pressure system off the coast of Mexico that is interacting with the AR.

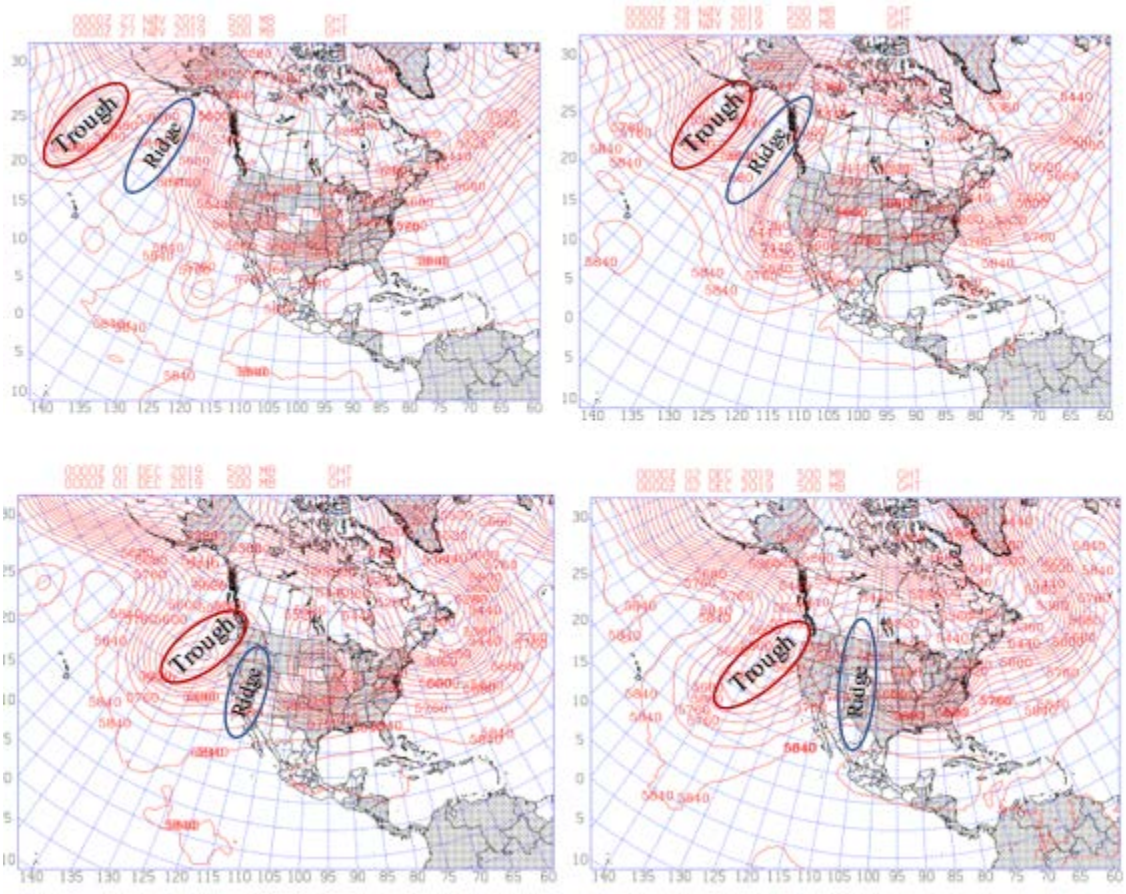

Upper-left: Upper-left: 0000 UTC 27 November 2019; upper-right: 0000 UTC 29 November 2019; lower-left: 0000 UTC 01 December 2019; lower-right: 0000 UTC 02 December 2019. 500 mb GHT are represented by the red lines in meters.

Figure 52. Case 4 500 mb GHT Plot Evolution

The SLP and 1000 mb winds in Figure 53 follow a similar evolution as the upper-levels of the November-December 2019 AR event. The surface low-pressure system was initially northwest of Hawaii (Figure 53 upper right), moves northward over the upper-level ridge, and then southeastward in the eastern Pacific to end up off the California coast by 02 December (Figure 53 bottom right). Case four has some similarities to case three in terms of water vapor transport but the low went over the top of the ridge while in case 3 the low undercut the ridge. Although a low-level high-pressure system occurs east of the surface cyclone and associated AR early in its evolution, there is evidence that that initial low-level high-pressure system dissipated, and a new low-level high-pressure system forms west of Mexico to subsequently interact with the AR. This low-level clockwise circulation (surface high) builds by 02 December (Figure 53 bottom right) and is drawing air from the tropics up into the AR.

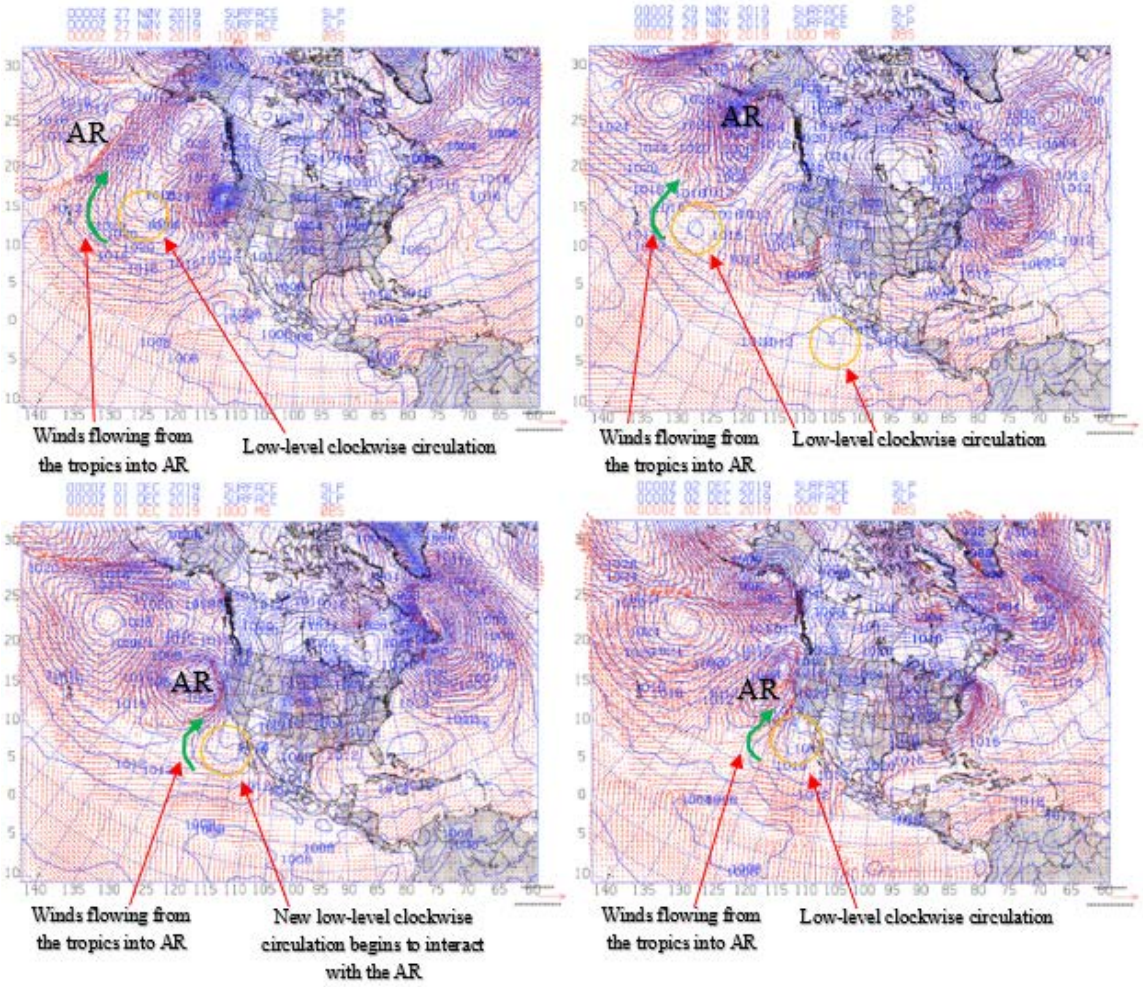

Upper-left: Upper-left: 0000 UTC 27 November 2019; upper-right: 0000 UTC 29 November 2019; lower-left: 0000 UTC 01 December 2019; lower-right: 0000 UTC 02 December 2019. SLP are represented by the blue lines in mb and the red arrows represent wind vectors.

Figure 53. Case 4 SLP and 1000 mb winds Plot.

Figure 54 shows the TQV and 700 mb GHT at specific times in the evolution of the November December 2019 AR event. Starting 27 November 2019 (Figure 54 upper left) values of 4 g/kg TQV interact in the north-south AR system. On 29 November 2019 (Figure 54 upper right) the position of the ridge and a different trough over California is preventing high TQV values from migrating toward the United States west coast. By 01 and 02 December 2019 (Figures 54 bottom left and bottom right), high TQV values enter California, but it appears the high TQV values are associated with the AR transport and did not occur over California prior to the arrival of the AR. It must be noted though, that the low-level clockwise circulation found in the 02 December IVT (Figure 54) is interacting with the AR and transporting water vapor into the AR. For the most part, high TQV values did not advance ahead of the AR, and all water vapor transport appeared to occur with the interaction of the AR and low-level high-pressure system.

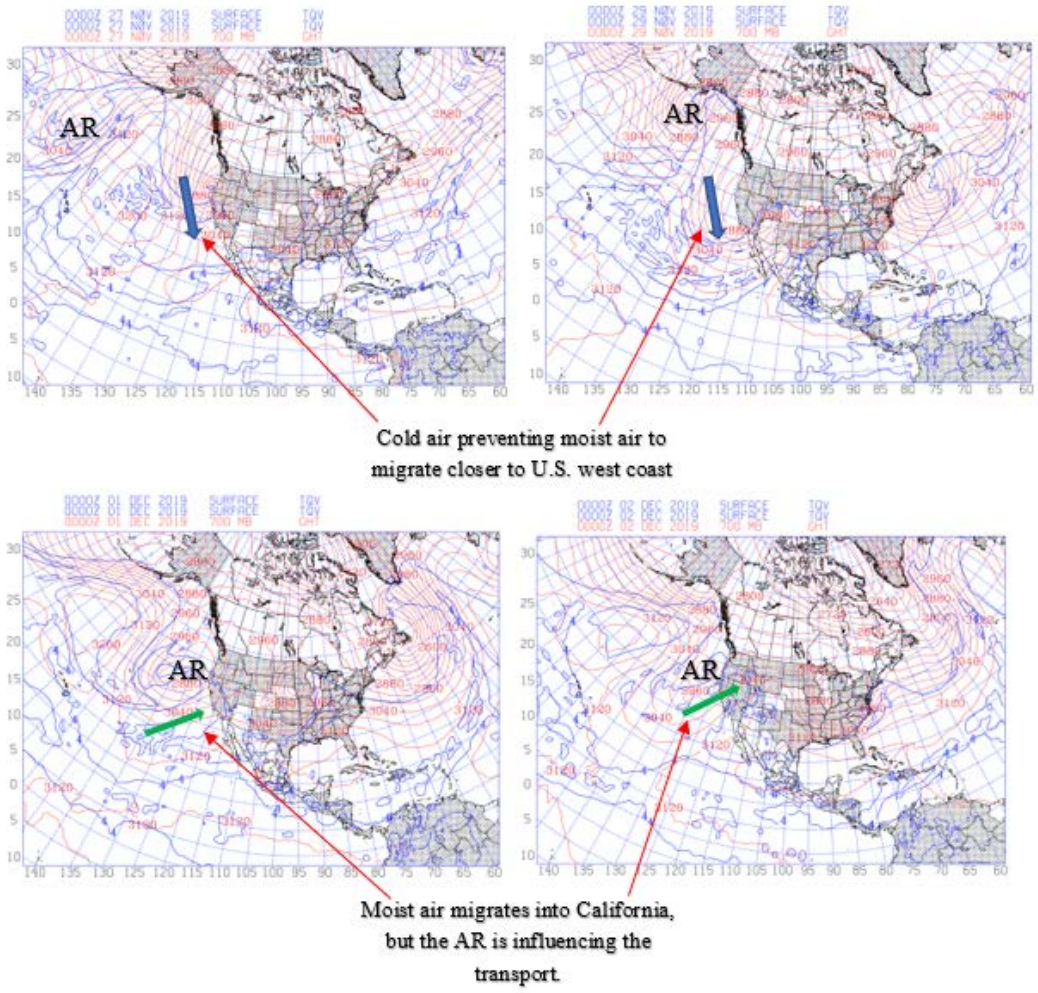

Upper-left: 0000 UTC 27 November 2019; upper-right: 0000 UTC 29 November 2019; lower-left: 0000 UTC 01 December 2019; lower-right: 0000 UTC 02 December 2019. Blue lines represent TQV and red lines represent 700 mb GHT.

Figure 54. Case 4 TQV and 700 mb GHT Plot Evolution.

Figure 55 shows the upper air jet stream at 250 mb and 500 mb GHT at specific times in the evolution of the November December 2019 AR event. Throughout the event the jet maximum windspeeds identified correspond to the cloud plume found in the IR images (Figure 50).

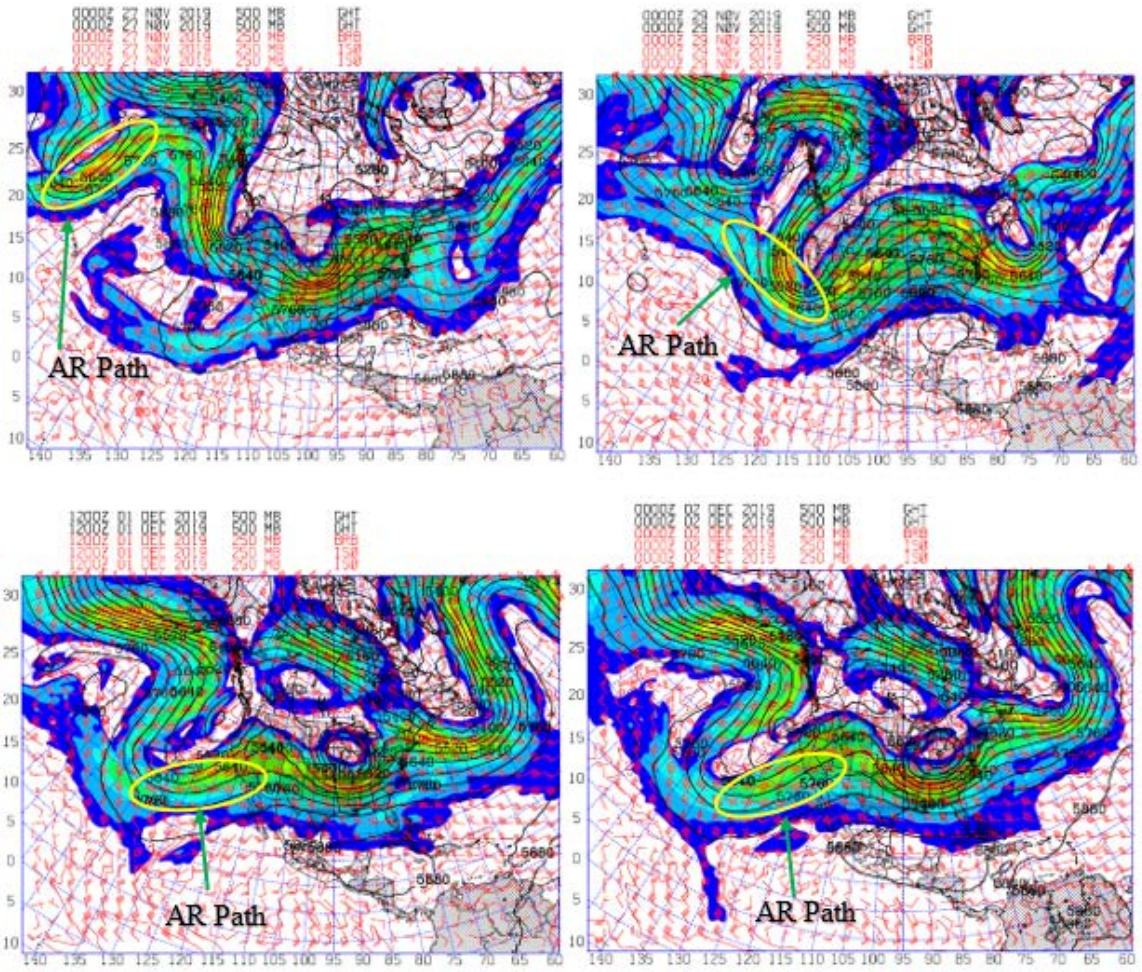

The 500 mb GPT is shown in black contours, the 250 mb wind is shown with red barbs, and the 250 mb jet stream is shown with a color fill. Upper-left: 0000 UTC 27 November 2019; upper-right: 0000 UTC 29 November 2019; lower-left: 1200 UTC 01 December 2019; lower-right: 0000 UTC 02 December 2019.

Figure 55. Case 4 Upper-Air Chart Evolution.

Figure 56 shows an air parcel trajectory ending at 700 mb on 1200 UTC 03 December 2019. The trajectory endpoint is over Blue Canyon California, and 48 hours prior the trajectory traced back to 23 N 127 W. The trajectory clearly shows that the moisture in the AR and associated precipitation originated to the south off the coast of Mexico. This trajectory suggests that the circulation around the high off the coast of Mexico was very important in feeding moisture into this AR, even though the cloud plume seen in Figure 50 extends back toward Hawaii.

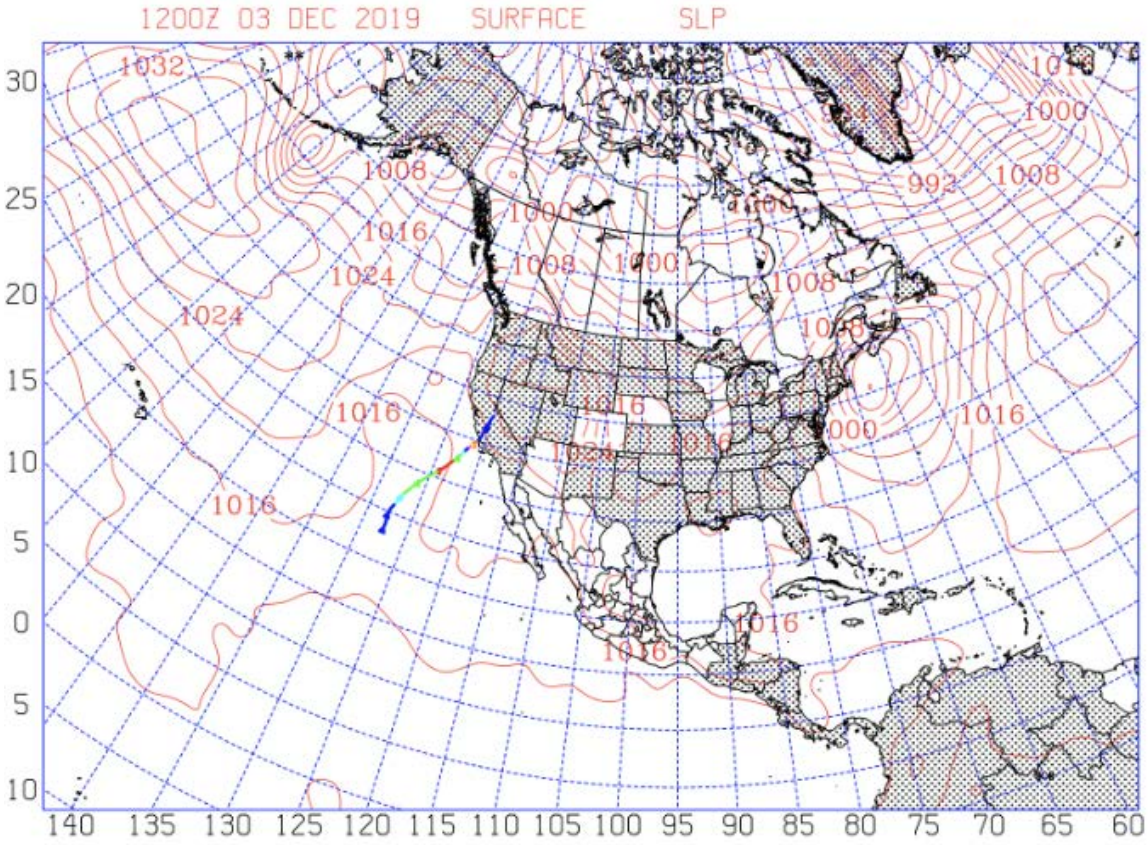

Figure 56. Case 4 700 mb Parcel Trajectory

V. CONCLUSION

In all four cases we examined three hypotheses for ARs that have similar characteristics. The hypotheses were: 1) that major (Pineapple Express) AR events form near Hawaii with the high-pressure system and low-pressure system interacting with each other; 2) that CBARs form as a result of the high-pressure system feeding moisture into the low-pressure system; 3) the relative source of moisture in different ARs and its potential impact on observed downstream precipitation.

In all cases, the IR image showed the formation of and AR northwest of the Hawaiian Islands. Examining the IVT and 700 mb GHT figures, a noticeable clockwise circulation would form east of the Hawaiian Islands. By analyzing the 500 mb GHT and SLP, this clockwise circulation was confirmed to be a high-pressure system. In three of the four cases, analysis in the IVT, 700 mb GHT, 500 mb GHT, 1000 mb winds and SLP figures, indicated the high-pressure system and AR were migrating and interacting with each other. The interaction and the migration were confirmed by analyzing the evolution of AR system just after making landfall on the west coast of the United States. For case four, the initial high-pressure system migrating and interacting with the AR would weaken and dissipate. However, a new high-pressure system formed further east to interact with the AR before making landfall in California.

In all cases, the IVT figures showed a high-pressure system appearing to be one of the main contributors for water vapor transport from the tropics into the AR. The high-pressure system in the IVT figures all displayed water vapor transport moving westward on the southern flank. On the western flank of the high-pressure system, the water vapor would turn northward and migrate into the AR's eastern flank. From there, high moisture would wrap into the AR. This was identified in the TQV figures. As the result, a cloud plume in the CBAR would be visible in the IR images.

Finally, in case one and two, it appeared high TQV values would migrate ahead of the AR. By examining the IVT, 700 mb GHT, 500 mb GHT, 1000 mb winds and SLP figures, it appears the high-pressure system was providing a transport of high TQV well

ahead of the AR and into the western United States. For case three, there was some evidence TQV was ahead of the AR due to the high-pressure system, but it did not migrate into the western United States before the AR arrived. This was most likely due to the prior low-pressure system already on the western United States. The orientation of this system and the high-pressure system would transport colder air from the north to the west coast of the United States and prohibited the moist air to migrate further. However, once the AR made landfall in California, the AR and high-pressure system were able to transport water vapor from the tropics once the colder air was cut off from influencing the western United States. In case four, there were similarities with case three. A prior low-pressure system transported colder air from north into the west coast of the United States. The high-pressure system was unable transport high water vapor values ahead of the AR. This was most likely due to the position of the high-pressure system. In case four the high-pressure system was further north than the previous three cases. The eastern flank of the high-pressure system drew in colder air into the western United States.

The purpose of this thesis was to bring awareness and focus attention on the role the high-pressure system plays on AR development and evolution. This study shows that there is a high possibility that the high-pressure system plays a significant role in the development of and transport of water vapor into an AR system, although the relative degree of this contribution was not quantified. There are still many other contributing factors that play roles into the ARs. One such factor not explored here is the enhanced precipitation from orographic lifting that occurs when any eastern Pacific storm hits the mountainous United States west coast (NWS 2020). Other areas that could be explored concerning the interaction of an AR and high-pressure system are as follows. What percentage of moisture is due to transport around the high versus along the AR from the southwest? Do high-pressure systems have to be strong or weak to have a significant contribution to an AR? Is there a correlation to the strength of pressure gradient force between the two systems and the transport of water vapor? These are just a few possibilities to examine between the interaction of an AR and high-pressure system.

LIST OF REFERENCES

AMS, 2019: Atmospheric river. Glossary of meteorology. Accessed 01 September 2020. http://glossary.ametsoc.org/wiki/Atmospheric_river.

CNRFC NOAA, 2019: Observed Precipitation. Accessed (15 January 2020), https://www.cnrfc.noaa.gov/rainfall_data.php.

Dacre, H. F., P. A. Clark, O. Martinez-Alvarado, M. A. Stringer, and D. A. Lavers, 2015: How do atmospheric rivers form? *Bull. Amer. Meteor. Soc.*, **96**,1243–1255, doi:10.1175/BAMS-D-14-00031.1.

Dettinger, M.D., F. M. Ralph, T. Das, P. J. Neiman, and D. Cayan, 2011. Atmospheric rivers, floods, and the water resources of California. *Water* **3**, 455–478.

Guan, B. and D. E. Waliser, 2017: Atmospheric rivers in 20 year weather and climate simulations: A multi-model, global evaluation. *J. Geophys Res Atmos.* **122,** 5556–5581, doi:10.1002/2016JD026174.

Hedstrom, S. L., 2014: Atmospheric rivers and the forcing of extreme precipitation in the Midwest U.S. M.S. thesis, Department of Meteorology, Naval Postgraduate School, 114 pp.

Ingram, B. L., and F. Malamud-Roam, 2013: *The West without Water: What Past Floods, Drought, and Other Climates Clues Tell Us about Tomorrow.* Berkley; Los Angeles: University of California Press.

Knapp, K. R., 2008: Scientific data stewardship of International Satellite Cloud Climatology Project B1 global geostationary observations. Accessed 01 February, 2020 GIBBS ISCCP B1 Browse System (noaa.gov)

Newell, R. E., N. E. Newell, Y. Zhu, and C. Scott, 1992: Tropospheric rivers? – A pilot study. *Geophysical Research Letters*, **12**, 2401–2404, https://doi.org/10.1029/92GL02916.

Nuss, W., and S. Drake, 1990: *VISUAL Meteorological Diagnostic and Display Program*, Naval Postgraduate School Department of Meteorology, 51 pp.

NWS Sacramento, 1996: Auburn CA Monthly Climate Data. National Weather Service Sacramento Forecast Office, Accessed (01 October 2020), https://w2.weather.gov/climate/xmacis.php?wfo=sto.

NWS Reno, 1996: Tahoe City CA Monthly Climate Data. National Weather Service Sacramento Forecast Office, Accessed (01 October 2020), https://w2.weather.gov/climate/xmacis.php?wfo=rev.

NWS Columbia, 2020: Weather Terms. National Weather Service Columbia Forecast Office, Accessed 02 September 2020, https://www.weather.gov/cae/weatherterms.html.

Ralph, F.M., P. J. Neiman, and G. A. Wick, 2004: Satellite and CALJET aircraft observations of atmospheric rivers over the Eastern North-Pacific Ocean during the winter of 1997⁄98. *Monthly Weather Review* 132:1721–1745.

Ralph, F. M., M. Dettinger, D. Lavers, I. V. Gorodetskaya, A. Martin, M.Viale, A. B. White, N. Oakley, J. Rutz, J. R. Spackman, H. Wernli, and J. Cordeira, 2017: Atmospheric rivers emerge as a global science an applications focus. Bull. Amer. Meteor. Soc. ,1969–1973, doi: 10.1175/BAMS-D-16-0262.1. https://doi.org/10.1175/BAMS-D-16-0262.1

Roos, M., 1997: The Great New Year's Flood of 1997 in Northern California. https://cepsym.org/Sympro1997/Roos.pdf.

Sexson, J. W., 2019: Baja Express: The emergence of convergent boundary atmospheric rivers and their effects in South Central United States. M.S. thesis, Department of Meteorology, Naval Postgraduate School, 84 pp.

INITIAL DISTRIBUTION LIST

1. Defense Technical Information Center
   Ft. Belvoir, Virginia

2. Dudley Knox Library
   Naval Postgraduate School
   Monterey, California